UCONN LIBRARY

University of Connecticut
OpenCommons@UConn

Master's Theses | University of Connecticut Graduate School

6-3-2011

Applied Control Strategies at a Cogeneration Plant

Joseph William Burns
University of Connecticut, jwb04001@gmail.com

Recommended Citation
Burns, Joseph William, "Applied Control Strategies at a Cogeneration Plant" (2011). *Master's Theses*. 129.
https://opencommons.uconn.edu/gs_theses/129

This work is brought to you for free and open access by the University of Connecticut Graduate School at OpenCommons@UConn. It has been accepted for inclusion in Master's Theses by an authorized administrator of OpenCommons@UConn. For more information, please contact opencommons@uconn.edu.

Applied Control Strategies in a Cogeneration Plant

Joseph W. Burns

B.S., Management and Engineering for Manufacturing, University of Connecticut, 2009

B.S., Mechanical Engineering, University of Connecticut, 2009

A Thesis

Submitted in Partial Fulfillment of the

Requirements for the Degree of

Master of Science

at the

University of Connecticut

2011

APPROVAL PAGE

Master of Science Thesis

Applied Control Strategies in a Cogeneration Plant

Presented by

Joseph W. Burns, B.S.

Major Advisor_____
Douglas Cooper, Ph.D.

Associate Advisor_____
Zbigniew Bzymek, Ph.D.

Associate Advisor_____
Chengyu Cao, Ph.D.

University of Connecticut

2011

ACKNOWLEDGEMENTS

Thank you to everyone who helped me along the way, making my education and research possible. I would like to thank my advisor, Professor Doug Cooper for providing me with this opportunity and preparing me for my career as a control systems engineer. Thank you to my family for the encouragement and support in so many different forms. To the staff at the UConn Cogeneration Plant and Array Systems, you guys have been great. I've truly enjoyed working with all of you. Thank you for taking the time to explain plant operation and controls to me. I would like to thank Professor Bzymek and Professor Cao, who have taught me so much in the classes that I have taken throughout the years, and served as my associate advisors. I would also like to acknowledge the State of Connecticut and the University of Connecticut for seven years of quality education and invaluable experiences that I've had here. To my girlfriend, Mackenzie, I could never have done it without you.

TABLE OF CONTENTS

LIST OF FIGURES

NOMENCLATURE

CO	controller output
D	disturbance variable
E	error
F	low pass filter transfer function
$f(CTG)$	function of combustion turbine generator fuel flow
G_C	controller transfer function
G_C^*	controller transfer function in IMC structure
$G_{C,1}$	cascade outer process controller transfer function
$G_{C,2}$	cascade inner process controller transfer function
G_D	disturbance transfer function
$G_{D,2}$	cascade inner process disturbance transfer function
G_{FF}	feed forward controller transfer function
G_P	process transfer function
G_P^*	process model transfer function in IMC structure
$G_{P,1}$	cascade outer process transfer function
$G_{P,2}$	cascade inner process transfer function
h	specific enthalpy
K_C	controller proportional gain
$K_{C,BFP}$	boiler feed water pressure controller proportional gain
$K_{C,DCLP}$	dump condenser low pressure steam pressure controller proportional gain
$K_{C,LP\ TEMP}$	low pressure steam temperature controller proportional gain
$K_{C,NH3}$	ammonia flow controller proportional gain

$K_{C,NOX}$	NO_X concentration controller proportional gain
$K_{C,TEMP}$	temperature controller proportional gain
K_D	controller derivative gain
$K_{D,LP\ TEMP}$	low pressure steam temperature controller derivative gain
K_P	process gain
K_I	controller integral gain
$K_{I,BFP}$	boiler feed water pressure controller integral gain
$K_{I,DCLP}$	dump condenser low pressure steam pressure controller integral gain
$K_{I,LP\ TEMP}$	low pressure steam temperature controller integral gain
$K_{I,NH3}$	ammonia flow controller integral gain
$K_{I,NOX}$	NO_X concentration controller integral gain
$K_{I,TEMP}$	temperature controller integral gain
$\dot{m}$	mass flow rate
n_{fans}	number of cooling tower fans operating
P_{fan}	cooling tower fan electric power consumption
P_{fans}	total electric power consumption of cooling tower fans
PV	process variable
$-\dot{Q}_{water}$	heat removal rate from water
SP	process set point
U	controller output
Y	measured process variable
Y^*	prediction of measured process variable
Y_{SP}	process set point

Δt	change in time for one time step
ΔT	change in temperature
θ_P	process dead time
τ_P	process time constant
τ_C	closed loop time constant
ω_{fans}	angular velocity of cooling tower fans
ω_{vapor}	ratio of the mass of water vapor to the mass of air in an air-vapor mixture

ABBREVIATIONS AND ACRONYMS

BPV	Bypass Valve
CEMS	Continuous Emissions Monitoring System
CTG	Combustion Turbine Generator
DCV	Dump Condenser Valve
DLO	Design Level of Operation
DSV	Desuperheater Valve
FOPDT	First Order Plus Dead Time
HMI	Human-Machine Interface
HP	High Pressure
HRSG	Heat Recovery Steam Generator
IMC	Internal Model Control
LP	Low Pressure
NGV	Natural Gas Valve
PI	Proportional, Integral
PID	Proportional, Integral, Derivative
PRV	Pressure Reduction Valve
RMS	Root Mean Square
SCADA	Supervisory Control And Data Acquisition
SCR	Selective Catalytic Reduction
SISO	Single Input Single Output
STG	Steam Turbine Generator
STGV	Steam Turbine Generator Valve
VFD	Variable Frequency Drive

CHAPTER 1: INTRODUCTION

1.1 Objectives

The purpose of this paper is to demonstrate the effectiveness of "classical strategies for dynamic control" on authentic cogeneration processes. These strategies are applied to several processes at the University of Connecticut's cogeneration plant. Case studies of their applications are presented in this paper. Strategies that are applied include the following:

1) The classical SISO feedback structure
2) The First Order Plus Dead Time (FOPDT) process model
3) The Internal Model Control (IMC) correlations for PI controller tuning
4) Static feed forward with feedback trim
5) Cascade Control

1.2 The Need for Simplicity in Cogen Control Logic

Cogeneration (cogen) plants tend to be small by nature. Their competitiveness is achieved by balancing a site's heating needs with power production. Despite smaller size, the complexity of a cogen plant is often greater than standard power plants. The small scale output and full scale complexity of a cogen plant demand simplicity in operations and maintenance. Control logic simplicity is particularly important.

A vast collection of customized control logic directs a plant's automated systems. The logic must be maintained along with ever changing processes, demands and environments. Simplicity is essential in order to understand and effectively manage the

evolution. Classical process control strategies are often the most appropriate solution. They provide satisfactory control performance while maintaining logic simplicity. Classical strategies tend to be well understood by plant personnel and are easy to implement, resulting in greater operational efficiency for the plant.

1.3 Overview of Cogen Case Studies

SCR NO_X Control of Combustion Turbine Exhaust

This case study details the NO_X control of cogen gas turbine exhaust using a nonlinear feed forward with cascade architecture. The proposed control structure incorporates the five control strategies listed in Section 1.1. A step-by-step process for implementing and tuning the control structure is presented. The resulting control performance is good and the logic is dramatically simplified.

Cooling Tower Temperature Control

The first four strategies outlined in Section 1.1 are applied to the cooling tower water temperature control system. Cooling tower system efficiency is also examined. Efficiency measures are integrated into a comprehensive logic, based on the classical control strategies. Resulting logic provides satisfactory temperature control and promotes efficiency.

Cogen Steam System

Three processes in the cogen plant's steam system are examined. The classical SISO feedback structure is applied to each process and the controllers are tuned using the FOPDT model and IMC correlations. This combination is the most basic control methodology of this paper. The simplicity of the methodology is its primary strength.

The results of these case studies are submitted as further evidence of the effectiveness of classical strategies for industrial process control.

1.4 Overview of the UConn Cogeneration Plant

The University of Connecticut Cogeneration Plant provides utilities for over 22,000 students at the Storrs, CT campus [21]. While typically referred to as a "cogeneration plant", it actually provides the campus with steam, chilled water and electricity, making it a combined heating, cooling and power facility. Before the cogen plant was built, a central utility plant on campus provided steam and chilled water; electricity was purchased from the grid. Faced with rising energy costs, UConn began construction of the cogen plant in 2003. It was completed by 2005, costing about $80 million [10]. The plant was mated with the existing central utility, which added electrical generation capability as well as the ability to utilize waste heat from power generation to produce steam and chilled water.

Three 7.5 MW Solar Taurus^{TM} 70 turbines are the main source of electrical power in the plant. They primarily burn natural gas for fuel but are also capable of burning fuel oil. Each turbine is coupled to a generator; collectively they are referred to as Combustion Turbine Generators (CTGs). Hot exhaust gases from the turbines pass through Rentech Heat Recovery Steam Generators (HRSGs) before being treated to reduce emissions and exiting through the stack. The HRSGs contain large heat exchangers used to capture heat from the exhaust gas which is then used to boil water and create steam. They also contain natural gas duct burners that are fired in the exhaust stream when more steam is required. The HRSGs produce high pressure and low pressure steam. High pressure

steam is used in a combined cycle configuration, driving a single stage, 5 MW Murray Steam Turbine Generator (STG), providing additional electricity generation. The steam exits the turbine at reduced pressure joining the low pressure steam from the HRSGs. An overview of the plant's steam system is provided in Figure 1.1.

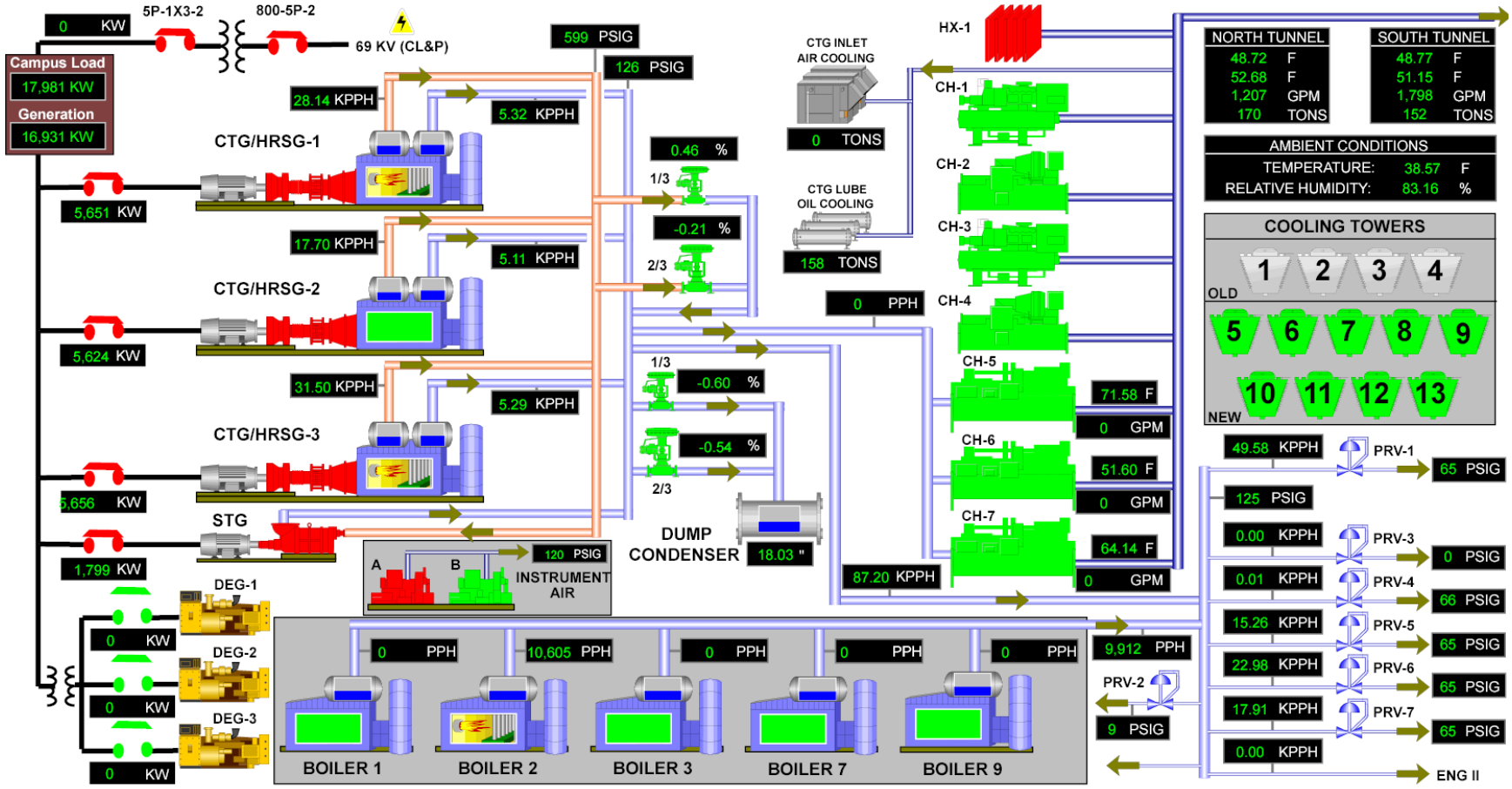

Figure 1.1: Overview of the UConn Cogeneration Plant's Steam System [17]

Low pressure steam is either used for heating or chilled water production, depending on the needs of the campus. When heating is required, low pressure steam passes through Pressure Reduction Valves (PRVs), and is distributed throughout the campus via an underground network of pipes. When additional steam capacity is required to meet campus heating demand, the plant can use its 100,000 lb/h gas fired boiler and its four older 70,000 lb/h boilers. When the HRSGs produce excess steam as a byproduct of electricity generation, it is sent to the dump condenser to be condensed and the resulting water sent to be conditioned and reused.

The cogen plant operates three York MaxE Steam-Turbine Drive Centrifugal Chillers for chilled water production. Each chiller's compressor is powered by a multi-stage Murray steam turbine. Heat rejection from the condensers is accomplished with a bank of nine mechanically driven cooling towers with VFD equipped fans on the roof of the facility. When the campus requires additional chilled water, the chiller plant from the original facility is used. The original facility contains four chillers. Two of them are Tecogen CH-1000 gas fired chillers and the other two are Carrier 19XR electric driven chillers. A bank of four mechanically driven cooling towers are used for heat rejection. When it is very cold outside, a free cooling heat exchanger is used to generate chilled water directly from the cooling tower water.

Heat that is normally rejected to the atmosphere at conventional power plants is captured at cogen plants and used to generate steam. Cogen plants are most efficient when the steam load at the location it serves matches the steam production generated as a byproduct of electricity generation. State rules prohibit the UConn Cogen Plant from selling power to the grid [3], therefore, the cogen plant attempts to produce exactly as

much electrical power as the campus demands. Consequently, steam produced as a byproduct of electricity generation rarely matches steam demand. The cogen steam supply may not fully meet campus demand, i.e., the steam/electricity balance is "steam deficient." In this case, less efficient, non-cogen sources of steam, such as boilers, must be used. The cogen plant may also produce too much steam as a byproduct of electricity generation, or have "excess steam." In this event some steam must be disposed of by the dump condenser. The cogen steam/electricity balance problem is expressed in the plant control logic.

The plant operates in three main control modes:

- Summer Mode: High ambient temperatures result in a low steam heating demand from campus, but chilled water demand is high. Cogen steam is used to drive the steam chillers to provide the campus with chilled water. Duct burners generate extra steam to meet peak chill water loads or natural gas and electric driven chillers are used.
- Shoulder Season Mode: Moderate ambient temperatures result in low steam heating demand and low chilled water demand. There is typically more than enough cogen steam to meet the demands. The excess steam is sent to the dump condenser.
- Winter Mode: Cold ambient temperatures result in high steam heating demand and minimal chilled water demand. Steam produced as a byproduct of electricity generation is not enough to meet campus demand, so duct burners and boilers are heavily used.

The UConn Cogen Plant's various systems are primarily controlled using Allen Bradley PLCs. The PLCs use Allen Bradley's RSLogix software. The PLCs are integrated into a SCADA/HMI powered by GE's Intellution software. The plant has hundreds of automated control loops functioning at all times to maintain critical process variables at their set points. The control logic requires frequent maintenance to keep up with the ever changing plant. The control algorithm of choice at the UConn Cogen is the standard PID controller due to its simplicity and effectiveness.

1.5 Review of Control Strategies

1.5.1 FOPDT Process Dynamic Modeling

Many self-regulating chemical processes can be adequately described by the First Order Plus Dead Time (FOPDT) dynamic model for control purposes [15]. The FOPDT model is linear and time invariant. The transfer function of a process, $G_P(s)$, which has been approximated by an FOPDT model, is described by a process gain, K_P, process time constant, τ_P, and process dead time, θ_P.

$$G_P(s) = \frac{K_P e^{-\theta_P s}}{\tau_P s + 1} \qquad \text{Equation 1.1}$$

The model parameters are used to calculate appropriate controller tuning values for plant processes. The three parameters of the FOPDT model can be derived using actual plant data from a "bump test" of the process [4]. A bump test involves perturbing the input to the process, the Controller Output (CO), in order to evoke a response in the Process Variable (PV), which is the output of the process and the variable to be controlled. The PV response should be strong enough to be distinguished from random fluctuations in process data. The step test is the most common form of bump test, where the CO is increased by a step function. A step test is performed on a simulated FOPDT process in Figure 1.2, showing the step response dynamics of the FOPDT model and the relevant process parameters.

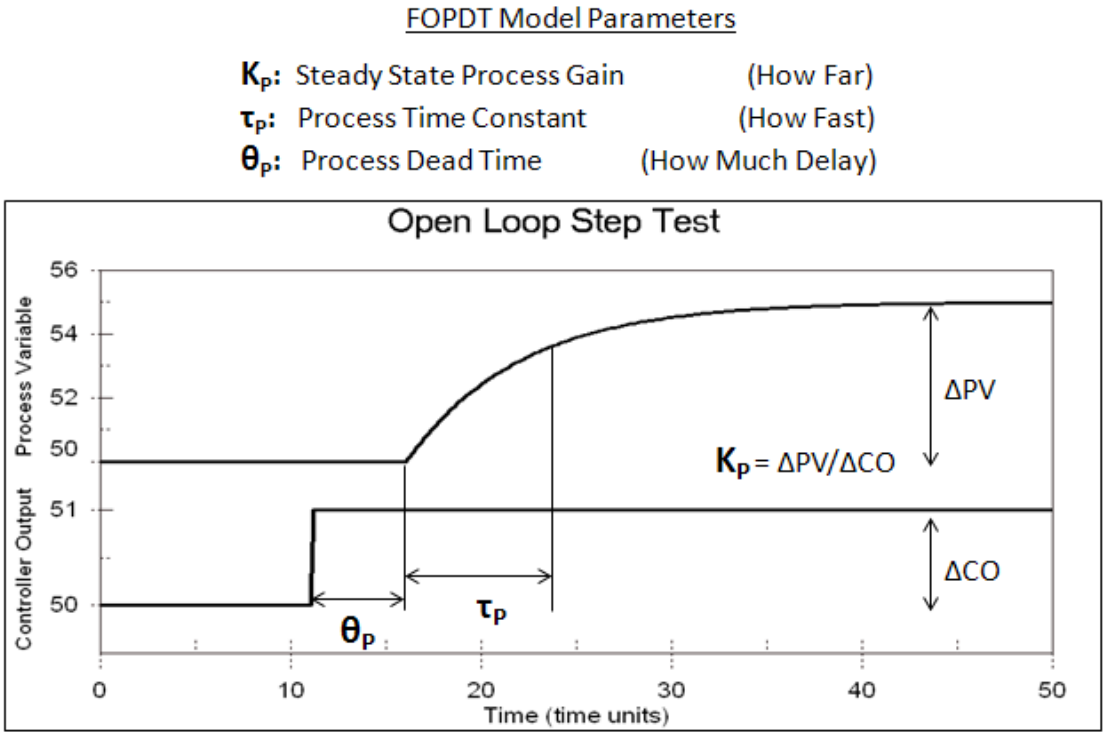

Figure 1.2: Simulated FOPDT Process Showing the Relevant Process Parameters

Many industrial processes are relatively time invariant, but not necessarily linear. Due to nonlinearities, it is important that the FOPDT model is based on data collected at the Design Level of Operation (DLO) [4]. The DLO represents the typical condition of the process, including the typical value of the PV and typical values of Disturbances (D) to the process. Any disturbances to the process should be held constant during the test to ensure the PV response is a direct result of the change in CO. Initially the CO is held constant, allowing the PV to reach steady state; then it is perturbed. A model fitting program can be used to generate a FOPDT best fit model to the bump test data. The model can be fit using an iterative procedure designed to minimize the sum of squared error over the time frame of the test [12]. An example of a process bump test with an FOPDT model fit is provided in Figure 1.3.

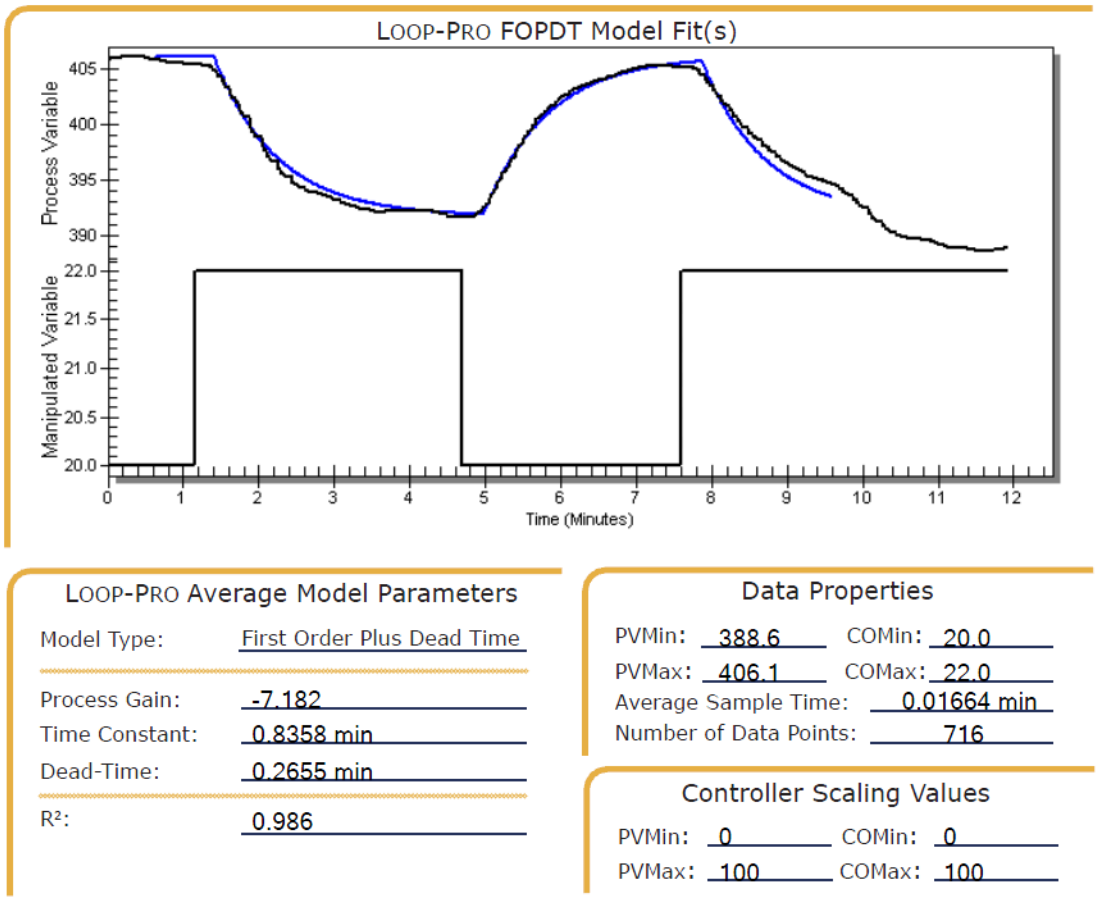

Figure 1.3: Example Process Bump Test Data with FOPDT Model Fit

1.5.2 The IMC Control Strategy

The Internal Model Control (IMC) tuning strategy was introduced by Rivera, et al. [18]. The IMC strategy is used to generate tuning values for controllers for the classic SISO control structure. Tuning values are generated based on a process model and the selection of a single parameter, the closed loop time constant, τ_C. As a result, controller tuning specifications and adjustments are drastically simplified. Decreasing τ_C results in a more aggressive, less damped, response. Increasing τ_C results in increased stability margins, but also a slower response. A heuristic can be used to select an initial τ_C appropriate for a given process. The heuristic used in this paper's case studies is discussed in Section 1.5.2.1.

1.5.2.1 Derivation of IMC Tuning Correlations for PI Controllers

This subsection, 1.5.2.1, has been written by Douglas J. Cooper. A version of this material has been published in [5] and is copyrighted by Control Station, Inc. Written permission for its use is provided in APPENDIX A.

Internal Model Control (IMC) can be used to derive PID controller tuning correlations. Figure 1.4 shows a simplified block diagram of the IMC structure. The unique aspect of IMC construction is the placement of a process model, $G_P^*(s)$, in parallel with the actual process it represents.

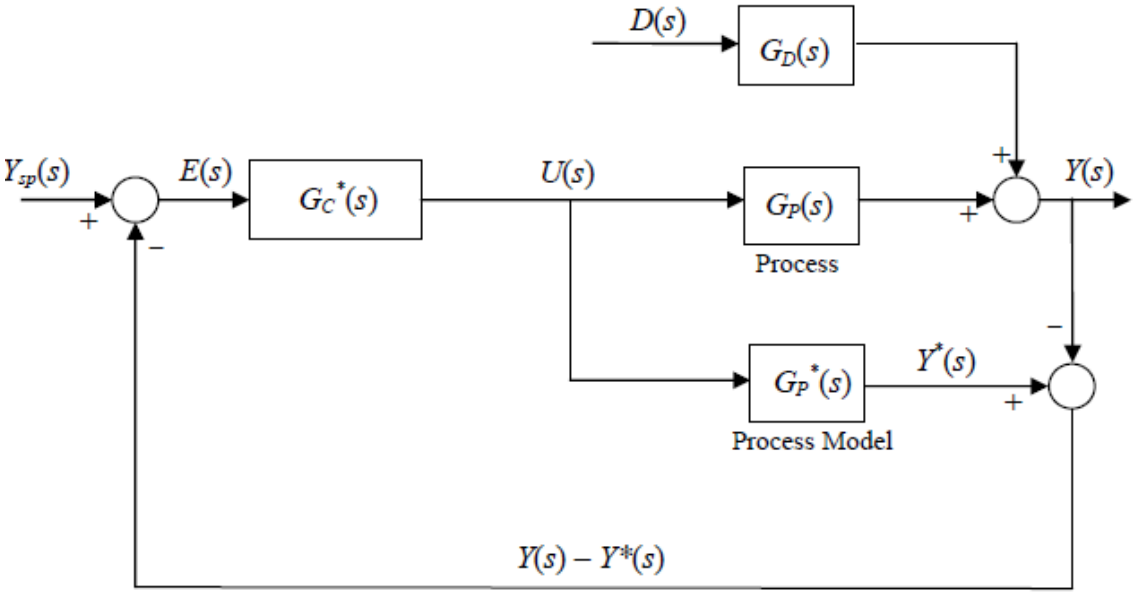

Figure 1.4: IMC Structure

As shown in the diagram, process model $G_P^*(s)$ receives the actual controller output signal, $U(s)$, and uses it to compute $Y^*(s)$, a prediction of the measured process variable, $Y(s)$. While in theory, the parallel process model must be derived and programmed as part of the controller, we show in the following sections that with certain assumptions, the structure of Figure 1.4 can be recast into a traditional feedback control architecture. Thus,

for the specific cases of interest here, this model is never actually created as a separate entity. The controller tuning correlations are based on the closed-loop transfer functions. To derive the closed-loop transfer functions, we perform balances on the IMC structure shown in Figure 1.4 by writing:

$$Y(s) = U(s)G_p(s) + D(s)G_D(s) \quad \text{Equation 1.2}$$

$$Y^*(s) = U(s)G_P^*(s) \quad \text{Equation 1.3}$$

$$U(s) = E(s)G_C^*(s) = \left[Y_{sp}(s) - Y(s) + Y^*(s)\right]G_C^*(s) \quad \text{Equation 1.4}$$

Substituting Equations 1.2 and 1.3 into Equation 1.4 yields:

$$U(s) = \left[Y_{sp}(s) - U(s)G_P(s) - D(s)G_D(s) + U(s)G_P^*(s)\right]G_C^*(s)$$

$$= Y_{sp}(s)G_C^*(s) - U(s)G_P(s)G_C^*(s) - D(s)G_D(s)G_C^*(s) + U(s)G_P^*(s)G_C^*(s)$$

We solve for *U(s)*:

$$U(s) = \frac{G_C^*(s)}{1+G_C^*(s)\left[G_P(s)-G_P^*(s)\right]}\ Y_{sp}(s) - \frac{G_D(s)G_C^*(s)}{1+G_C^*(s)\left[G_P(s)-G_P^*(s)\right]}\ D(s) \quad \text{Equation 1.5}$$

Substitute Equation 1.5 into Equation 1.2 to obtain:

$$Y(s) = \frac{G_C^*(s)G_P(s)}{1+G_C^*(s)\left[G_P(s)-G_P^*(s)\right]}\ Y_{sp}(s) - \frac{G_D(s)G_C^*(s)G_P(s)}{1+G_C^*(s)\left[G_P(s)-G_P^*(s)\right]}\ D(s) + D(s)G_D(s)$$

And rearrange into the closed loop transfer function:

$$Y(s) = \frac{G_C^*(s)G_P(s)}{1+G_C^*(s)\left[G_P(s)-G_P^*(s)\right]}\ Y_{sp}(s) - \frac{G_D(s)\left[1-G_C^*(s)G_P(s)\right]}{1+G_C^*(s)\left[G_P(s)-G_P^*(s)\right]}\ D(s) \quad \text{Equation 1.6}$$

Equation 1.6 yields a set-point tracking (servo response) transfer function assuming a constant disturbance, and disturbance rejection (regulator response) transfer function assuming a constant set point:

Set-Point Tracking: $$\frac{Y(s)}{Y_{sp}(s)} = \frac{G_C^*(s)G_P(s)}{1+G_C^*(s)\left[G_P(s)-G_P^*(s)\right]}$$ Equation 1.7

Disturbance Rejection: $$\frac{Y(s)}{D(s)} = \frac{G_D(s)\left[1-G_C^*(s)G_P(s)\right]}{1+G_C^*(s)\left[G_P(s)-G_P^*(s)\right]}$$ Equation 1.8

Three basic steps are used to derive IMC tuning correlations; the first two steps detail the creation of the IMC model. The last step relates the IMC model to a classical feedback controller transfer function to obtain controller tuning correlations.

Step 1: The poles of a transfer function (the roots of the characteristic equation in the denominator of the transfer function) indicate system stability. If the real part of any root is positive, the system is unstable. This concept plays a central role in the IMC analysis. The approach we take is to invert the process model to create the controller. One problem with such an approach is that any zeros (roots in the numerator of a transfer function) of the process model that lie in the right hand of the complex plane, when inverted, become unstable poles. If we permit this to occur, our controller will be unstable. To avoid creating an unstable controller, factor the process model, $G_P^*(s)$, into an invertible and noninvertible part. The classification is based on the numerator of the transfer function because this becomes the denominator when the model is inverted in Step 2.

The noninvertible part, $G_{P+}^*(s)$, contains all right-hand plane zeros (roots in the numerator of a transfer function that have positive real parts) and the dead time term. The invertible part, $G_{P-}^*(s)$, contains left hand plane zeros (roots in the numerator that have negative real parts) that produce stable behavior when in the denominator of a transfer function. Using this notation, the process model is factored as:

$$G_P^*(s) = G_{P+}^*(s)G_{P-}^*(s)$$ Equation 1.9

Step 2: Specify the controller transfer function as:

$$G_C^*(s) = \frac{1}{G_{P-}^*(s)} F(s) \qquad \text{Equation 1.10}$$

where *F(s)* is a low-pass filter with gain equal to 1. The term "low-pass" is used to indicate that high frequencies (rapid controller output changes) are lost. For deriving tuning correlations, the IMC filter has the form:

$$F(s) = \frac{1}{\tau_C s + 1} \qquad \text{Equation 1.11}$$

where τ_C is the closed loop time constant, and indicates the speed of the response of a process to set point changes. A popular heuristic for achieving a 10% to 15% overshoot to step changes in set point is:

τ_C is the larger of $0.1\tau_P$ or $0.8\theta_P$

A heuristic for a more conservative "no overshoot" response to set point changes is:

τ_C is the larger of $0.5\tau_P$ or $4\theta_P$

Step 3: Relate the IMC transfer function models to those from classical feedback control. We recall that the closed loop transfer function for a classical feedback control architecture is:

$$Y(s) = \frac{G_P(s)G_C(s)}{1+G_P(s)G_C(s)} Y_{sp}(s) + \frac{G_D(s)}{1+G_P(s)G_C(s)} D(s) \qquad \text{Equation 1.12}$$

We compare set point tracking forms:

IMC: $\frac{Y(s)}{Y_{sp}(s)} = \frac{G_P(s)G_C^*(s)}{1+G_C^*(s)\left[G_P(s)-G_P^*(s)\right]}$ Classical: $\frac{Y(s)}{Y_{sp}(s)} = \frac{G_P(s)G_C(s)}{1+G_P(s)G_C(s)}$

And equate the two:

$$G_P(s)G_C^*(s)[1 + G_P(s)G_C(s)] = G_P(s)G_C(s)\left[1 + \left(G_P(s) - G_P^*(s)\right)G_C^*(s)\right]$$

$$G_C^*(s) + G_C^*(s)G_P(s)G_C(s) = G_C(s) + G_C^*(s)G_P(s)G_C(s) + G_C^*(s)G_P^*(s)G_C(s)$$

Rearranging we obtain:

$$G_C(s) = \frac{G_C^*(s)}{1 - G_C^*(s)G_P^*(s)} \qquad \text{Equation 1.13}$$

We can use Equation 1.13 to obtain a classical feedback controller from one derived from the IMC structure. This enables us to determine the controller PI tuning parameters K_C and K_I. Assume a FOPDT process model:

$$G_P^*(s) = \frac{K_P e^{-\theta_p s}}{\tau_P s + 1}$$

Substitute the first order expansion for $e^{-\theta_p s}$:

$$e^{-\theta_p s} \approx 1 - \theta_p s$$

Resulting in Equation 1.14:

$$G_P^*(s) = \frac{K_P\left(1 - \theta_p s\right)}{\tau_P s + 1} \qquad \text{Equation 1.14}$$

Factor $G_P^*(s)$ into invertible and noninvertible parts:

$$G_P^*(s) = G_{P+}^*(s)G_{P-}^*(s)$$

so following the discussion above:

$$G_{P+}^*(s) = \left(1 - \theta_p s\right) \qquad \text{Equation 1.15}$$

$$G_{P-}^*(s) = \frac{K_P}{\tau_P s + 1} \qquad \text{Equation 1.16}$$

We can now express the IMC controller model, $G_C^*(s)$, in terms of the invertible process model term and a first-order filter term, $F(s)$:

$$G_C^*(s) = \frac{1}{G_{P-}^*(s)}\, F(s)$$ Equation 1.17

where the IMC filter has the form:

$$F(s) = \frac{1}{\tau_C s+1}$$ Equation 1.18

Substituting Equations 1.15, 1.16 and 1.18 into Equation 1.17 yields the controller:

$$G_C^*(s) = \left(\frac{\tau_P s+1}{K_P}\right)\left(\frac{1}{\tau_C s+1}\right) = \frac{\tau_P s+1}{K_P(\tau_C s+1)}$$ Equation 1.19

We can relate this IMC controller model, $G_C^*(s)$, to a classical feedback controller model via Equation 1.13:

$$G_C(s) = \frac{G_C^*(s)}{1-G_C^*(s)G_P^*(s)}$$ Equation 1.13

We substitute Equations 1.14 and 1.19 into Equation 1.13 and simplify:

$$G_C(s) = \frac{\tau_P}{K_P(\tau_C+\theta_P)}\left[1+\frac{1}{\tau_P s}\right]$$ Equation 1.20

Compare Equation 1.20 to the classical feedback model for a PI controller,

$$G_C(s)_{PI} = K_C + \frac{K_I}{s}$$

We obtain the following controller tuning parameters:

IMC PI Tuning Correlations: $K_C = \frac{\tau_P}{K_P(\tau_C+\theta_P)}$ and $K_I = \frac{K_C}{\tau_P}$

1.5.3 Static Feed Forward

The standard feedback control structure's disturbance rejection performance is limited because it neutralizes disturbances by reacting to errors. The error must already be present before action is taken to correct it. The addition of a feed forward controller can improve disturbance rejection performance by taking preemptive action to neutralize the effects of a disturbance on the process variable [19]. Figure 1.5 shows the traditional feedback control structure with the addition of a feed forward controller.

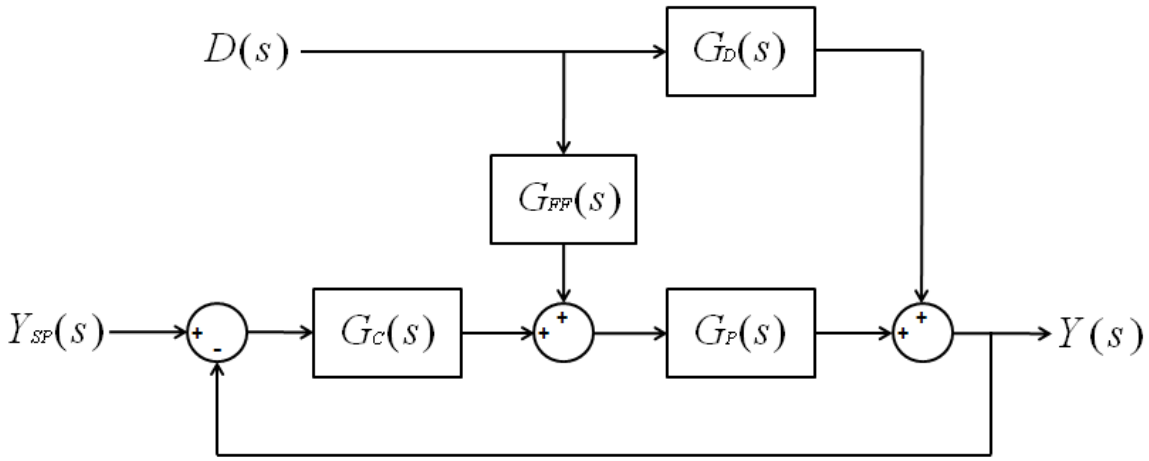

Figure 1.5: Traditional Feedback Control Structure with Feed Forward

The closed loop transfer function of the control structure of Figure 1.5 is as follows:

$$Y(s) = \frac{G_P(s)G_C(s)}{1+G_P(s)G_C(s)}\,Y_{sp}(s) + \frac{G_D(s)+G_{FF}(s)G_P(s)}{1+G_P(s)G_C(s)}\,D(s) \qquad \text{Equation 1.21}$$

Ideally the transfer function of the feed forward controller, $G_{FF}(s)$, would be set to

$$G_{FF}(s) = -\frac{G_D(s)}{G_P(s)}$$

This reduces the disturbance coefficient, the second term of Equation 1.21, to zero. The resultant in the closed loop transfer function is

$$Y(s) = \frac{G_P(s)G_C(s)}{1+G_P(s)G_C(s)}\, Y_{sp}(s)$$

which is simply the set point tracking servo response. It may not be practical to accurately model the disturbance process, and program the dynamic feed forward transfer function into the PLC. In many cases, a static feed forward may dramatically improve disturbance rejection performance. The logic for a static feed forward is simpler to implement, understand and maintain. A static feed forward neglects the relative dynamics of the disturbance and process, only considering the relative gains. For a static feed forward, the feed forward transfer function is set to

$$G_{FF}(s) = -\frac{K_D}{K_P}$$

where K_D and K_P are the static gains of the disturbance and process, respectively. The static feed forward generally proves useful if the dynamics of $G_D(s)$ are similar in speed to the dynamics of $G_P(s)$ [14]. In many cases, the ratio of the static gains may not be constant at all levels of the disturbance. For these cases a nonlinear, static function for $G_{FF}(s)$ can be useful.

1.5.4 Cascade Control Structure

A cascade controller can be useful when an intermediate process is used to control a process variable of interest as depicted in Figure 1.6.

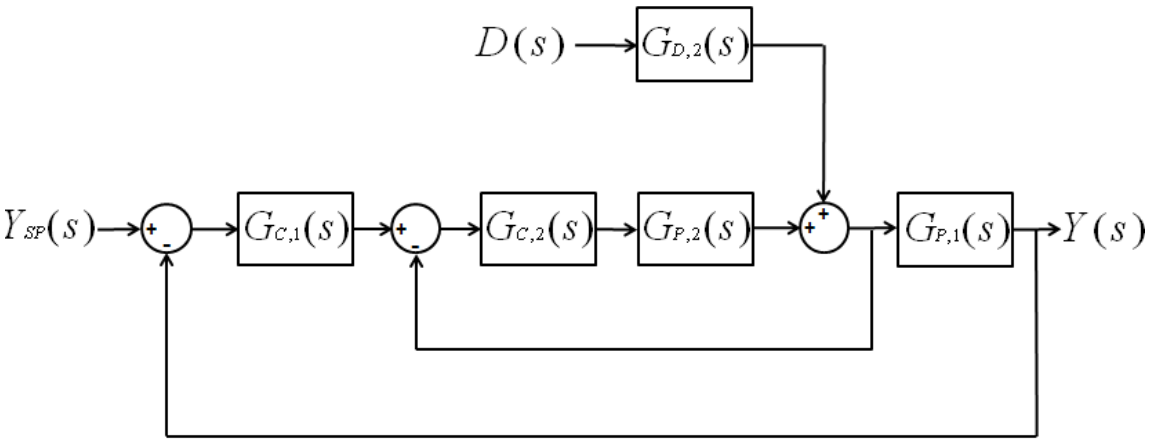

Figure 1.6: Traditional Cascade Structure

The inner loop is used to track a set point generated by the controller of the outer loop, $G_{C,1}(s)$. The inner loop's process variable is the input to the outer loop's process, $G_{P,1}(s)$. The inner process, $G_{P,2}(s)$, could be controlled in open loop mode, with the outer loop feedback handling deviations in the process variable, $\mathrm{Y}(s)$, however, disturbances to the inner process would be allowed to propagate to the outer process. The cascade structure is used to reject disturbances to the inner process limiting the effect on the outer loop [9]. Inner loop feedback may also make the process behave linearly. If $G_{P,2}(s)$ is very nonlinear, the cascade can make control simpler than the single loop alternative.

Cascade control should only be used if the dynamics of the inner process, time constant and dead time, are approximately three or more times faster than the dynamics of the

outer process [14]. Flow and pressure control loops are often the inner loops of cascade structures and are typically quite fast.

Cascade controllers can be tuned using a similar process to single loop controllers. First, the inner process should be approximated with a FOPDT model from bump test data as described in Section 1.5.1. The FOPDT model can be used to derive PI controller tuning values using the IMC correlations derived in Section 1.5.2.1. For cascades with inner processes that are slow compared to the outer processes, a P-only controller is generally more appropriate, because faster closed loop settling times can be achieved. With the inner loop tuned and in automatic mode, the outer loop controller can be tuned. The outer loop controller is tuned using a process model which includes the automatic inner loop as well as the outer process. The outer loop controller output is perturbed to collect bump test data for FOPDT approximation. The IMC correlations can then be used to generate PI tuning values for the outer controller.

CHAPTER 2: SCR NO_X CONTROL OF COMBUSTION TURBINE EXHAUST

2.1 Abstract

This section discusses a model based strategy for controlling the NO_X concentration of natural gas turbine emissions. The strategy addresses a typical cogeneration configuration where NO_X is removed from turbine exhaust via Selective Catalytic Reduction (SCR). A case study of its application to a 7.5 MW Solar Taurus^{TM} 70 turbine with lean, premixed combustion is presented. The unit is equipped with a Rentech HRSG, iron zeolite SCR catalysts and cool, dry Continuous Emissions Monitoring Systems (CEMS). A control logic structure is proposed, as well as a method of plant-specific deployment. The structure is simple, intuitive and highly effective.

The experimental data presented in this work shows that NO_X concentration can be reasonably controlled with a NO_X → ammonia flow rate → ammonia valve position cascade architecture. However, the cascade feedback cannot adequately address disturbances to NO_X concentration caused by rapid adjustments in turbine load. A feed forward controller based on turbine load is shown to provide excellent dynamic support to the feedback controller in mitigating the disturbance. A regression of ammonia flow vs. turbine load data is used to establish a static, nonlinear relationship for the feed forward controller. Data presented in this paper demonstrates that the proposed control strategy provides improved performance over the previous NO_X control logic at the UConn Plant while retaining simplicity.

2.2 Introduction

2.2.1 Overview of the Combustion and NO_X Reduction Processes

The University of Connecticut's cogen plant operates three 7.5 MW Solar Taurus^{TM} 70 natural gas turbines. The turbines drive generators which are used to produce electricity to power the UConn campus. The turbine and generator units are collectively referred to as Combustion Turbine Generators (CTGs). Each unit is connected to a Rentech Heat Recovery Steam Generator (HRSG) which captures waste heat from combustion turbine exhaust to produce steam for the campus's heating and cooling needs. The HRSGs also contain natural gas duct burners which are fired when additional steam is required. Downstream of the heat exchangers, the HRSGs contain integrated iron zeolite NO_X catalysts and ammonia injection systems. After being dosed with ammonia vapor, the exhaust passes through a catalyst grid where NO_X is removed via Selective Catalytic Reduction (SCR). The exhaust gas continues up through the stack where it is sampled by a Continuous Emissions Monitoring System (CEMS) before being released into the atmosphere. A diagram of UConn's combustion and NO_X reduction processes is provided in Figure 2.1.

UConn's natural gas turbines produce low levels of NO_X by using lean, premixed combustion. Thoroughly premixing the air and natural gas before it enters the combustion chamber reduces hot areas in the combustion process [2]. The lower temperature results far less NO_X production than higher temperatures. The lean fuel/air ratio also reduces the overall combustion temperature; however, this also reduces the power cycle efficiency. The turbines are operated lean in order to maintain the turbine

exit temperature below 900°F, thus preventing damage to the turbine blades. The low level NO_X production combined with the SCR NO_X treatment of the exhaust allows UConn to control NO_X emissions at a low level of 1.8 Parts Per Million (PPM).

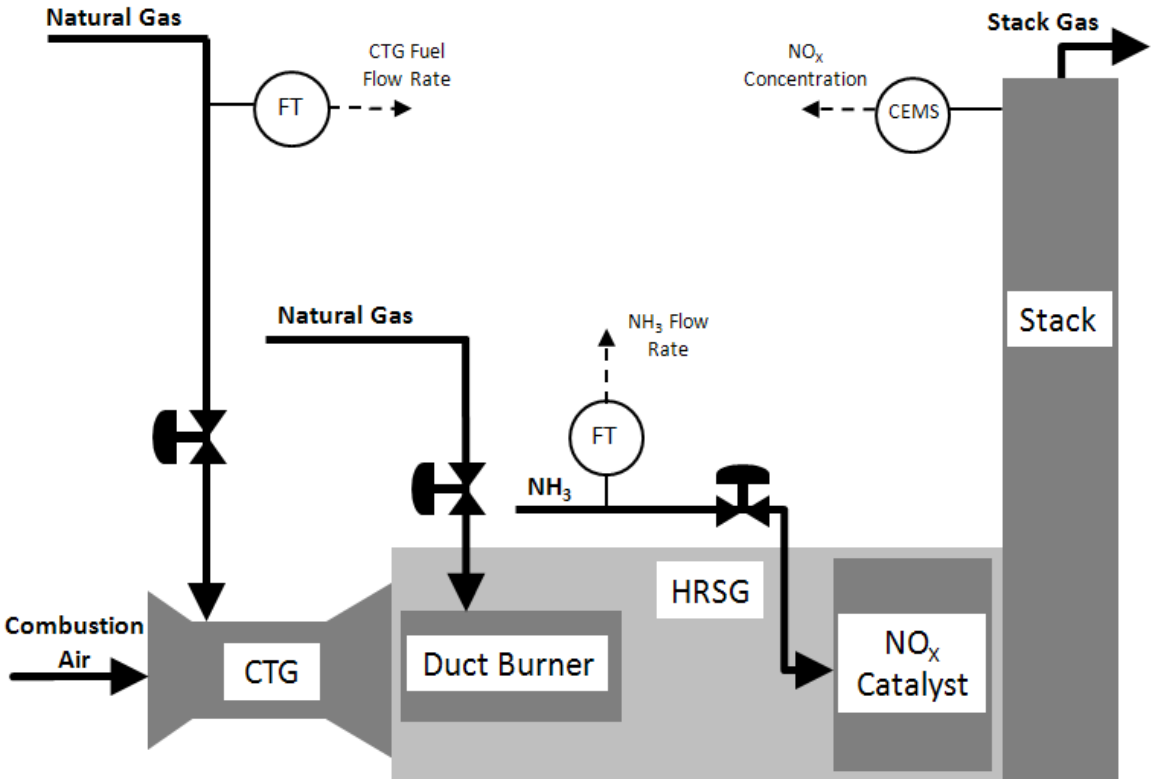

Figure 2.1: Diagram of UConn's Combustion and NO_X Reduction Processes

2.2.2 Selective Catalytic Reduction of NO_X

SCR is accomplished by reacting ammonia with the NO_X contained in exhaust gases in the presence of a catalyst. SCR of NO_X is achieved based on the following reactions [8]:

$$4NH_3+4NO+O_2 \rightarrow 4N_2+6H_2O \quad (1)$$

$$2NH_3+NO+NO_2 \rightarrow 2N_2+3H_2O \quad (2)$$

$$8NH_3+6NO_2 \rightarrow 7N_2+12H_2O \quad (3)$$

Excess oxygen is available in lean burning natural gas turbine exhaust and >90% of NO_X in the untreated exhaust generally consists of NO [8]. Reaction (1) dominates the overall NO_X reduction in these conditions. The objective of NO_X control is to adjust the rate of this reaction in order to maintain a specific concentration of NO_X exiting the stack. This balances two objectives: to emit a low level of NO_X while also keeping ammonia usage and emissions low.

2.2.3 Variables Affecting NO_X Production and Reduction

Variables affecting NO_X production and reduction rates include: CTG load, fuel flow rate, air/fuel ratio, fuel mixing and combustion, inlet air temperature, pressure and humidity [16], duct burner firing rate, catalyst temperature, catalyst condition, and ammonia surface concentration and distribution over the catalyst [11]. From a control perspective, only some of these variables must be considered.

The surface ammonia concentration of the catalyst is the most important variable affecting NO_X. It provides a means to control NO_X emissions to the atmosphere. Increasing the level of ammonia on the catalyst increases the rate of the NO_X reduction reaction and reduces the concentration of NO_X emitted to the atmosphere. Ammonia surface concentration is not measured in UConn's plant so ammonia flow rate to the catalyst must be considered in its place.

A number of CTG operating variables impact NO_X, but the CTG internal controls are such that the variables are correlated. At any given loading, the CTG operating variables are controlled to prescribed operating levels. The effect of the CTG operating variables on NO_X production can be described simply as a function of CTG load. CTG fuel flow

rate is used to indicate CTG load throughout this study. The CTG load at UConn's cogeneration plant constantly fluctuates to satisfy the instantaneous power requirements of the campus. A CTG is typically brought online and offline everyday causing large load swings in the other two CTGs twice daily. These rapid changes in the CTG load induce a strong and rapid NO_X response that is damaging to NO_X control performance.

Other variables affecting NO_X production and reduction include ambient air conditions, catalyst temperature and condition, and duct burner firing rate. These variables do not require special consideration because they only induce a weak NO_X response or they change very slowly during normal plant operation. The impact on NO_X emissions due to changes in these variables can be adequately addressed by feedback control.

2.2.4 NO_X System Processes

Sensors are available at UConn's cogen plant that can be used to examine the input and output relationships of the NO_X processes. The sensors, shown in Figure 2.1, include: a combustion turbine fuel flow rate sensor, an ammonia flow rate sensor, and a CEMS unit that provides NO_X concentration data for the exhaust gas after it has been treated by SCR.

$\underline{NH_3 \rightarrow NO_X \text{ Process}}$

NO_X emissions can be adjusted by changing the ammonia flow rate to the catalyst. Increasing the ammonia flow rate increases the rate of the NO_X reduction reaction. Figure 2.2 shows dynamic response data showing the effect of ammonia flow rate on NO_X concentration for UConn's unit #2.

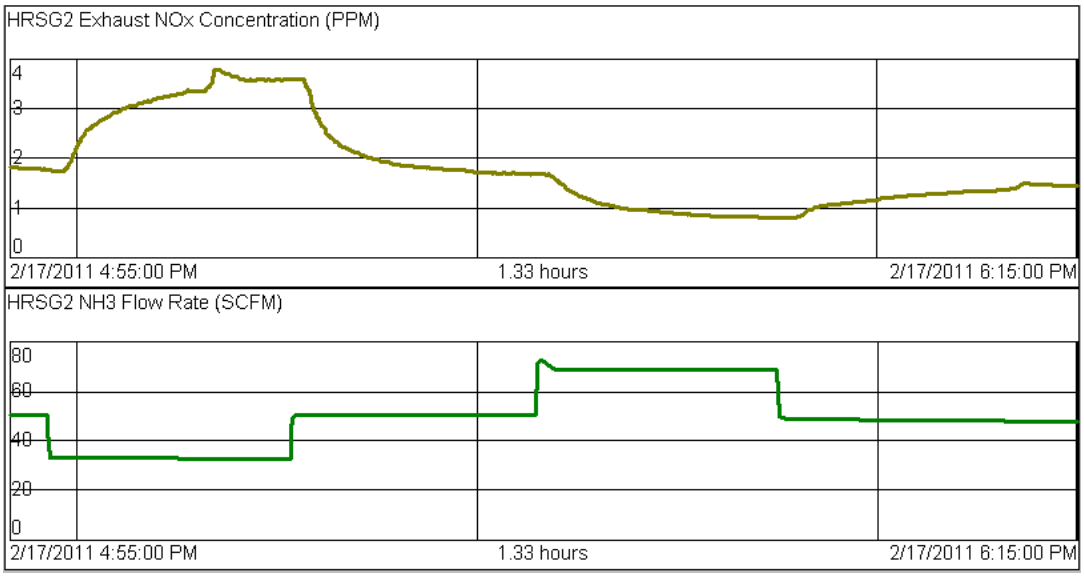

Figure 2.2: Unit #2 NO_X Concentration Response to Steps in Ammonia Flow Rate

The exit NO_X concentration data of Figure 2.2 is taken at time when the major disturbance, the CTG fuel flow, is held constant. On all three of UConn's units, step tests similar to the ones of Figure 2.2 consistently show that the exit NO_X concentration

reaches a steady state given a constant ammonia flow rate. This indicates that the process is self-regulating. Furthermore, it is observed that the ammonia flow rate's impact on the NO_X concentration process is reverse-acting and nonlinear.

Valve → NH_3 Process

The next component of the NO_X system that needs to be examined is the ammonia flow rate process. The ammonia flow control valve, shown in Figure 2.1, can be adjusted to manipulate ammonia flow rate. Dynamic response data showing the effect of ammonia flow control valve position on ammonia flow rate for UConn's unit #2 is presented in Figure 2.3.

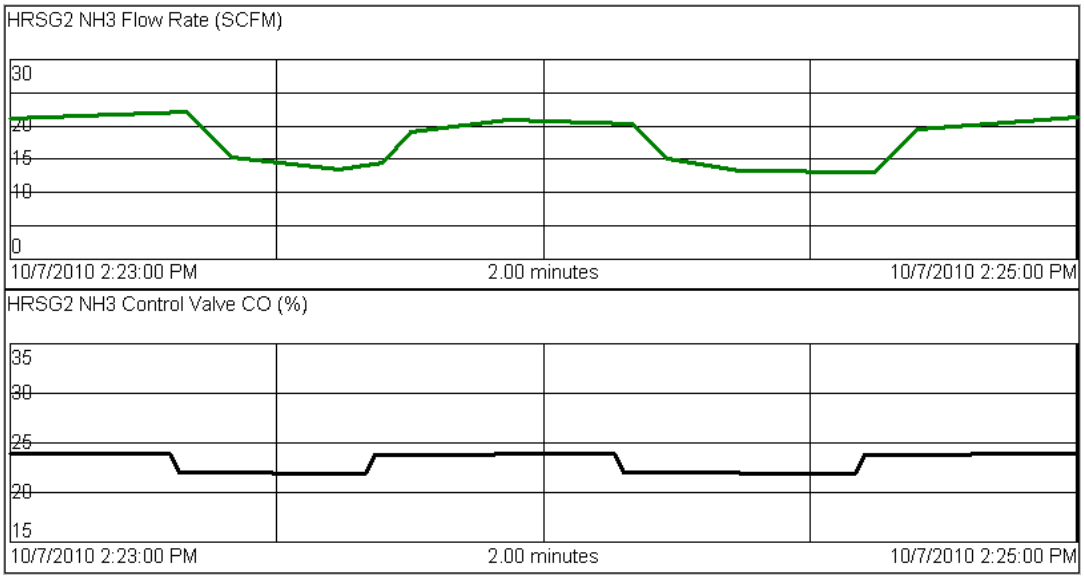

Figure 2.3: Unit #2 NH3 Flow Rate Response to Steps in NH3 Flow Valve Position

The ammonia flow rate data of Figure 2.3 is taken at time when the upstream ammonia pressure, the main disturbance to the ammonia flow rate process, is constant. The ammonia flow rate process is also self-regulating on all three of UConn's units. It is observed that the impact of the ammonia flow control valve position on the ammonia flow rate process is direct-acting and nonlinear.

CTG → NO_X Disturbance

CTG load changes have a strong impact on NO_X production. CTG load is the primary disturbance to the NO_X concentration process. Throughout this paper CTG fuel flow rate is used as an indicator of CTG load. Dynamic response data showing the effect of CTG fuel flow on NO_X concentration for UConn's unit #2 is presented in Figure 2.4.

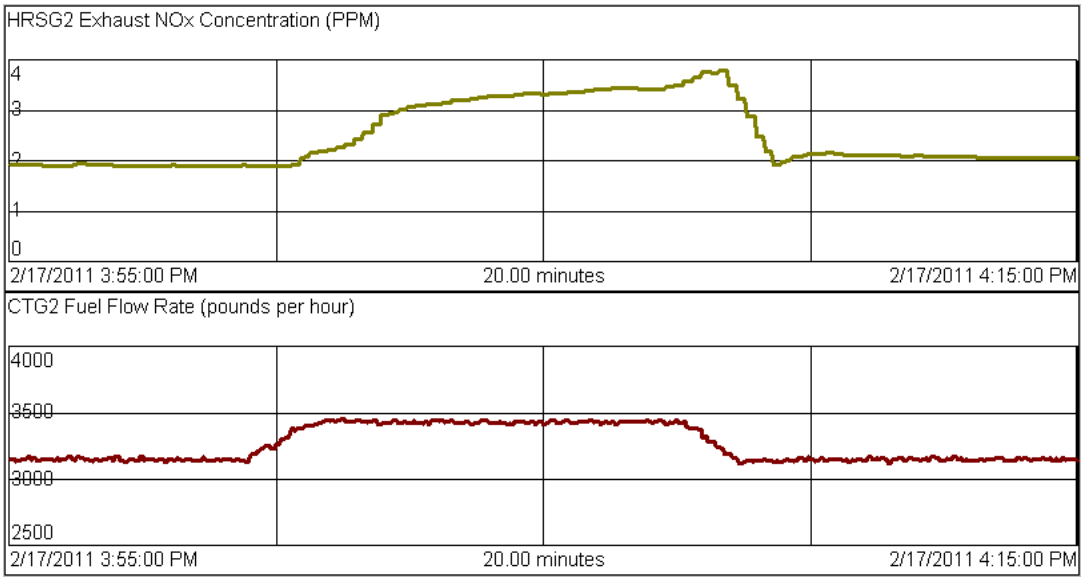

Figure 2.4: Unit #2 NO_X Concentration Response to Steps in CTG Fuel Flow Rate

The exit NO_X concentration data of Figure 2.4 is taken at time when the ammonia flow rate is held constant. On all three of UConn's units, step tests similar to the ones of Figure 2.4 consistently show that the exit NO_X concentration reaches a steady state given a constant CTG fuel flow rate. This indicates that the process is self-regulating. Furthermore, it is observed that the impact of CTG fuel flow rate on the NO_X concentration process is direct-acting and nonlinear.

2.3 Methodology

2.3.1 Proposed Control Structure

UConn's environmental objectives require that the NO_X concentration of exhaust gas emitted to the atmosphere be controlled to 1.8 PPM. To satisfy the control objective with the NO_X reduction system in place at UConn, the correct amount of ammonia must be injected onto the catalyst at the right time. The problem can be broken into two parts: determining the proper ammonia flow rate to the catalyst, and maintaining that flow rate.

The NO_X control methodology of this paper employs an exit NO_X concentration → ammonia flow rate → ammonia valve position cascade architecture. A diagram of the NO_X processes and the proposed control structure is presented in Figure 2.5.

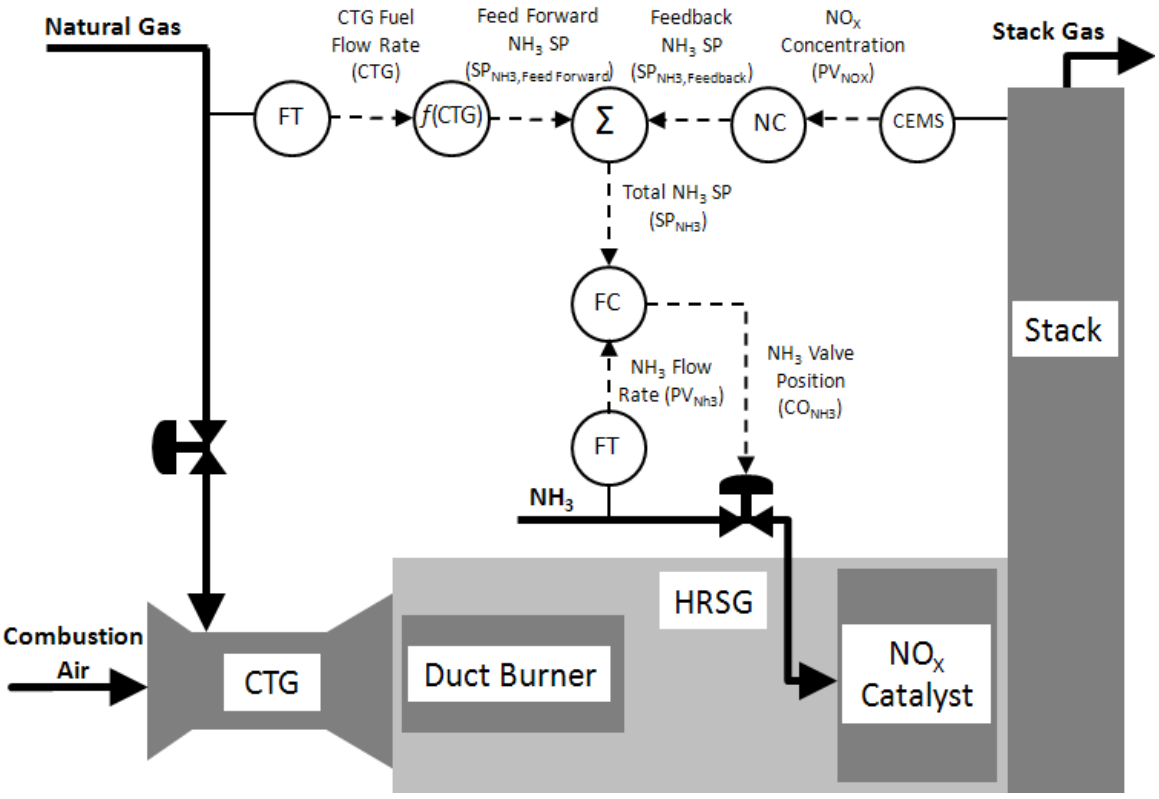

Figure 2.5: Diagram of Exit NO_X Concentration Control Scheme

This structure uses a NO_X feedback controller (NC) to correct deviations in the NO_X concentration process variable (PV) by adjusting an ammonia flow rate set point (SP). The cascade uses another feedback loop to ensure the ammonia flow rate set point is tracked by adjusting the ammonia control valve. PI control algorithms are used in both controllers to reject disturbances without offset. A static feed forward controller provides an estimate of the required ammonia flow rate set point based on the CTG fuel flow (f(CTG)). The NO_X feedback controller refines the estimate to achieve the desired NO_X concentration.

Several parameters are required for the control structure to function. These parameters are specific to the system and should be derived from plant data. Fine tuning can be done according to performance observations and the parameters should be adjusted as the plant evolves. The following parameters are required for the NO_X control algorithm:

1) Proportional and integral tuning values for the ammonia flow controller, $K_{C,NH3}$ and $K_{I,NH3}$
2) Proportional and integral tuning values for the NO_X feedback controller, $K_{C,NOX}$ and $K_{I,NOX}$
3) Predicted ammonia flow rate as a function of CTG fuel flow for the NO_X feed forward controller, f(CTG)

A control block diagram of the NO_X control algorithm with the required parameters is provided in Figure 2.6.

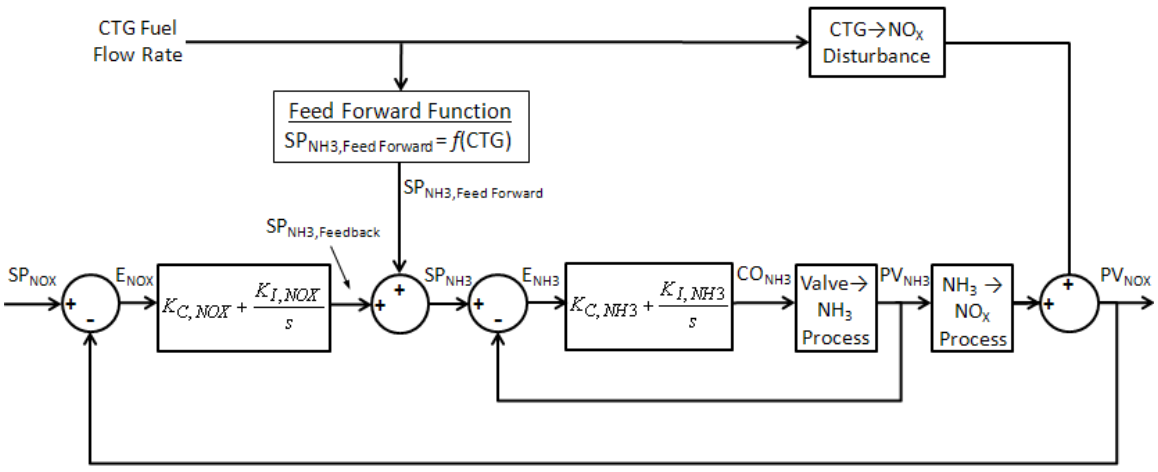

Figure 2.6: Proposed NO_X Concentration Control Block Diagram

2.3.2 Conversion from the Previous Control Structure

The UConn Cogen NO_X control structure that existed at the beginning of this study was overly complex. The structure was based on theoretical NO_X production and reduction models; the parameters could not be derived from available plant data. It was not practical to improve the NO_X control performance by tuning the existing structure. The logic from the original structure is presented in Figure 2.7.

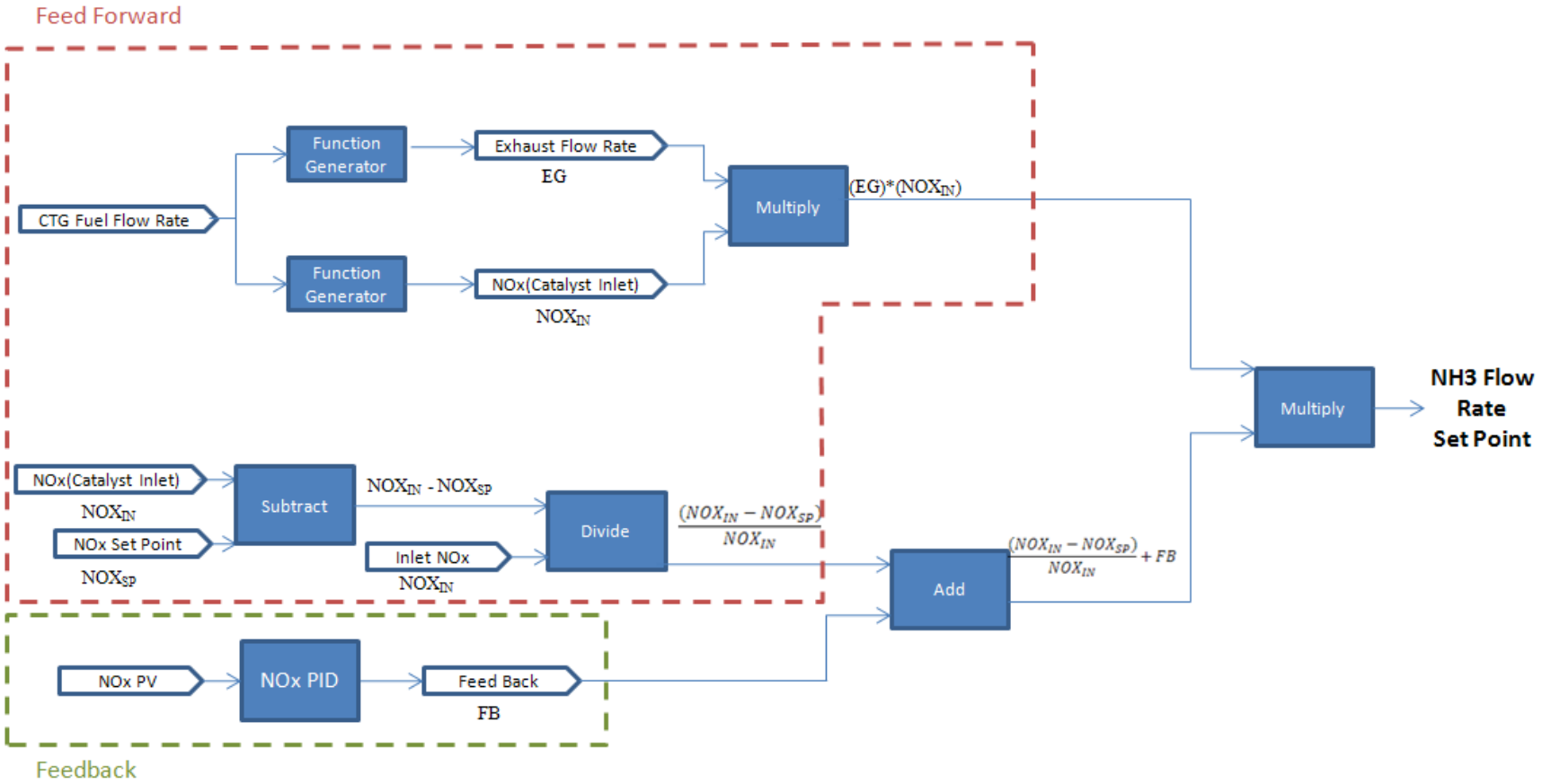

Figure 2.7: Logic from the Original NO_X Control Structure at the UConn Cogeneration Plant

The logic of Figure 2.7 is used to generate an NH_3 flow rate set point, which is tracked by another controller in a cascade format. The new logic proposed by this paper also uses a cascade, but generates the NH_3 flow rate set point differently. Upon inspection of the logic of Figure 2.7, it is clear that there are only two independent variables: Gas Flow Rate and NO_X PV. This is also similar to the new logic proposed by this paper, therefore, the logic of Figure 2.7 can be converted to a mathematically equivalent logic, structured in the manner proposed by this paper.

The tuning parameters required by the new structure, listed in Figure 2.6, are derived from the old structure to create a mathematically equivalent control logic. Adaptive tuning for $K_{C,NOX}$ and $K_{I,NOX}$ and a nonlinear function *f*(CTG) are derived from the old structure to generate an equivalent control response. This is done as a precaution, to verify that the new structure provides the same NO_X control performance as the old structure before it is improved upon. One week of NO_X control performance data is provided in the plot of Figure 2.8. Halfway through the plot of Figure 2.8, the new, mathematically equivalent control structure is brought online.

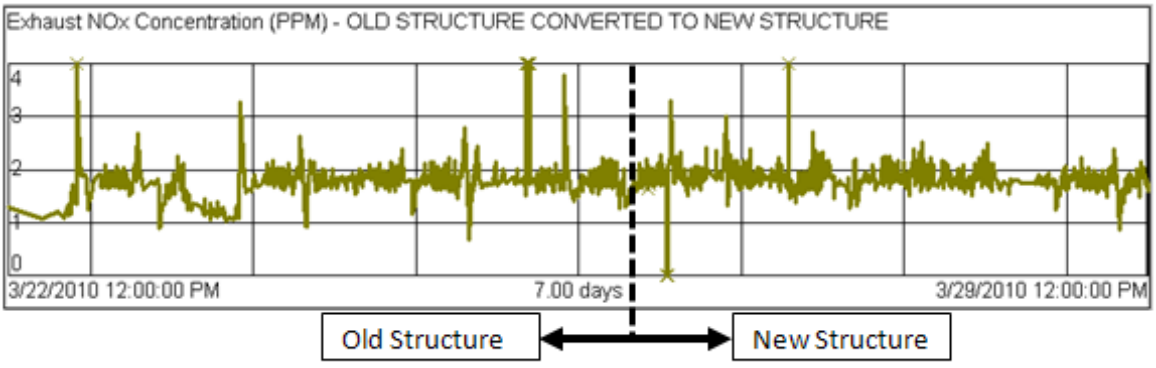

Figure 2.8: One Week of NO_X Control Data Showing the Conversion of the Old Control Structure to the New, Mathematically Equivalent Structure

Figure 2.8 confirms that the new structure provides similar control performance as the old structure, as expected. With the new structure in place, improvements to the NO_X control system can be made.

2.3.3 FOPDT Modeling and PI Tuning Using the IMC Method

The controllers for the self-regulating $NH_3 \rightarrow NO_X$ and Valve$\rightarrow NH_3$ processes are tuned according to the strategy of Section 1.5.

$NH_3 \rightarrow NO_X$ Process Modeling and PI Tuning

The desired set point for the NO_X concentration process is 1.8PPM. The CTG varies a great deal in operating level, but again a midrange value is selected. Together, these conditions represent an average DLO and are used for tuning purposes. The NO_X concentration is allowed to reach steady state at the DLO and is bumped by changing the flow rate of ammonia. The flow rate of ammonia is the input to this process and is treated as the CO. Figure 2.9 shows the process being bumped around the DLO in order to produce a dynamic response for modeling and tuning.

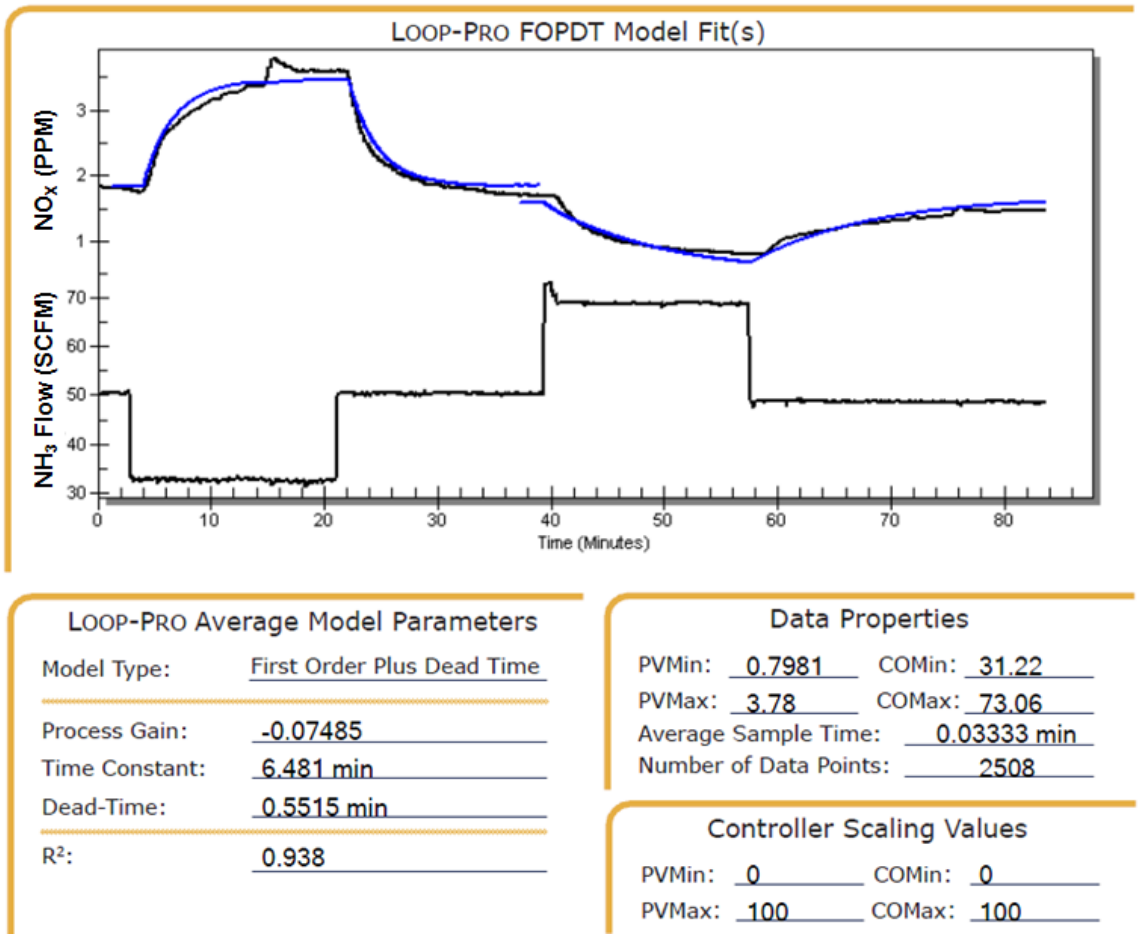

Figure 2.9: NO_X Concentration Dynamic Response to Change in Ammonia Flow and FOPDT Approximation

Control Station's LOOP-PRO software is used again to approximate an FOPDT model. The process is nonlinear, so an average of two fits is used from tests above and below the DLO. IMC tuning correlations are applied using the parameters of the approximated model. LOOP-PRO is used to adjust the aggression of tuning values so the resulting closed loop response approximates a critically damped response. The resultant tuning values are as follows:

$K_{C,NOX} = -12\ SCFM/PPM$ $K_{I,NOX} = -1.9\ SCFM/PPM \cdot min$

Valve→NH_3 Process Modeling and PI Tuning

For the ammonia flow rate process, the DLO includes a wide range of flow rates. Depending upon the CTG load, the expected ammonia flow rate could be anywhere from 5 Standard Cubic Feet per Minute (SCFM) to 90 SCFM. A mid-range value, approximately 40 SCFM, is selected to be the DLO for tuning purposes. Barring a major nonlinearity in the ammonia flow rate process, tuning values derived at this DLO should provide adequate control throughout the expected range. The ammonia flow rate is allowed to settle and then is bumped by changing the controller output to the valve. Figure 2.10 shows the process being bumped in this range.

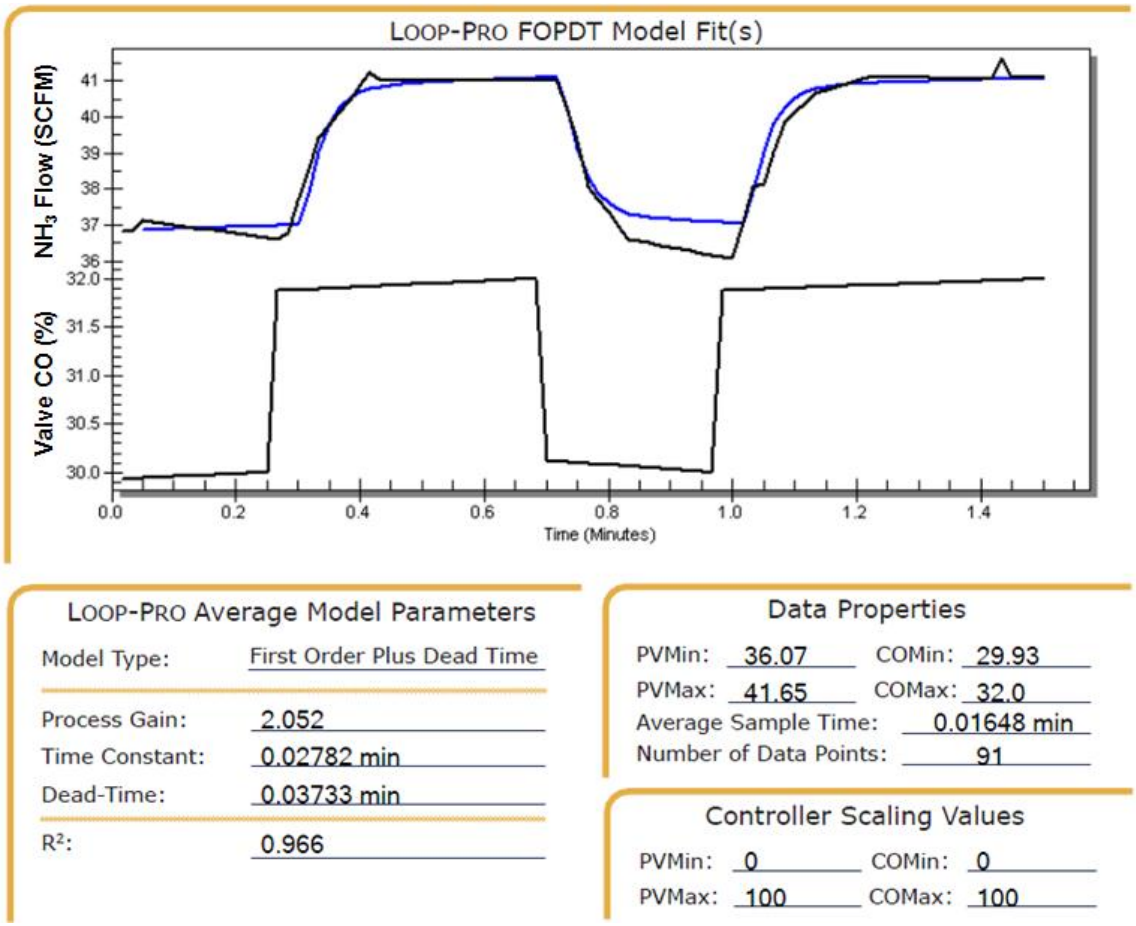

Figure 2.10: Ammonia Flow Dynamic Response to Change in Valve CO and FOPDT Approximation

Figure 2.10 also shows a FOPDT approximation to the process data, generated by Control Station's LOOP-PRO software. IMC tuning correlations are applied using the parameters of the approximated model. LOOP-PRO is used to adjust the aggression of tuning values so that the resulting closed loop response approximates a critically damped response. The resulting tuning values are as follows:

$K_{C,NH3} = 0.11$ %/SCFM $\qquad\qquad$ $K_{I,NH3} = 3.8$ %/SCFM·min

2.3.4 Derivation of the Static Feed Forward Function

The third parameter required for the control structure is the function $SP_{NH3,Feed\ Forward} = f(CTG)$. The ammonia flow rates, $SP_{NH3,Feed\ Forward}$, are the typical values that result in an exit NO_X concentration of 1.8 PPM at given steady state CTG fuel flow rates. The CTG load is the dominant variable determining the magnitude of the ammonia flow rate required to reduce exit NO_X concentration to 1.8 PPM. However, as previously stated, a number of other factors affect NO_X production and reduction; the actual ammonia flow rate required at a given fuel flow varies.

To estimate the function, the units are placed in automatic control. The cascade controller, tuned in the previous steps, uses feedback to reasonably control the exit NO_X concentration. The units are allowed to run in this mode for a long period of time to capture data that will provide the basis for the feed forward function. This data should represent a full range of normal operating conditions of the system. The data must be filtered so that only instances when NO_X concentration is near the set point are considered. For this project, instances when the NO_X concentration is between 1.7 PPM and 1.9 PPM are considered; the rest of the data is filtered out. We can correlate the flow

rate of ammonia to the CTG fuel flow rate during these times. Figure 2.11 shows a plot of ammonia flow rates vs. CTG fuel flow rates for this data.

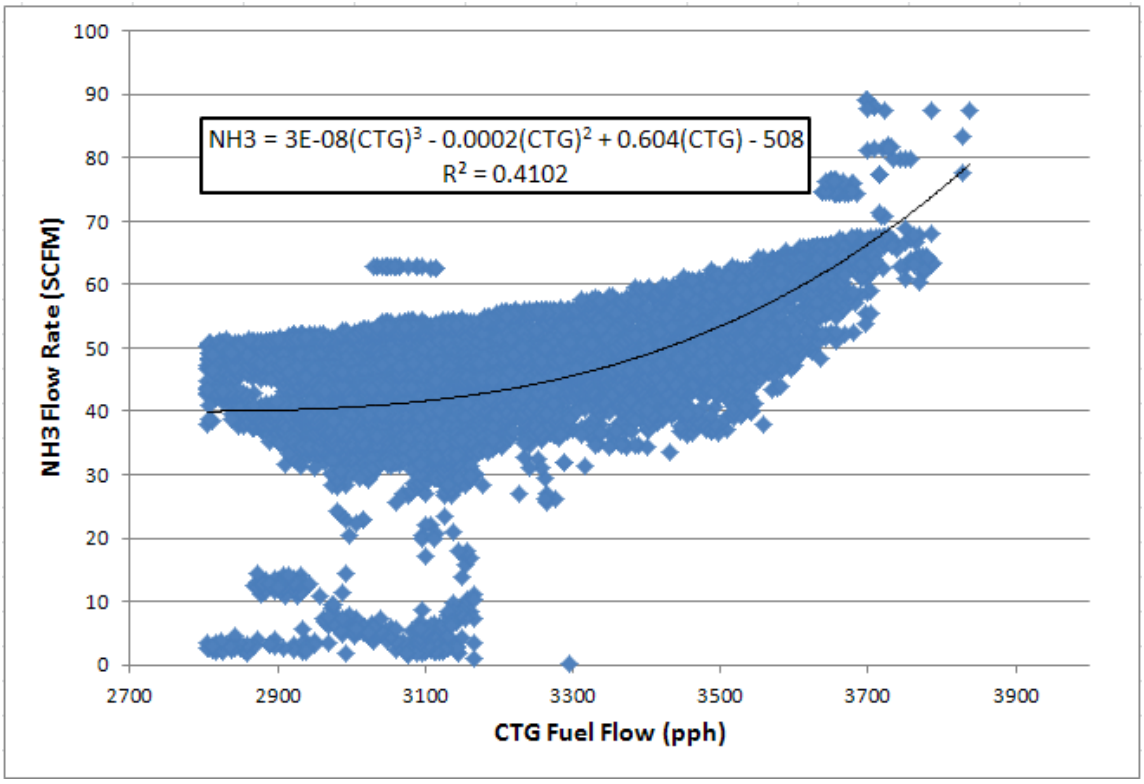

Figure 2.11: Ammonia Flow Rates vs. CTG Fuel Flow and Polynomial Regression for UConn's Unit #2

The control structure's feed forward function, $SP_{NH3,Feed\ Forward} = f(CTG)$, is the regression equation of Figure 2.11. The slope of the ammonia flow rate vs. CTG fuel flow is much greater at the high end of the CTG operating range, so a nonlinear regression function is necessary.

2.4 Results

The tuned ammonia flow rate control loop is put in automatic to test its set point tracking performance. A plot of closed loop, set point step responses is provided in Figure 2.12. The plot shows the ammonia flow rate set point is tracked with no overshoot and a settling time of approximately 1.5 minutes.

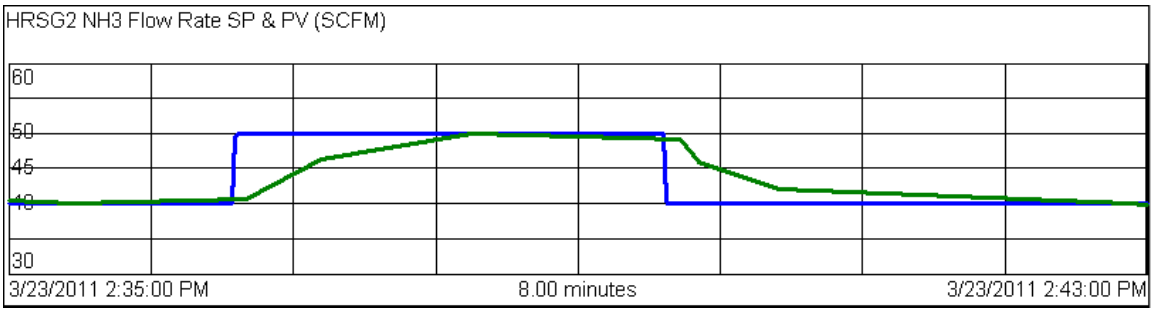

Figure 2.12: Tuned Ammonia Flow Rate Set Point Tracking on UConn's Unit #2

With the ammonia flow rate set point tracking loop in automatic, the tuned NO_X feedback loop is also put in automatic to test its disturbance rejection performance. A plot of closed loop CTG step responses is provided in Figure 2.13. The NO_X disturbances are corrected with no overshoot and the observed settling time of each event is approximately 15 minutes.

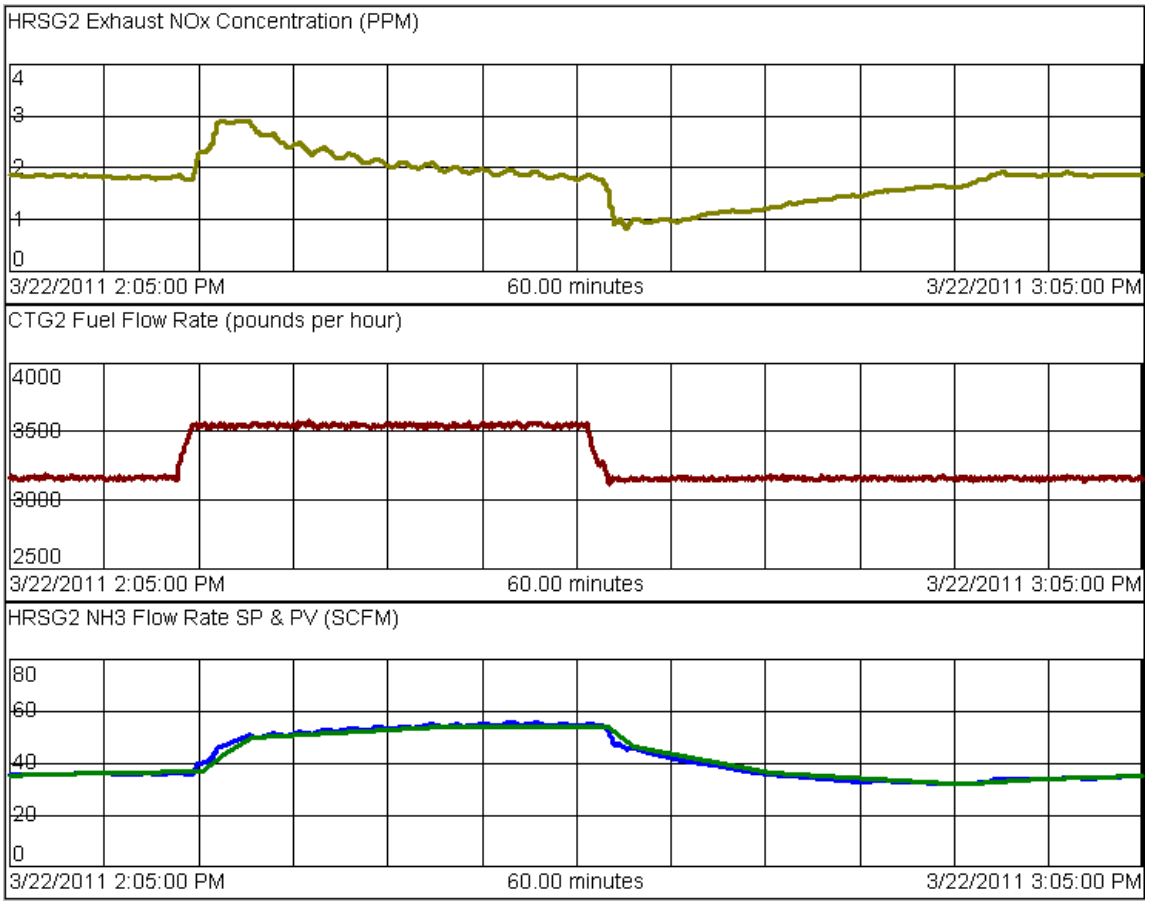

Figure 2.13: CTG Steps with Tuned NO_X Disturbance Rejection (no Feed Forward) on UConn's Unit #2

The feed forward function is added to the cascade feedback structure to test the overall CTG disturbance rejection performance. A plot of CTG step responses using the combined feed forward with feedback trim → ammonia flowrate cascade is provided in Figure 2.14. The NO_X disturbances are corrected with minimal overshoot. The observed settling time of each event is approximately 8 minutes. The ammonia flow rate slightly lags the ammonia setpoint but its response is still very fast when compared to the NO_X process.

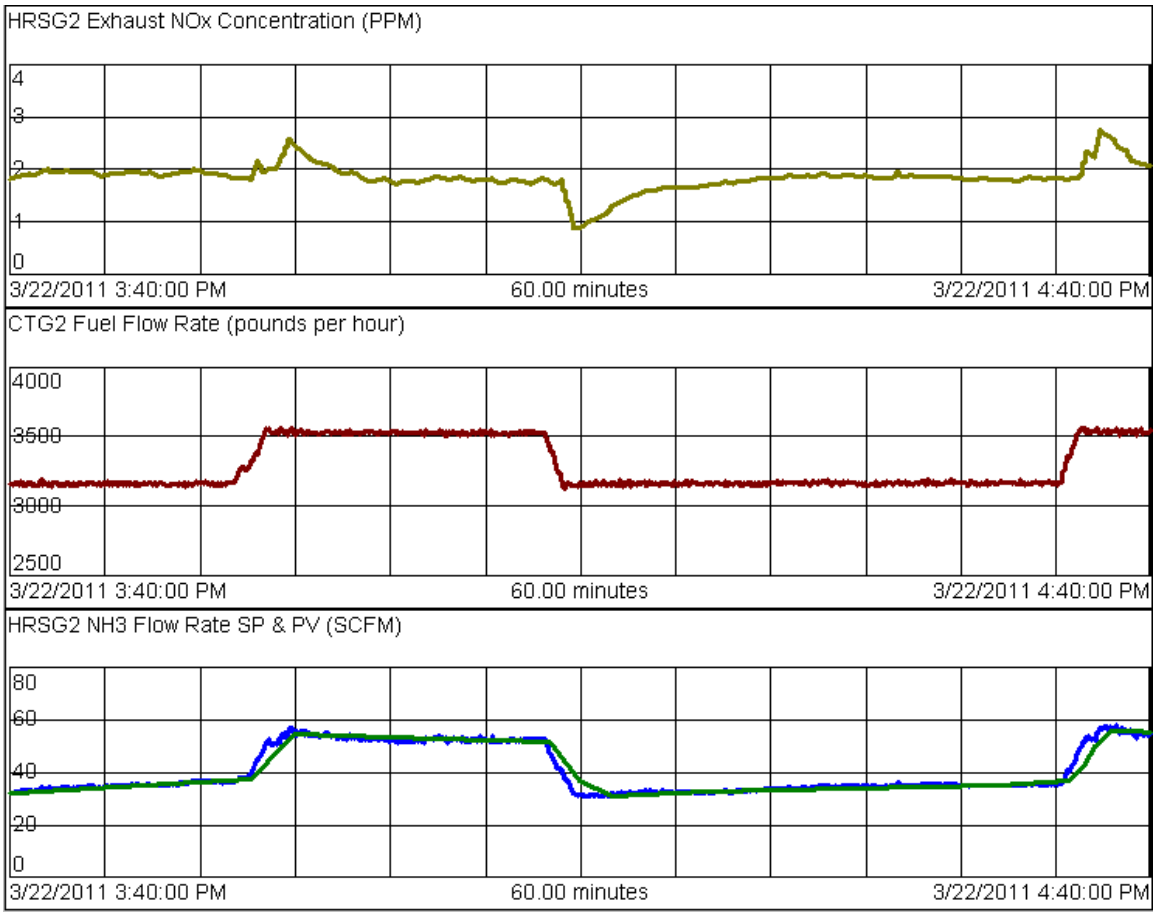

Figure 2.14: CTG Steps with Tuned NO_X Disturbance Rejection and Feed Forward on UConn's Unit #2

A performance comparison of the new, tuned NO_X control structure to the old NO_X control structure is provided in Figure 2.15. Three days of NO_X and CTG data is provided. It's clear that the new, tuned structure dramatically reduces the variance in exit NO_X concentration. Its performance is particularly improved at low CTG fuel flow rates.

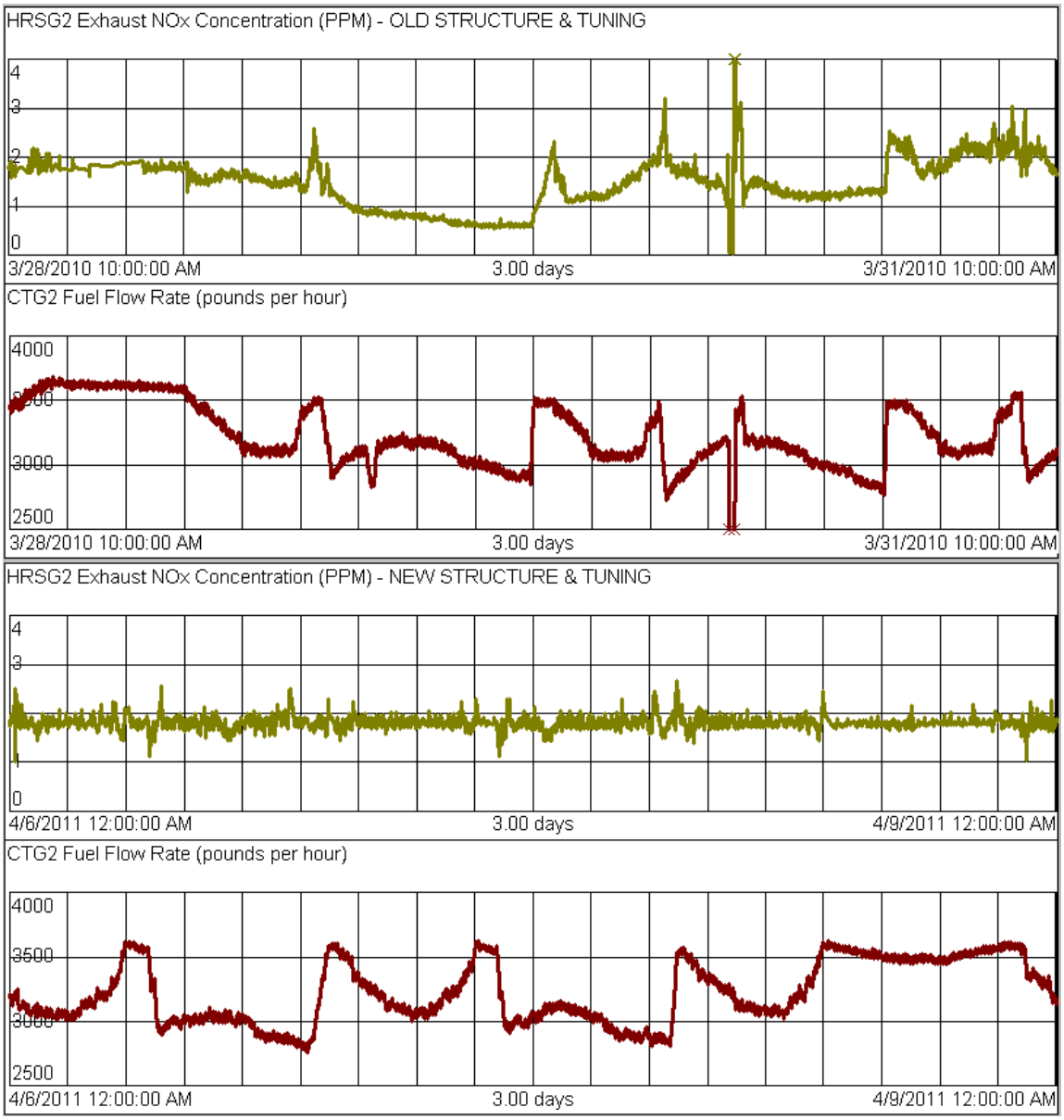

Figure 2.15: Three Days of NO_X Control Performance Data with the Old Structure and Tuning and the New Structure and Tuning

2.5 Conclusions

The tuned NO_X control cascade and feed forward provides dependable NO_X control for UConn's three CTG/HRSG units. The conservative tuning values selected for the feedback loops provide disturbance rejection with negligible overshoot, and a stability margin that will protect the loop's stability against nonlinearities and changes in the processes. While conservative tuning values deliver robust stability, they also result in slower disturbance rejection. The addition of the feed forward function improves the disturbance rejection performance of the structure, reducing the settling time of the main disturbance by nearly 50%. This dramatically reduces the standard deviation of NO_X concentration of emissions during normal cogen operation.

The control methodology not only provides favorable NO_X control performance and robust stability, it's also user friendly. Cascade and feed forward are industry standard tools, while alternative NO_X control strategies may require messy logic and physical models. The parameters used in the control structure are calculated from simple plant tests. Commercially available software such as LOOP-PRO enables an engineer to complete the four step tuning process in minutes, with a high level of confidence. Finally, no additional sensors are required beyond what is already available in cogeneration configurations. The structure successfully meets the UConn Cogeneration Plant's operational and environmental objectives. This methodology is recommended for similar configurations because it is effective and can be easily and confidently deployed and maintained.

CHAPTER 3: COOLING TOWER TEMPERATURE CONTROL

3.1 Abstract

Presented is a model based strategy for controlling the temperature of cogen cooling tower water. The strategy is applied to the UConn Cogen Plant's cooling water system which includes multiple mechanical draft cooling towers. The cooling tower fans' electric motors are driven by VFDs, allowing for a continuous range of fan speed. The speed and number of fans operating are manipulated to control cooling tower water temperature.

The energy efficiency of deploying different numbers of cooling tower fans is examined. Theoretical models are proposed relating fan speed to both power consumption and relating cooling power. Empirical data from UConn's plant has been provided to corroborate the theory. Logic is included to automate fan starting and stopping to maintain operation of the most efficient number of fans.

The classical SISO structure is employed for temperature control and tuned using the IMC method. Adaptive tuning is used to compensate for changes in process dynamics according to the number of fans operating. The control structure also includes a feed forward to reject the disturbance of fan starts and stops. The strategy improves the efficiency of the cooling process and is shown to provide improved control over the previous control strategy employed at the UConn Cogen Plant.

3.2 Introduction

3.2.1 Overview of the Cooling Water System

The University of Connecticut's cogen plant operates an array of nine mechanically driven cooling towers. The cooling towers facilitate evaporation from warm water into the atmosphere. This has a powerful cooling effect due to the energy required for phase change. Evaporation is promoted by increasing the contact area between water and air. In mechanically driven cooling towers, a fan is used to increase airflow over the water-air interface. A picture of one of UConn's cooling towers is provided in Figure 3.1.

Figure 3.1: Cooling Tower at the UConn Cogeneration Plant

Warm water is held in a basin at the top of the cooling tower. It is allowed to trickle down through a metal mesh on the sides of the tower, coating it and providing increased surface area for mass transfer. The metal mesh is known as the fill. A large fan at the top

of the cooling tower draws air in through the fill. A closer view of the fill on one of UConn's cooling towers is provided in Figure 3.2.

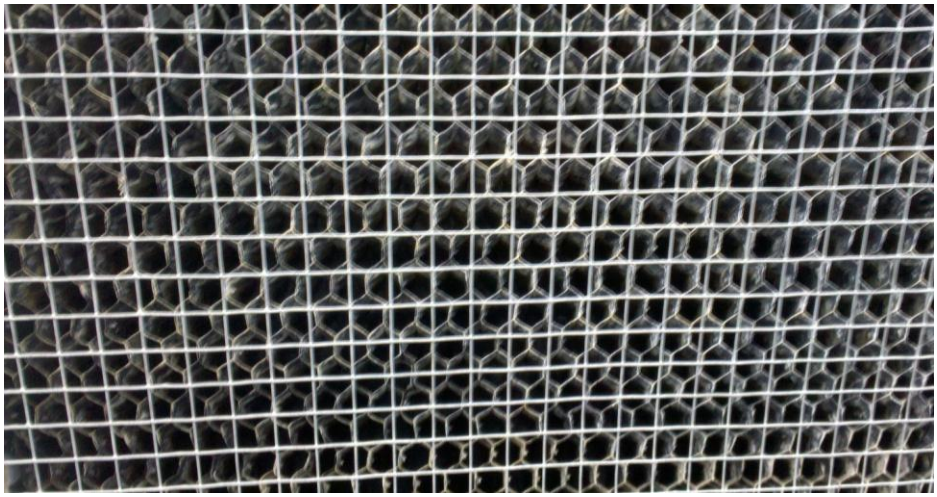

Figure 3.2: Cooling Tower Fill

The atmospheric air drawn through the fill already contains water vapor, but is typically well below saturation point. A concentration gradient exists at the interface of the water are unsaturated air; consequently there is mass transfer of water vapor into the air. The remaining water that trickles down to the bottom of the tower has a significantly lower temperature as a result of the evaporative cooling. Makeup water is added to this water to compensate for evaporative losses and to maintain a constant volume in the system.

The cooling towers are used to reject waste heat from the plant's power cycle, chiller plant, and for other cooling needs. Hot water from these processes passes through heat exchangers to transfer waste heat to the cooling tower water. The warmed cooling tower water continues to the cooling towers to be cooled, and is pumped back to the heat exchangers, completing the cycle.

The cooling tower fans' motors are driven by Variable Frequency Drives (VFDs) that can adjust the fan speeds continuously within their operating ranges. The temperature of the cooled water exiting the array of towers can be controlled by adjusting the fan speeds. The temperature can also be adjusted by starting an additional cooling tower fan, or taking one offline. A diagram of the cooling water system is presented in Figure 3.3.

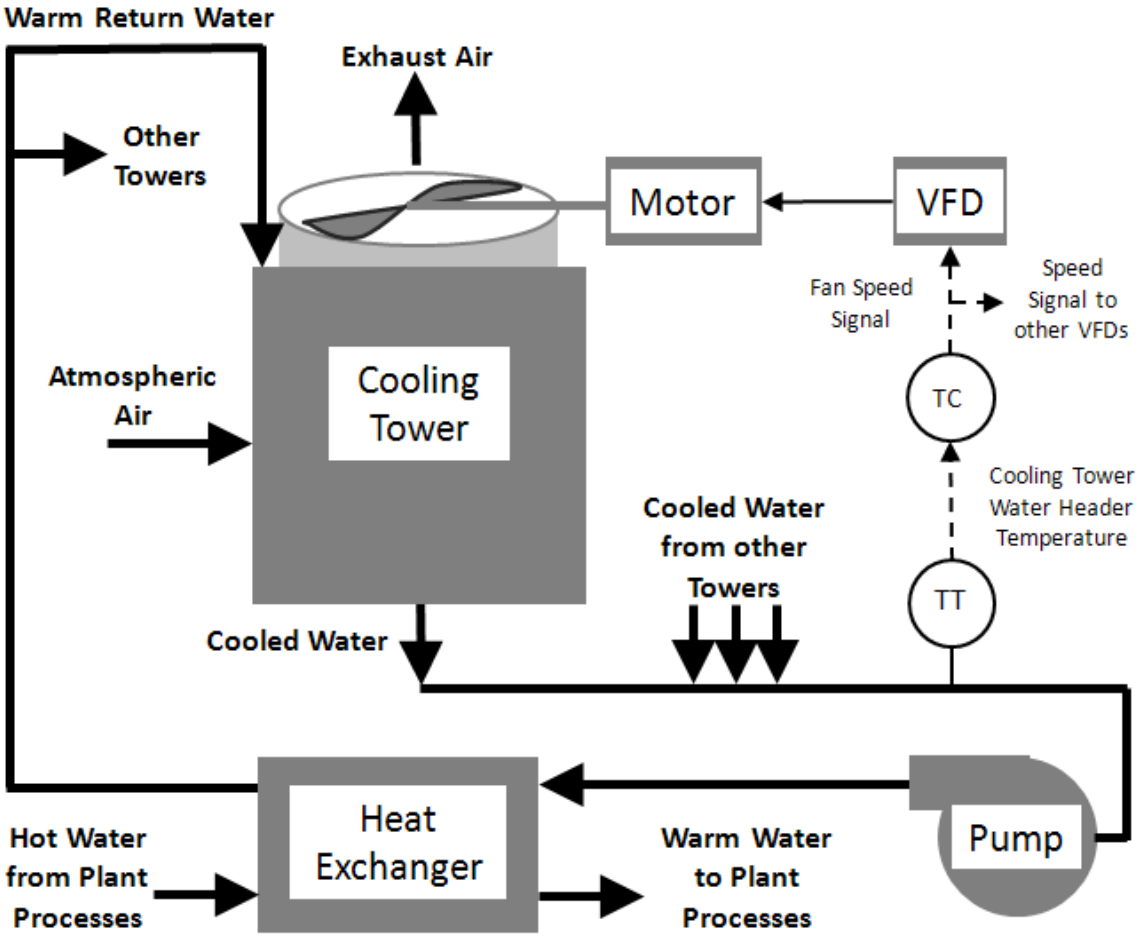

Figure 3.3: Diagram of UConn's Cooling Water System

3.2.2 Cooling Water Temperature Process

Fan Speed → Temperature Process Dynamics

The temperature of the cooling water can be adjusted by adjusting the speed of the cooling tower fans, or by turning an additional cooling tower fan on or off. Higher fan speeds, or the addition of a fan results in a lower cooling water header temperature. Dynamic response data showing the effect of fan speed on the cooling water header temperature when five fans are running is presented in Figure 3.4.

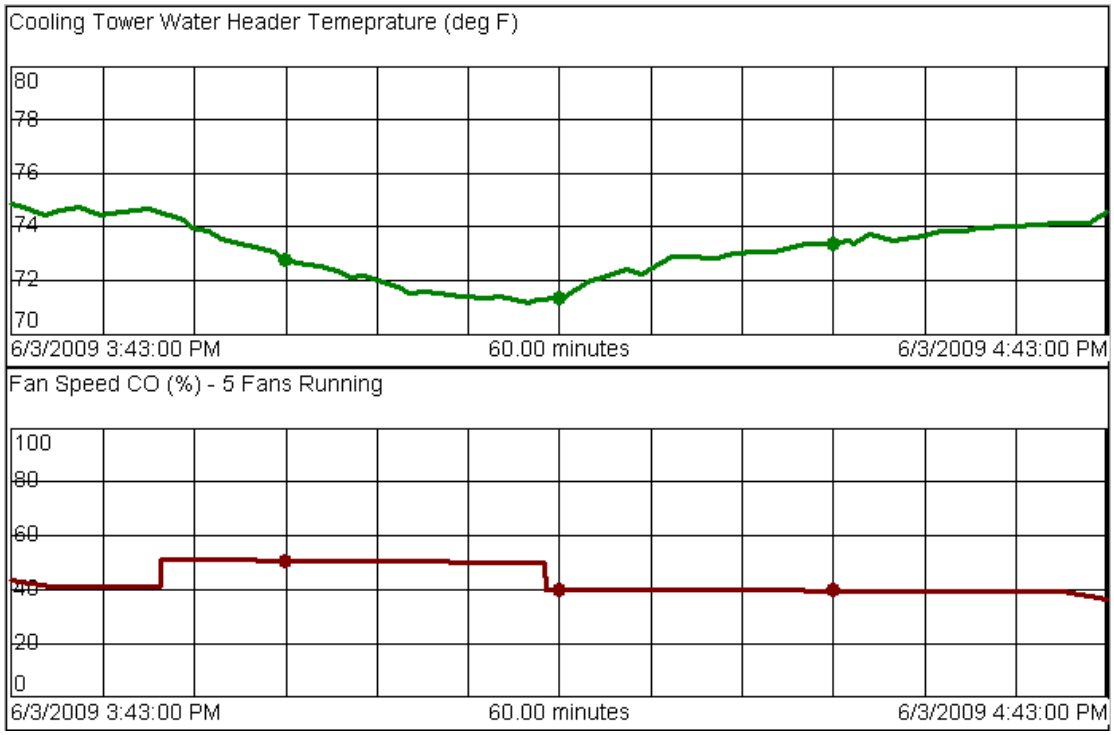

Figure 3.4: Cooling Tower Water Temperature Response to Steps in Fan Speed with 5 Fans Running

The cooling tower header temperature data is taken at a time when the major disturbance, chiller load, is relatively constant, reducing its impact on the data. Step tests similar to the ones of Figure 3.4 consistently show that the cooling tower header temperature reaches a steady state given a constant fan speed. This indicates that the process is self-

regulating. It is also observed that the process is reverse acting. A similar test is conducted when only one fan is running, and is presented in Figure 3.5.

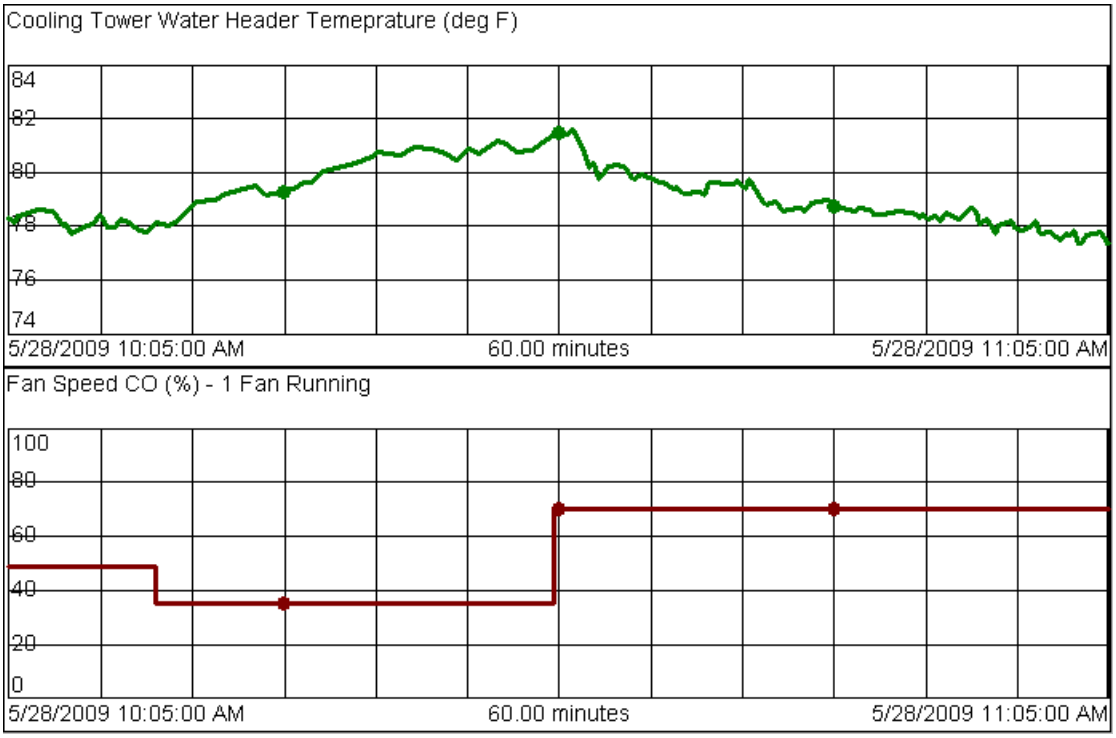

Figure 3.5: Cooling Tower Water Temperature Response to Steps in Fan Speed with 1 Fan Running

Tests similar to those of Figures 3.4 and 3.5 demonstrate that the Fan Speed→Temperature process dynamics tend to be different when a different number of fans are on. This result is due to a combination of factors, most importantly the different number of fans, but also the different atmospheric humidity, temperature and plant loading conditions that tend to exist when different numbers of fans are engaged. For example, if nine fans are on, it is probably a very hot and humid day, and the chiller plant is probably running at a high load. The days when only one fan is engaged tend to be cold and dry.

Fan Starts and Stops

When a cooling tower fan is started or stopped, the cooling power that the bank of towers delivers is changed. Figure 3.6 shows the response of the cooling water system when two fans are initially running, and then one is shut off. During this time the system is in automatic, and the fan speed CO is adjusted to control the cooling water header temperature to 78°F.

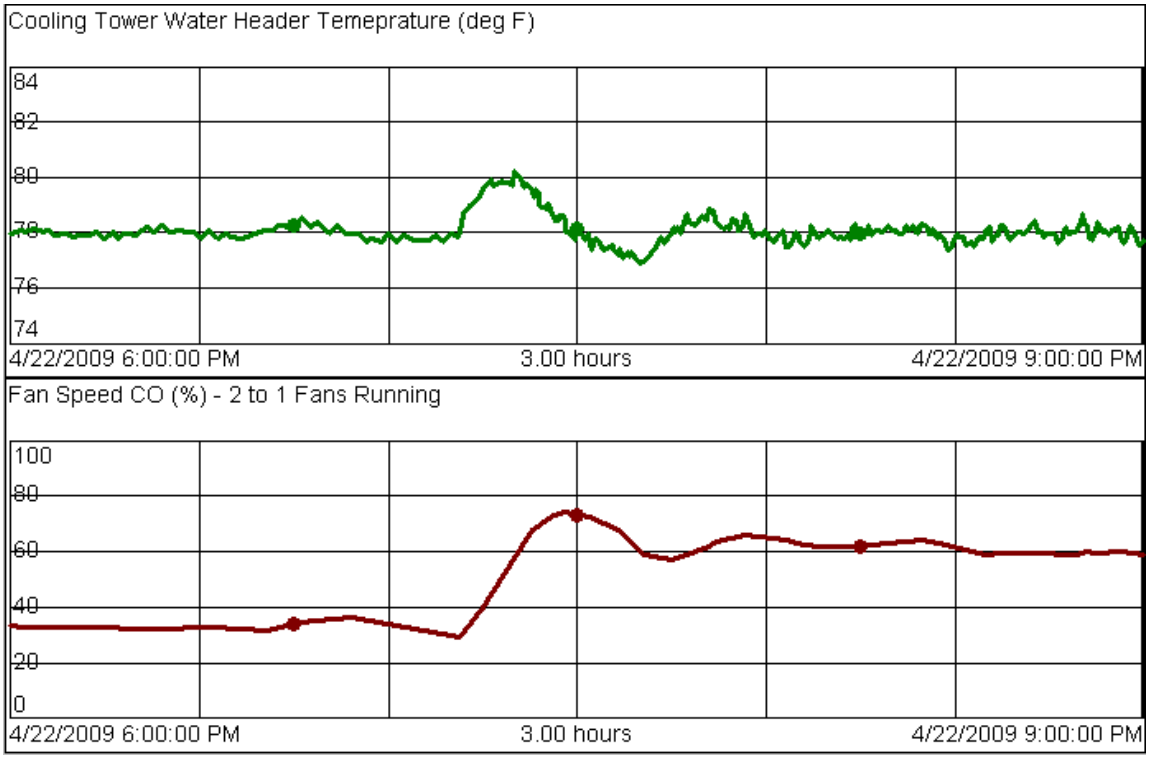

Figure 3.6: Cooling Tower Water Temperature Response to a Fan Shut Off (Initially 2 Fans Running)

3.3 Methodology

To control the cooling water system in a manner best suited to the cogen plant, it's necessary to consider the operational objectives of the process. The cooling system control strategy should:

1) operate in a manner that is energy efficient,
2) ensure the cooling water provided to the plant's processes is controlled at the temperature set point, 75°F, with low variability,
3) retain simplicity so it can be easily understood and adapted.

3.3.1 Steady State Modeling

Any strategy must first consider the fundamental question of whether it is more efficient to run a few of the cooling tower fans at a high speed or many fans at a low speed to achieve the plants cooling needs. The fan laws state the power consumed by a fan is proportional to the cube of the fan's angular velocity [6].

$$P_{fan} \propto \omega_{fan}{}^{3} \qquad \text{Equation 3.1}$$

Electric power input to the fan is calculated from the RMS current and voltage data available from the VFD. The calculated power is plotted versus the fan speed signal in Figure 3.7.

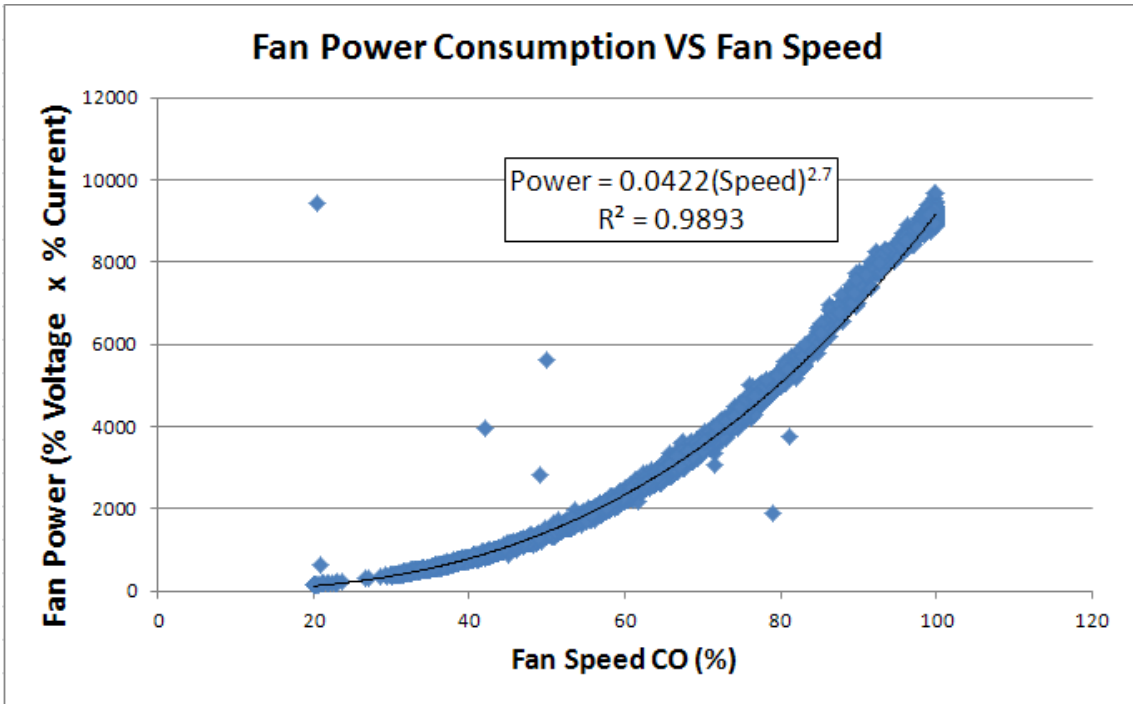

Figure 3.7: Fan Electric Power Consumption vs. Fan Speed Data with Regression

A regression of Figure 3.7 shows that fan power consumption is approximately proportional to fan speed raised to the power of 2.7. This confirms that the approximation of Equation 3.1 is reasonable. Equation 3.1 is extended to include the power consumed by the sum of all the fans operating, n_{fans}, yielding Equation 3.2.

$$P_{fans} \propto n_{fans}{\omega_{fans}}^3 \qquad \text{Equation 3.2}$$

The fan laws also state, the air flow generated by a fan is proportional to its angular velocity [6].

$$\dot{m}_{air} \propto \omega_{fans} \qquad \text{Equation 3.3}$$

There is no sensing equipment to measure the air flow through the towers but the relationship of Equation 3.3 is used as an approximation.

A cooling tower control volume diagram is provided in Figure 3.8, including energy balance variables. Mass flow rate is represented by $\dot{m}$, specific enthalpy is represented by h, and the humidity ratio, the ratio of the mass of water vapor to the mass of air, is represented by ω_{vapor}.

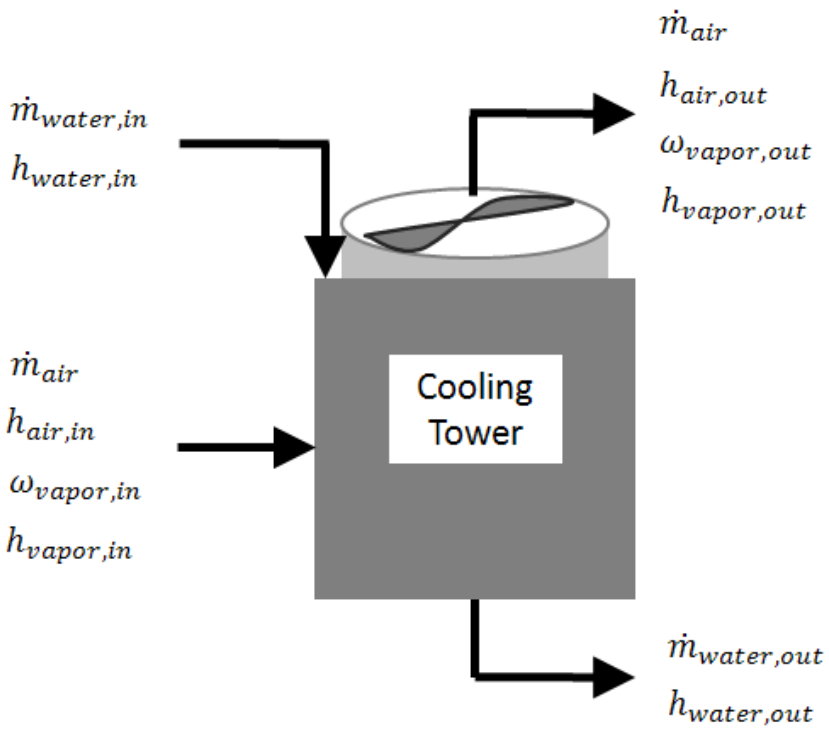

Figure 3.8: Control Volume of a Cooling Tower

Assuming steady state conditions, negligible heat addition by the fan work, and the only heat transfer that occurs is due to fluid flow, Figure 3.8 results in the following energy balance equation [13]:

$$\dot{m}_{water,in}h_{water,in} + \dot{m}_{air}\left(h_{air,in} + \omega_{vapor,in}h_{vapor,in}\right)$$

$$= \dot{m}_{water,out}h_{water,out} + \dot{m}_{air}\left(h_{air,out} + \omega_{vapor,out}h_{vapor,out}\right) \qquad \text{Equation 3.4}$$

Assuming the mass flow of the water that evaporates from the system is negligible compared to the mass flow rate of water through the system [20], we see that $\dot{m}_{water,in} = \dot{m}_{water,out} = \dot{m}_{water}$. Using this assumption, and rearranging Equation 3.4, we arrive at Equation 3.5.

$$\dot{m}_{water}\left(h_{water,in} - h_{water,out}\right)$$

$$= \dot{m}_{air}\left(h_{air,out} + \omega_{vapor,out}h_{vapor,out} - h_{air,in} - \omega_{vapor,in}h_{vapor,in}\right) \qquad \text{Equation 3.5}$$

We define $-\dot{Q}_{water}$ as the heat rejection rate from the cooling tower water. From our assumptions and the first law of thermodynamics:

$$\dot{m}_{water}\left(h_{water,in} - h_{water,out}\right) = -\dot{Q}_{water} \qquad \text{Equation 3.6}$$

Substituting the relationship of Equation 3.6 into Equation 3.5 and rearranging, we arrive at Equation 3.7.

$$-\dot{Q}_{water} =$$

$$\dot{m}_{air}\left(h_{air,out} + \omega_{vapor,out}h_{vapor,out} - h_{air,in} - \omega_{vapor,in}h_{vapor,in}\right) \qquad \text{Equation 3.7}$$

It is assumed that the state of the air-vapor mixture exiting the cooling tower is independent of the air mass flow rate through the tower, i.e. $\left(h_{air,out} + \omega_{vapor,out}h_{vapor,out}\right) \neq f(\dot{m}_{air})$. This would be true under the assumption that the air-vapor mixture reached thermodynamic equilibrium with the incoming water stream before exiting. It is also assumed that inlet air conditions are constant. Using these assumptions, and Equation 3.7, we arrive at the relationship of Equation 3.8.

$$-\dot{Q}_{water} \propto \dot{m}_{air}$$ Equation 3.8

Equation 3.8 simply states, under the assumptions we have made, that the heat rejection rate from the cooling tower water, $-\dot{Q}_{water}$, is proportional to the mass flow rate of air through the cooling tower. The relationship of Equation 3.8 is extended to the entire bank of cooling towers by multiplying the airflow by the number of towers in operation, n_{fans}, resulting in Equation 3.9.

$$-\dot{Q}_{water} \propto n_{fans}\dot{m}_{air}$$ Equation 3.9

Combining Equation 3.9 and Equation 3.2 yields Equation 3.10,

$$-\dot{Q}_{water} \propto n_{fans}\omega_{fans}$$ Equation 3.10

which states, the cooling power of the fan bank is equal to the number of fans running times the angular velocity of the fans.

The relationship of Equation 3.10 is supported by empirical data. Tests are run by allowing the cooling system to reach steady state, then either shutting off a fan or engaging a new fan. With the speed of the fans in automatic temperature control, the system again reaches steady state. During this period we assume the heat rejection load of the cooling towers, $-\dot{Q}_{water}$, and atmospheric conditions remain constant. Under these conditions, Equation 3.10 predicts, the initial number of fans times the initial speed of the fans should equal the final number of fans times the final speed of the fans.

$$n_{fans,i}\omega_{fans,i} = n_{fans,f}\omega_{fans,f}$$ Equation 3.11

Data collected during a sample test run is provided in Figure 3.9.

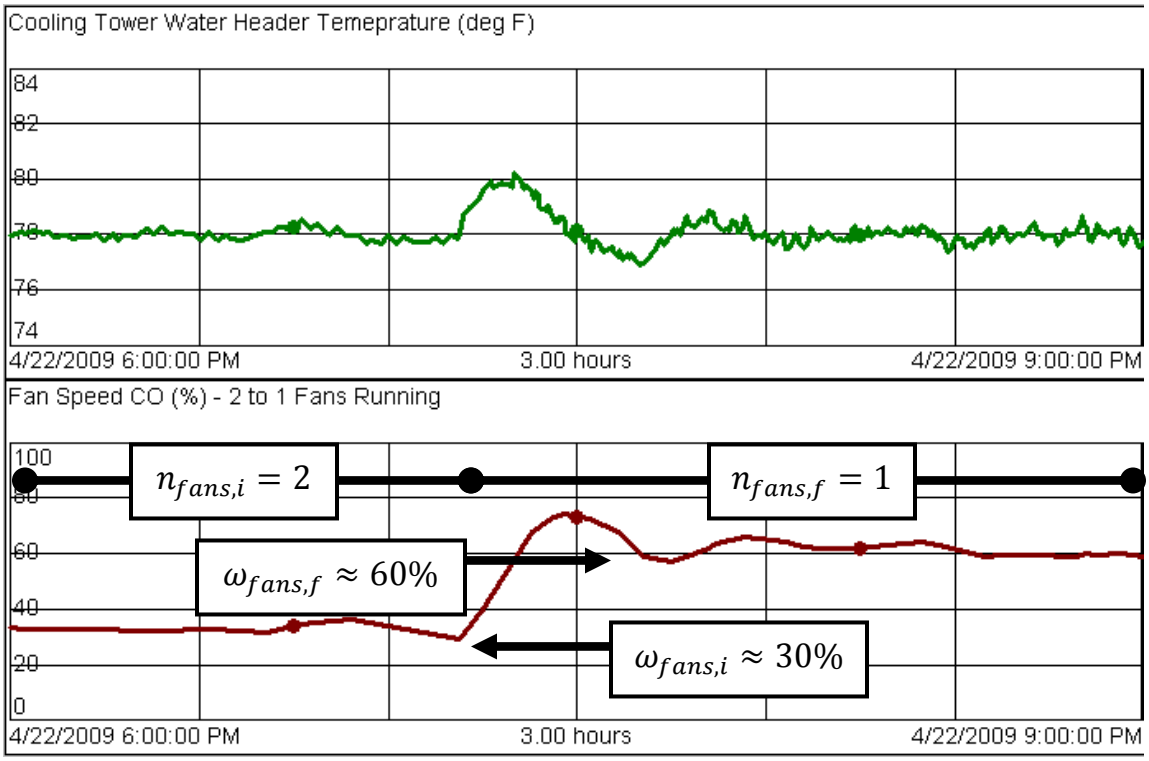

Figure 3.9: Cooling Tower System Test. Initially 2 Fans, 1 is Shut Down

The test case of Figure 3.9 is in close agreement with Equation 3.11, which validates Equation 3.10. Additional fan start and stop tests, similar to the one of Figure 3.9, have been conducted. The results are provided in Figure 3.10. The observed final equilibrium fan speeds of each test are plotted next to those predicted by Equation 3.11.

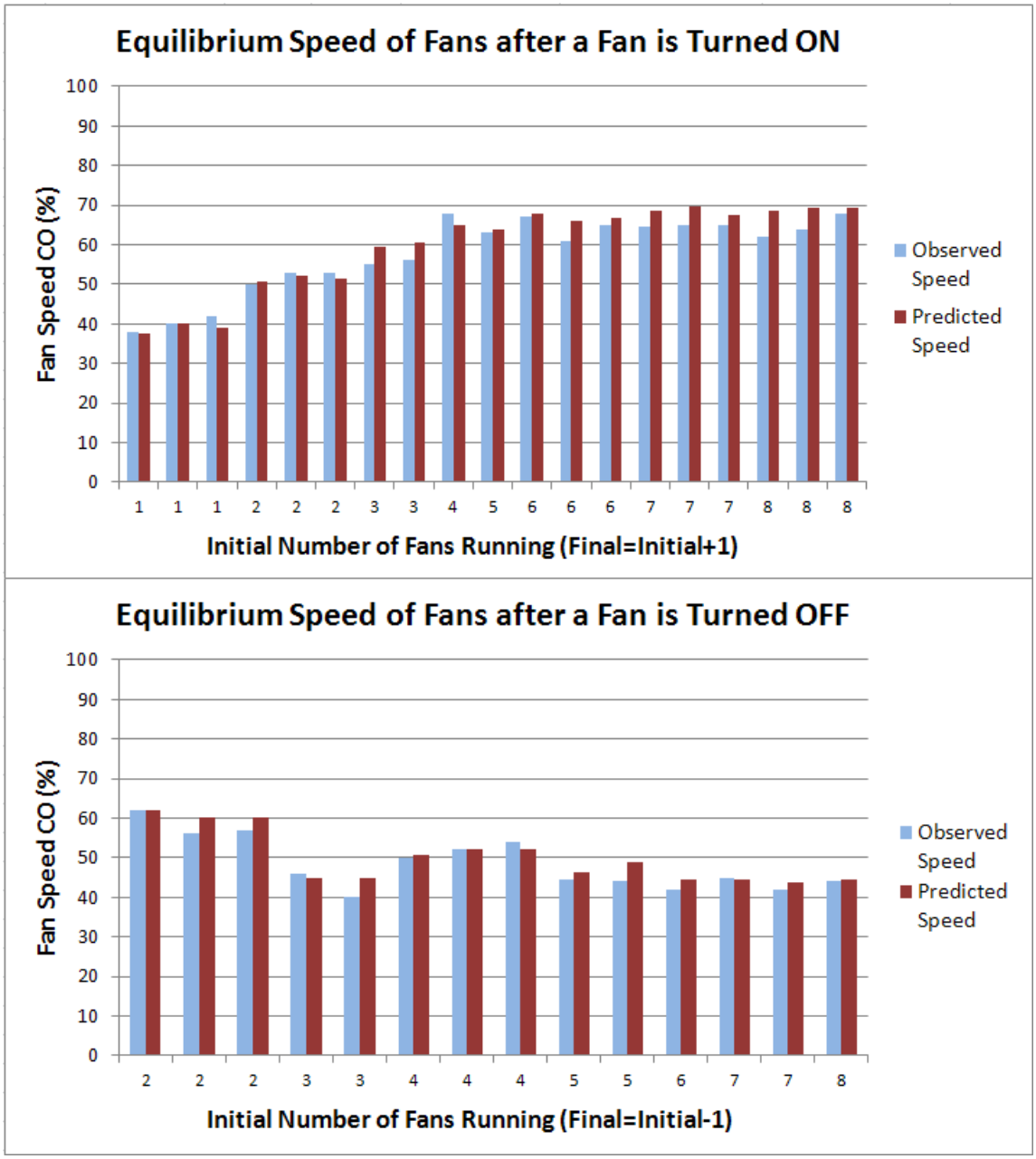

Figure 3.10: Fan Starts and Stops. Actual vs. Predicted Final Speeds.

The test data of Figure 3.10 demonstrates the predicted equilibrium speeds are a good approximation. This supports the theoretical model from Equation 3.10, which indicates the cooling power of the cooling tower bank is proportional to the number of fans running and the speed of the fans.

This paper has proposed theoretical models relating fan speed to power consumption and cooling power. Empirical data from UConn's plant has been provided to corroborate the theory. The two models, described in Equation 3.2 and Equation 3.10 can be combined to describe cooling tower system efficiency, defined as the ratio of the cooling power of the system divided by the electrical power input to the fans.

$$\frac{-\dot{Q}_{water}}{P_{fans}} \propto \frac{1}{{\omega_{fans}}^2} \qquad \text{Equation 3.12}$$

Equation 3.12 reveals, the energy efficiency of the system is significantly greater when the fans are running at lower speeds. From an energy efficiency standpoint, it makes sense to operate many fans at lower speed rather than a few fans at higher speed.

3.3.2 Proposed Control Structure

A traditional feedback structure is proposed to control cooling tower water temperature by adjusting fan speed. The structure is effective, easy to deploy and maintain, and is well understood by plant personnel. Figure 3.11 shows the control block diagram of the single loop control structure. The traditional feedback loop is appended by additional logic. The additional logic can adjust the loop to account for changes in the number of fans operating.

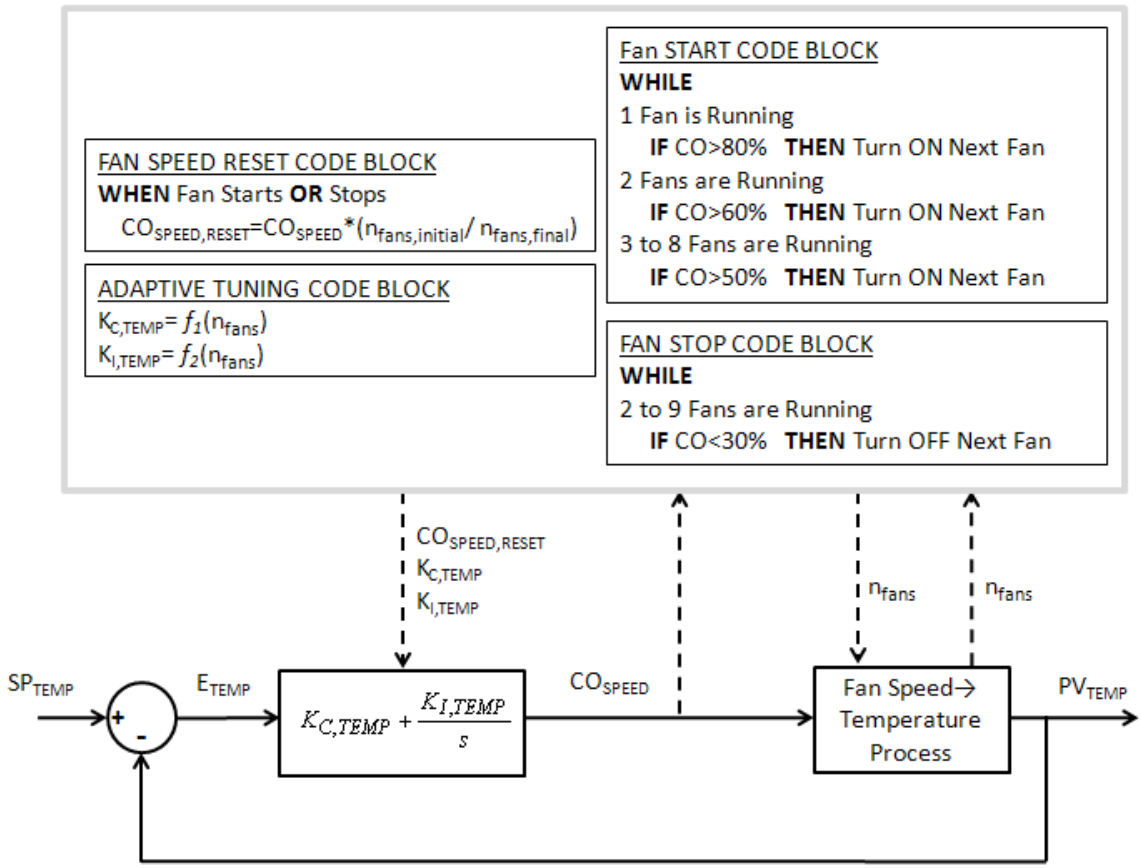

Figure 3.11: Cooling Tower Control Structure

The plant's efficiency criterion suggests the cooling tower system should operate all fans at low speed to provide the necessary cooling. This strategy must also consider wear and tear on the system. The manufacturer states, the fans should not be operated below 20% of rated speed. Therefore, as the cooling load changes, some fans are periodically turned on and shut off. The frequency of these starts and stops should be minimized to reduce wear and tear.

The FAN START CODE BLOCK and the FAN STOP CODE BLOCK are added to the traditional structure to automate starting and stopping of cooling tower fans. When fan speed drops below 30%, a fan is turned off, preventing the speed of the fans from

reaching the 20% speed lower limit prescribed by the manufacturer. Similarly, fan speed reaches an upper threshold, an additional fan is turned on. This promotes energy efficiency by using more fans at lower speeds whenever possible. The upper threshold is varied based upon the number of fans running. The upper threshold must be increased when only a few fans are running. This prevents the speed of the fans from immediately dropping below the lower limit, triggering the FAN STOP CODE BLOCK, and entering an on/off cycle. At the given upper speed thresholds, Equation 3.11 predicts that the speed of the fans will be approximately 40% after a fan is started. This gives the fan speed a 10% buffer before it reaching the 30% lower threshold, reducing unnecessary starts and stops.

The FAN SPEED RESET CODE BLOCK shown in Figure 3.11 is a feed forward function. It is used to reject the temperature disturbance that occurs when a fan is turned on or off. Equation 3.11 predicts the new fan speed required when a fan is turned on or off, and is the basis of the feed forward function.

The ADAPTIVE TUNING CODE BLOCK of Figure 3.11 is used to change the temperature controllers PI tuning. The process changes significantly when different numbers of fans are running, so different tuning values may deliver better performance.

3.3.3 FOPDT Modeling and Tuning Using the IMC Method

The Fan Speed→Temperature process changes when different numbers of fans are operating. In all cases, the process can be well approximated by a FOPDT dynamic model. The tuning values are generated using the IMC tuning method as described in Section 1.5. Step tests are performed on fan speed with 1, 4, 5, 7 and 9 fans operating, according to the IMC strategy. Loop-Pro tuning software is used to fit FOPDT models to the process data in each case. Results of the FOPDT model fitting are presented for the 4 fan case in Figure 3.12. The FOPDT model fits for other numbers of fans are provided in APPENDIX B.

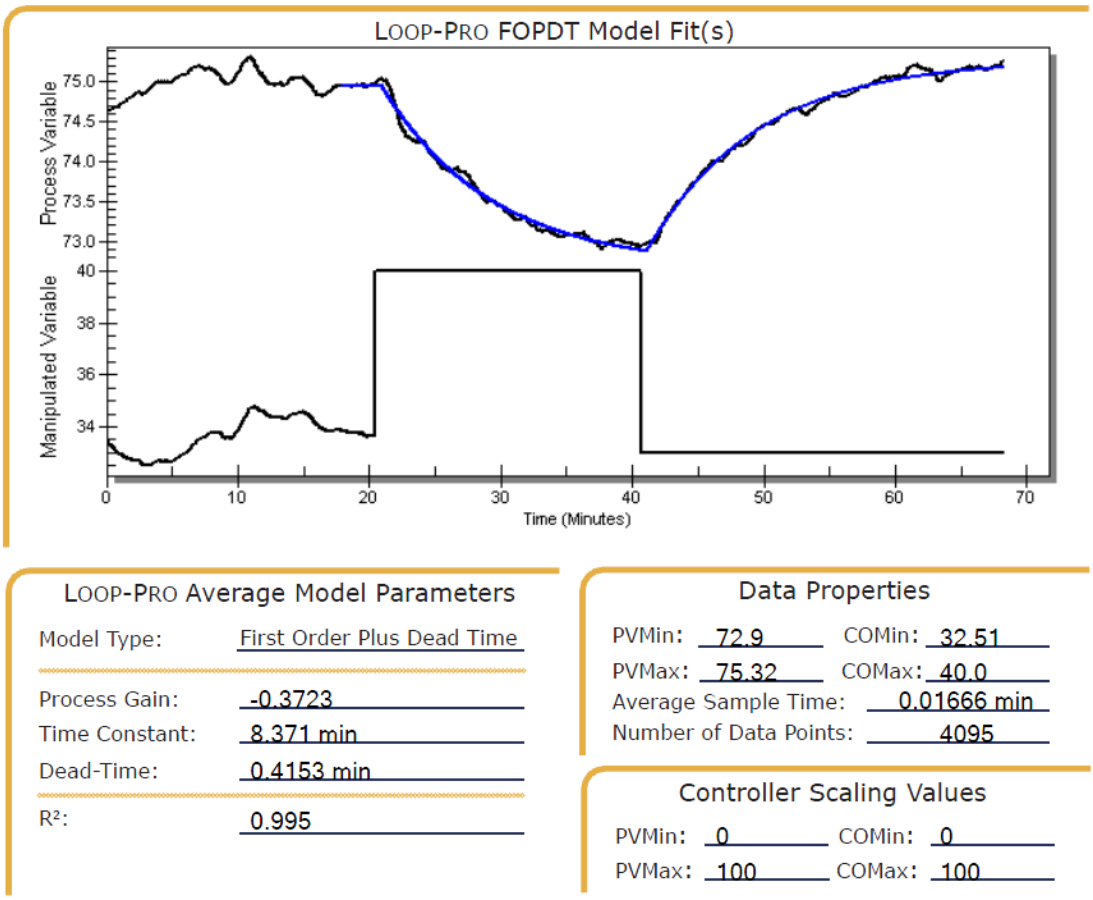

Figure 3.12: Temperature Dynamic Response to Change in Fan Speed with 4 Fans Running and FOPDT Approximation

A summary of the FOPDT approximations fit to process data with different numbers of fans running is given in Figure 3.13.

# Fans Operating	K_P [°F/%]	τ_P [min]	θ_P [min]	R^2
1	-0.28	14	0.017	.958
4	-0.37	8.4	.42	.995
5	-0.47	12	0.017	.974
7	-0.28	7.7	1.1	.948
9	-0.23	7.2	0.99	.935

Figure 3.13: FOPDT Model Approximation Parameters and Goodness of Fit Values for Different Numbers of Fans Operating

It is interesting to note that the process gain, K_P, becomes smaller when nine fans are operating. Additional bump test data confirms this phenomenon. This result is due to the hotter and more humid atmospheric conditions that generally exist when nine fans are operating. The result also shows the effect of the DLO on bump tests for process tuning. Tuning values are generated using the IMC correlations from the FOPDT model fits of Figure 3.13. The heuristic introduced in Section 1.5.2.1 is used to select a closed loop time constant, τ_C, that targets a 10-15% overshoot in the closed loop set point tracking response. The results are presented in Figure 3.14.

# Fans Operating	$K_{C,TEMP}$ [%/°F]	$K_{I,TEMP}$ [%/°F·min]
1	-12	-0.84
4	-7.7	-0.92
5	-7.1	-0.60
7	-7.6	-0.99
9	-9.1	-1.27

Figure 3.14: IMC Tuning Values and Closed Loop Time Constants Corresponding to the FOPDT Models

The actual tuning values used for adaptive tuning in the control structure are presented in Figure 3.15. Reduced tuning values were used for higher numbers of fans. This reflects the fact that they may need to operate in colder, less humid conditions than when the bump tests were performed. More conservative values will protect the stability of the system and reduce oscillations. The integral gains, $K_{I,TEMP}$, values are set to the same number for logic simplicity, and because the calculated values were all around -0.85. Tuning values for cases not tested were set equal to the nearest number of fans that were tested.

# Fans Operating	$K_{C,TEMP}$ [%/°F]	$K_{I,TEMP}$ [%/°F·min]
1 or 2	-10	-0.85
3 or 4	-8	-0.85
5 or 6	-7	-0.85
7, 8 or 9	-6	-0.85

Figure 3.15: Actual PI Tuning Values used for Adaptive Tuning

3.4 Results

3.4.1 Feedback Performance

To objectively describe the closed loop performance of the tuned control structure, it is compared to previous tuning values. The cooling water system was initially tuned using the guess and check method, with $K_{C,TEMP}$ =-2 %/°F and $K_{I,TEMP}$ = -2%/°F·min. Two plots of the cooling system closed loop performance are provided in Figure 3.16. The upper plot shows 1.5 hours of temperature data while 2 fans are continuously operating, using the old tuning values. The lower plot shows similar data for 2 fans using the new tuning values. During these time periods there were no major disruptions to the major disturbance, the cooling tower return water temperature, so a more objective comparison can be made.

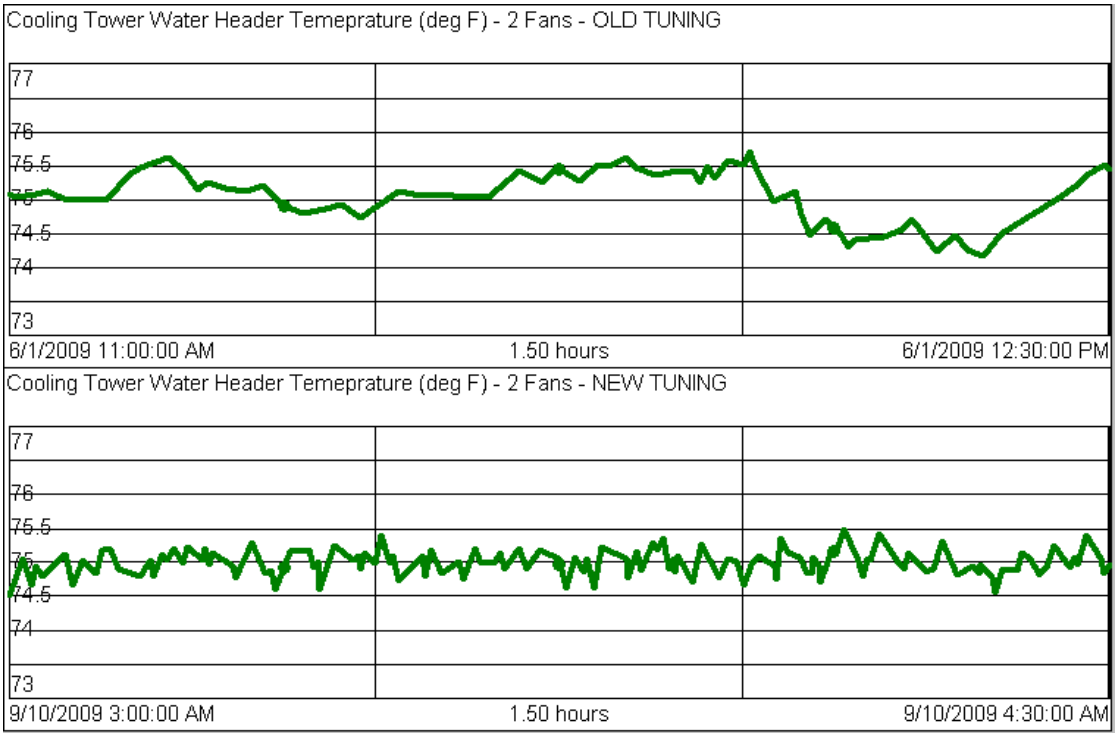

Figure 3.16: Comparison of Temperature Regulation Performance with 2 Fans Operating Before and After Tuning

Plots of temperature regulation performance comparison data similar to Figure 3.16 for 1 to 9 fans are provided in APPENDIX C. A summary of the temperature control performance plots is provided in Figure 3.17.

# Fans Operating	Temperature Std. Dev. using Old Tuning Values	Temperature Std. Dev. using New Tuning Values
1	0.19	0.13
2	0.36	0.15
3	0.20	0.11
4	0.18	0.13
5	0.21	0.23
6	0.22	0.21
7	0.22	0.23
8	0.20	0.15
9	0.11	0.09

Figure 3.17: Table of Temperature Regulation Performance for 1.5 Hours of Data Using Old Tuning Values vs. New Tuning Values

3.4.2 Feed Forward Performance

When a cooling tower fan is shut down, it causes a change in the Fan Speed→Temperature process. The process dynamics change and a disturbance occurs. Adaptive tuning addresses the change in the process dynamics, and the feed forward function of Equation 3.11 is used to neutralize the disturbance. Figure 3.18 shows how the temperature control loop performs before and after the feed forward function was implemented, when two fans are initially operating and one is shut down.

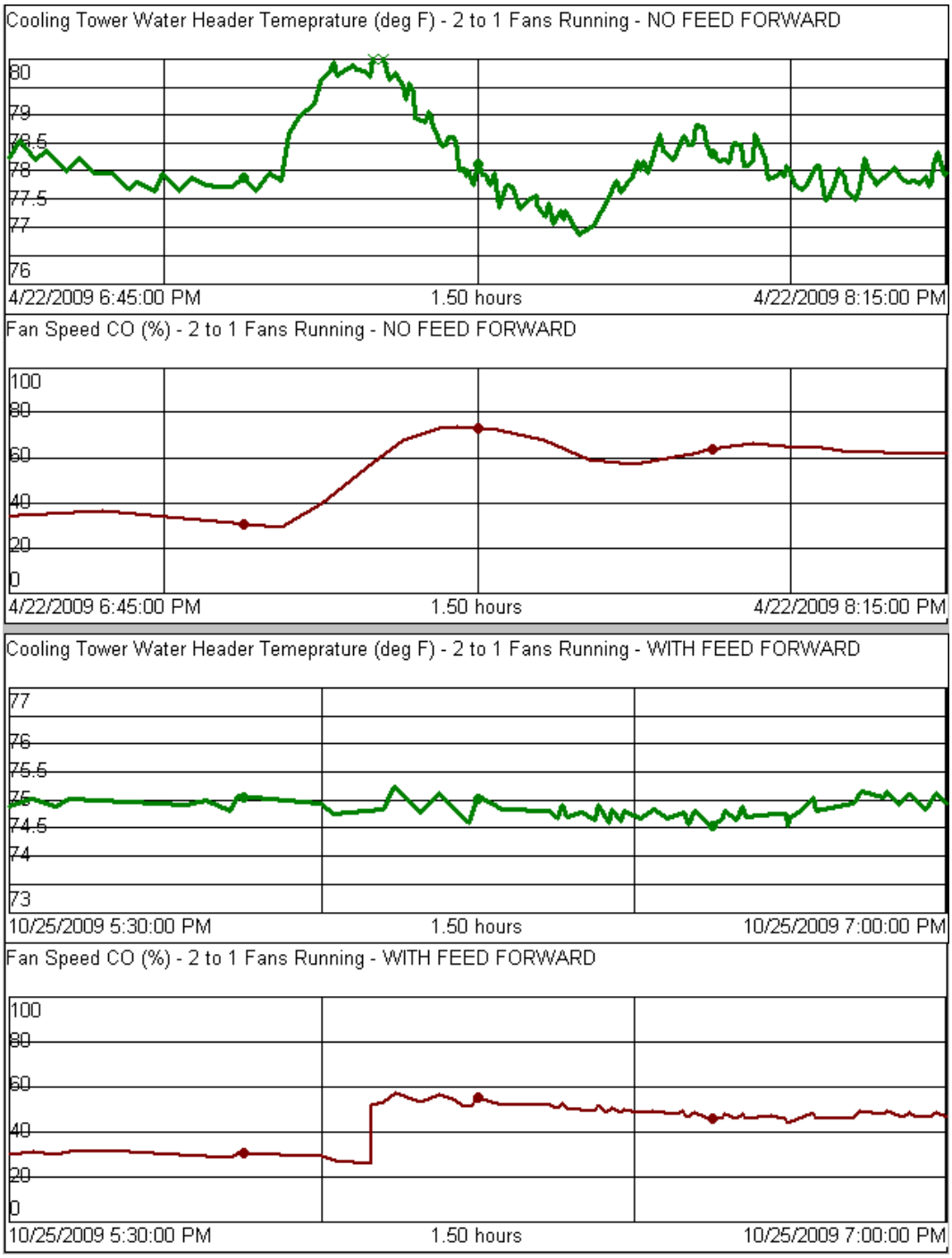

Figure 3.18: Comparison of Disturbance Rejection Performance, No Feed Forward vs. Feed Forward, 2 Fans Initially Operating, 1 Fan Stopped

Without the feed forward function, the temperature deviates approximately 2.1°F from the set point. When the feed forward function is used, the temperature deviates

approximately 0.3°F from the set point. Plots similar to those of Figure 3.18, when 3 to 9 fans are initially running, are presented in APPENDIX D. The figures show the benefit of the feed forward function on rejecting fan shut down temperature disturbances. Figure 3.19 is a summary of the fan stop disturbance rejection comparison data in table form. "Negligible" indicates that the resultant temperature disturbance due to a fan being stopped is not distinguishable in the process data.

Number of Fans Before and After Shut Down	Max ΔT, No Feed Forward [°F]	Max ΔT with Feed Forward [°F]
2 to 1	2.1	Negligible
3 to 2	1.5	Negligible
4 to 3	2.0	Negligible
5 to 4	1.0	Negligible
6 to 5	0.8	Negligible
7 to 6	Negligible	Negligible
8 to 7	1.1	Negligible
9 to 8	Negligible	Negligible

Figure 3.19: Table of Fan Stop Disturbance Rejection Performance Data without Feed Forward and with Feed Forward

3.5 Conclusions

The temperature control structure, tuned for each number of fans using the IMC method, provided similar or better temperature regulation than the guess and check method for each time period analyzed. The temperature standard deviations were most dramatically reduced with lower numbers of fans operating. The tuning values for low numbers of fans were also changed more dramatically from the original guess and check values.

The IMC tuning method provided improved performance over the guess and check method on the initial try. This is further proof the method is practical for industrial applications. A single bump test and simple calculation can provide better control performance than a lengthy and unpredictable guess and check process. The IMC tuning method allows the control engineer to tune processes with ease and confidence.

The feed forward function provided similar or improved temperature control performance when a cooling fan was stopped in every instance examined. The function provides support to the traditional feedback loop by helping neutralize the main disturbance, fan starts and stops. It adapts its control action according to the number of fans running, adding only little additional logic to the structure.

The adaptive feed forward and feedback together improve the temperature control performance of the control loop while retaining logic simplicity. Fan start and stop logic adds complexity to the logic, yet it automates the process. This allows operators to focus on other plant issues, and ensures the most energy efficient number of fans are operating whenever possible.

CHAPTER 4: COGEN STEAM SYSTEM

4.1 Abstract

A study of the UConn Cogen Plant's steam system is presented. The steam pressure control system's various processes are described. Different processes are used to control the steam pressures, according to the production rate of cogen-sourced steam versus campus demand, as described in Section 1.4. Multiple controllers are used to safely and efficiently maintain pressure set points. Different steam pressure set points are assigned to different controlling processes. A summary of the various steam pressure control modes is presented.

Three individual steam system related processes are also studied. The classical SISO structure tuned using the IMC method is used to control the systems. A problem with the dump condenser control algorithm is examined. The physical limit of the dump condenser valve results in a nonlinear process requiring anti-integral windup logic. The physical limit of the process, combined with the anti-integral windup logic causes the dump condenser valve to "pop open" when it should remain closed. Retuning the dump condenser pressure controller is shown to resolve the problem and provides improved pressure control in normal operating conditions.

An oscillation problem in the low pressure steam temperature control system is examined. A PID algorithm tuned using the IMC method is shown to decrease oscillations.

A new pressure control valve is commissioned in the boiler feed water system. An analysis of the system is provided. PI tuning of the pressure controller using the IMC

method is shown to provide satisfactory pressure control. The strategy results in simple control logic and the controller is tuned in a few short steps.

4.2 Description of the Steam System

4.2.1 Steam System Overview

The steam system at the UConn Cogen Plant is comprised of many individual processes that maintain a delicate pressure balance. Steam flow demand from the campus and chillers must be matched by steam production. There are a number of control modes the steam system uses, depending on the supply and demand for steam. Different actuators and pressure set points are used in each mode.

High Pressure (HP) and Low Pressure (LP) steam is generated by the HRSGs as a byproduct of electricity generation. When the cogen steam and electricity loads are in balance, the entire steam load is satisfied by waste heat from the CTGs. If the plant needs additional steam, duct burners can be used. If the steam load is even greater, boilers can be operated to generate more LP steam. When the CTGs are produce too much steam due to electrical load, some steam must be removed from the system. A dump condenser is used to dispose of the excess steam.

HP steam is converted to LP steam by passing it through the STG. The STG extracts electrical energy from the HP steam and reduces its pressure. The HP and LP steam pressures can be manipulated by the STG by controlling the flow of steam from the HP side to the LP side. A bypass valve can quickly convert HP steam to LP steam, as a safety in the event the HP steam pressure gets too high or the LP steam pressure gets too low.

Production and flow of steam is controlled in order to maintain the HP and LP steam pressures in each control mode. Four actuators are used to maintain the steam pressures. Six pressure controllers direct the valves, each with a different pressure set point. An additional valve and controller is used to control the LP steam temperature. The main components of the steam system are diagrammed in Figure 4.1.

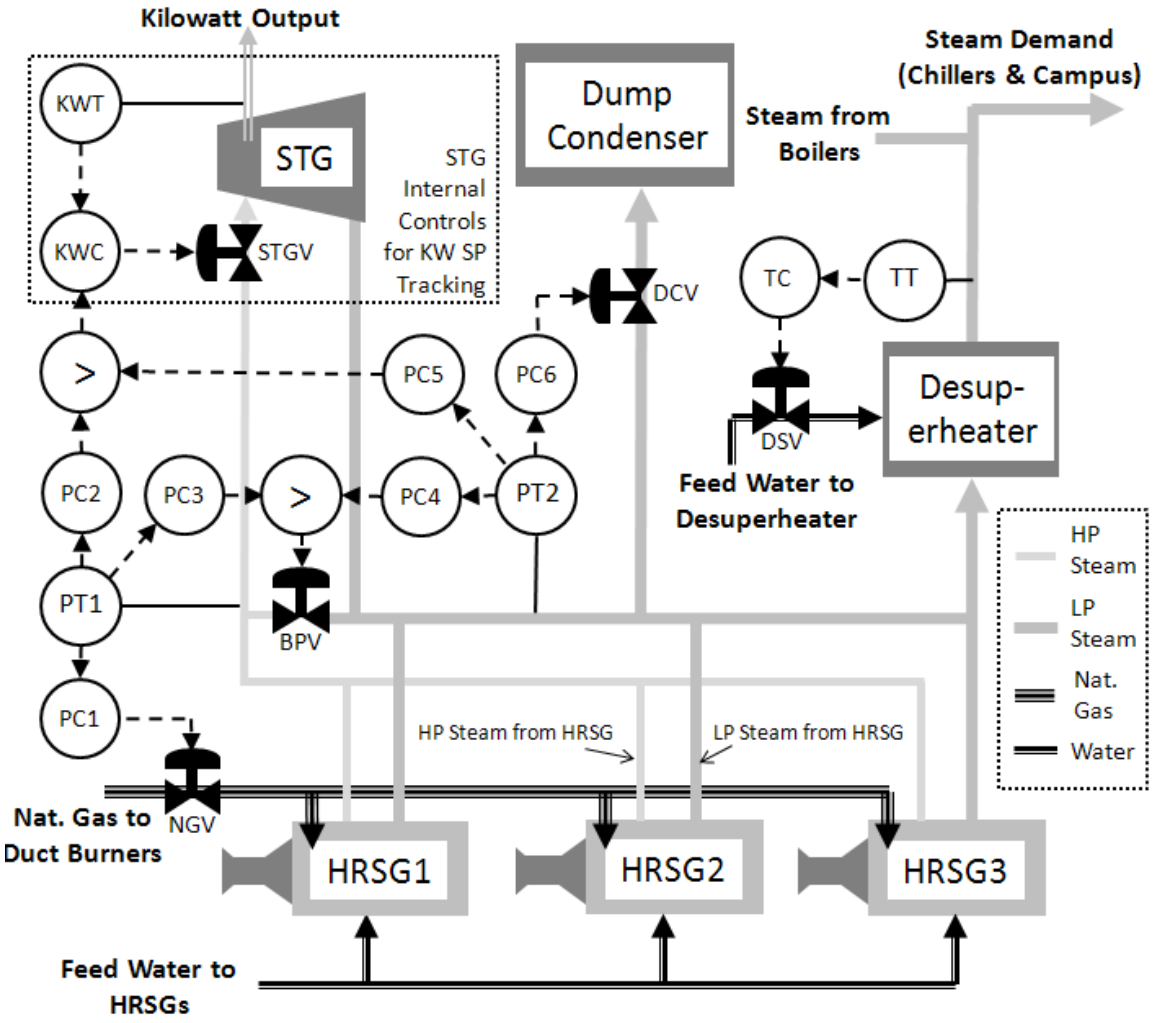

Figure 4.1: Simplified Piping & Instrumentation Diagram of the Steam System

4.2.2 Descriptions of Steam Pressure Processes

There are seven main processes involved in the steam pressure system:

NGV → HP Steam Pressure Process

- Description: The Natural Gas Valve (NGV) is used to regulate fuel flow to the duct burners. The combustion turbine exhaust is used by the HRSGs to produce steam. The duct burners marginally increase steam production from the HRSGs to balance steam production with demand, maintaining a stable HP steam pressure. This is the most common mode of control for the HP steam pressure. When fuel flow to the duct burners is adjusted to control HP steam pressure, the control action also affects LP steam pressure and is considered a disturbance to the LP steam pressure process.
- Process Variable: HP Steam Pressure
- Set Point: 600 psi
- Manipulated Variable: NGV Opening %
- Controller: PC1
- Cogen Condition when in Auto: Balanced Electricity/Steam or Steam Deficient

STGV → STG KW Process

- Description: The Steam Turbine Generator (STG) is used in a combined cycle configuration to produce electrical energy from HP steam generated by the HRSGs. The STG has internal controls that can track a kilowatt (KW) set point; these internal controls cannot be accessed or retuned. The controller adjusts the

STG Valve (STGV) to manipulate steam flow through the turbine to achieve the desired KW output.

- Process Variable: STG KW Output
- Set Point: Generated by HP pressure controller PC2 or LP pressure controller PC5. The larger of the two is selected.
- Manipulated Variable: STGV Opening %
- Controller: KWC
- Cogen Condition when in Auto: All Cases

STG KW → HP Steam Pressure Process

- Description: The power output of the STG is related to the steam flow rate through the STG from the HP side to the LP side. The STG has internal controls that can track a kilowatt (KW) set point. A cascade controller adjusts HP steam pressure by manipulating the KW set point to the STG. This mode of control is used when production of steam, as a byproduct of turbine electricity generation, is greater than demand for steam. The duct burners would already be fully off in this case. When HP steam pressure gets too high, the STG is directed to produce more kilowatts, reducing HP steam pressure, and generating electricity. The LP steam pressure is also affected by the STGs action; the STG is considered a disturbance to the LP steam in this control mode.
- Process Variable: HP Steam Pressure
- Set Point: 625 psi
- Manipulated Variable: STG KW Set Point

- Controller: PC2
- Cogen Condition when in Auto: Excess Steam

BPV → HP Steam Pressure Process

- Description: The Bypass Valve (BPV) is used as a safety to reduce pressure if HP steam pressure becomes very high. The valve is directed to open and HP steam is dumped into the LP side. This causes a major disturbance to the LP steam pressure. The BPV as a safety for the LP side when the pressure is very low. The greater of the two control signals is sent to the valve.
- Process Variable: HP Steam Pressure
- Set Point: 650 psi
- Manipulated Variable: BPV Opening %
- Controller: PC3
- Cogen Condition when in Auto: HP Steam Pressure Too High

BPV → LP Steam Pressure Process

- Description: In this case, the BPV is controlled by the low pressure safety controller on the LP side. The valve is directed to open and HP steam is dumped into the LP side to increase LP steam pressure. This causes a major disturbance to the HP steam pressure.
- Process Variable: LP Steam Pressure
- Set Point: 124 psi
- Manipulated Variable: BPV Opening %

- Controller: PC4
- Cogen Condition when in Auto: LP Steam Pressure Too Low

STG KW → LP Steam Pressure Process

- Description: The power output of the STG is related to the steam flow rate through the STG from the HP side to the LP side. The STG has internal controls that can track a kilowatt (KW) set point. A cascade controller is used to adjust LP steam pressure by manipulating the KW set point to STG. This is the most common mode of control for LP steam pressure. The STG is operated so just enough steam flow is supplied through the STG to meet demand, maintaining stable LP steam pressure. The HP steam pressure is also affected, and the STG is considered a disturbance to the HP steam pressure in this mode. When steam pressure gets too low on the HP side and the duct burners are fully off, the STG is directed to produce more kilowatts, reducing pressure on the HP side.
- Process Variable: HP Steam Pressure
- Set Point: 126 psi
- Manipulated Variable: STG KW Set Point
- Controller: PC5
- Cogen Condition when in Auto: Balanced Electricity/Steam or Steam Deficient

DCV → LP Steam Pressure Process

- Description: The Dump Condenser Valve (DCV) is used to regulate the flow of LP steam sent to the dump condenser. The dump condenser is used to control LP

steam pressure when there is excess steam in the system. This condition exists when the duct burners are fully off, but steam generated as a byproduct of CTG electricity production is greater than demand. In this case, the STG would control the HP steam pressure, and a portion of steam allowed into the LP side is dumped so LP steam pressure remains constant. The dump condenser is also used as a safety if LP steam pressure suddenly increases beyond the acceptable limit. In this event some LP steam is dumped.

- Process Variable: LP Steam Pressure
- Set Point: 128 psi
- Manipulated Variable: DCV Opening %
- Controller: PC6
- Cogen Condition when in Auto: Excess Steam or LP Steam Pressure Too High

4.2.3 Summary of Steam Pressure Control Modes

A summary of the steam system's various control modes, showing the active controllers and actuators at different HP and LP pressure set points, is provided in Figure 4.2.

LP Set Point **HP Set Point**	**124 psi**	**126 psi**	**128 psi**
600 psi	**LP:** PC4, Bypass Valve **HP:** PC1, Duct Burners	**LP:** PC5, STG Cascade **HP:** PC1, Duct Burners	**LP:** PC6, Dump Condenser **HP:** PC1, Duct Burners
630 psi	**LP:** PC4, Bypass Valve **HP:** PC2, STG Cascade	**LP:** Wanders **HP:** PC2, STG Cascade	**LP:** PC6, Dump Condenser **HP:** PC2, STG Cascade
650 psi	**LP:** Wanders **HP:** PC3, Bypass Valve	**LP:** Wanders **HP:** PC3, Bypass Valve	**LP:** PC6, Dump Condenser **HP:** PC3, Bypass Valve

Figure 4.2: Summary of Steam Pressure Controlling Actuators at the Various Set Points

The most typical control mode has been underlined. The term "wanders" indicates the pressure is not being controlled. These are transient states and the process variable will enter a new range where it will be controlled. For instance, when HP steam pressure is being controlled at 630 psi by the STG cascade and the LP is "wandering" between 124 psi and 128 psi, variation in steam supply and demand will cause LP steam pressure to drop lower to 124 psi, or increase to 128 psi, and control will resume.

4.2.4 Disturbances to Steam Pressure Control

Certain steam pressure processes interact with other parts of the system, where they behave as disturbances, as described in Section 4.2.2. There are four additional disturbances to steam pressure:

CTG → HP Steam Pressure Disturbance

- Description: The Combustion Turbine Generators (CTGs) are operated at levels that match campus electricity load. The flow rate of hot exhaust gases produced by the CTGs varies according to the load. That flow rate affects the amount of steam produced by the HRSGs, and consequently the HP and LP steam pressures are disturbed.

CTG → LP Steam Pressure Disturbance

- Description: The CTGs disturb the LP and HP steam pressures as detailed in the CTG → HP Steam Pressure Disturbance description.

Boiler → LP Steam Pressure Disturbance

- Description: The boilers are fired when an additional base load of LP steam is required. This generally occurs during winter months when campus steam demand for heating is high. When the output of the boilers is changed, it causes a disturbance to the LP steam pressure.

Steam Demand → LP Steam Disturbance

- Description: The demand for LP steam from the campus for heating, and from the steam chillers for chilled water production, must always be met. Changes in these flow rates disturb the LP steam pressure.

4.2.5 Steam Temperature Process

An additional process is used to control the LP steam temperature:

DSV → LP Steam Temperature Process

- Description: The desuperheater sprays liquid water into the LP steam to control its temperature and to increase the quantity of the steam. The Desuperheater Valve (DSV) is used to adjust the flow of water sprayed into the LP steam.
- Process Variable: LP Steam Temperature
- Set Point: 400°F
- Manipulated Variable: DSV Opening %
- Controller: TC
- Cogen Condition when in Auto: All conditions

4.3 Dump Condenser Anti-Windup Issue

4.3.1 Review of PI Controller Integral Windup

Integral windup is a control issue that occurs due to the finite operating range of a Final Control Element (FCE). When a valve, one type of FCE, reaches the fully open or fully closed position, the dynamic process model considered during controller tuning is no longer valid. Any decrease in controller output to a valve that is already fully closed, will have no effect on the valve, therefore no effect on the process. The result is the loss of control of the process. When process disturbances subside, and the process returns near its DLO, the controller should be able to resume control of the process within the valve's effective range. If the controller algorithm included integral action, the controller output may have "wound up" while the valve was at its physical limit. The controller continues to integrate error during this period, when the valve has no effect on the process. The integration of the persistent error causes the controller output to grow unbounded. When the process returns to a controllable level, the controller output remains far outside the valve's effective range, and control does not resume as it should.

A process controlled with a PI controller has been simulated to show the effect of integral windup when its FCE, a valve, reaches its limit by closing completely. The valve cannot shut beyond its physical limit of 0% open, yet the controller output continues to drop below 0%. The simulation results are shown in Figure 4.3.

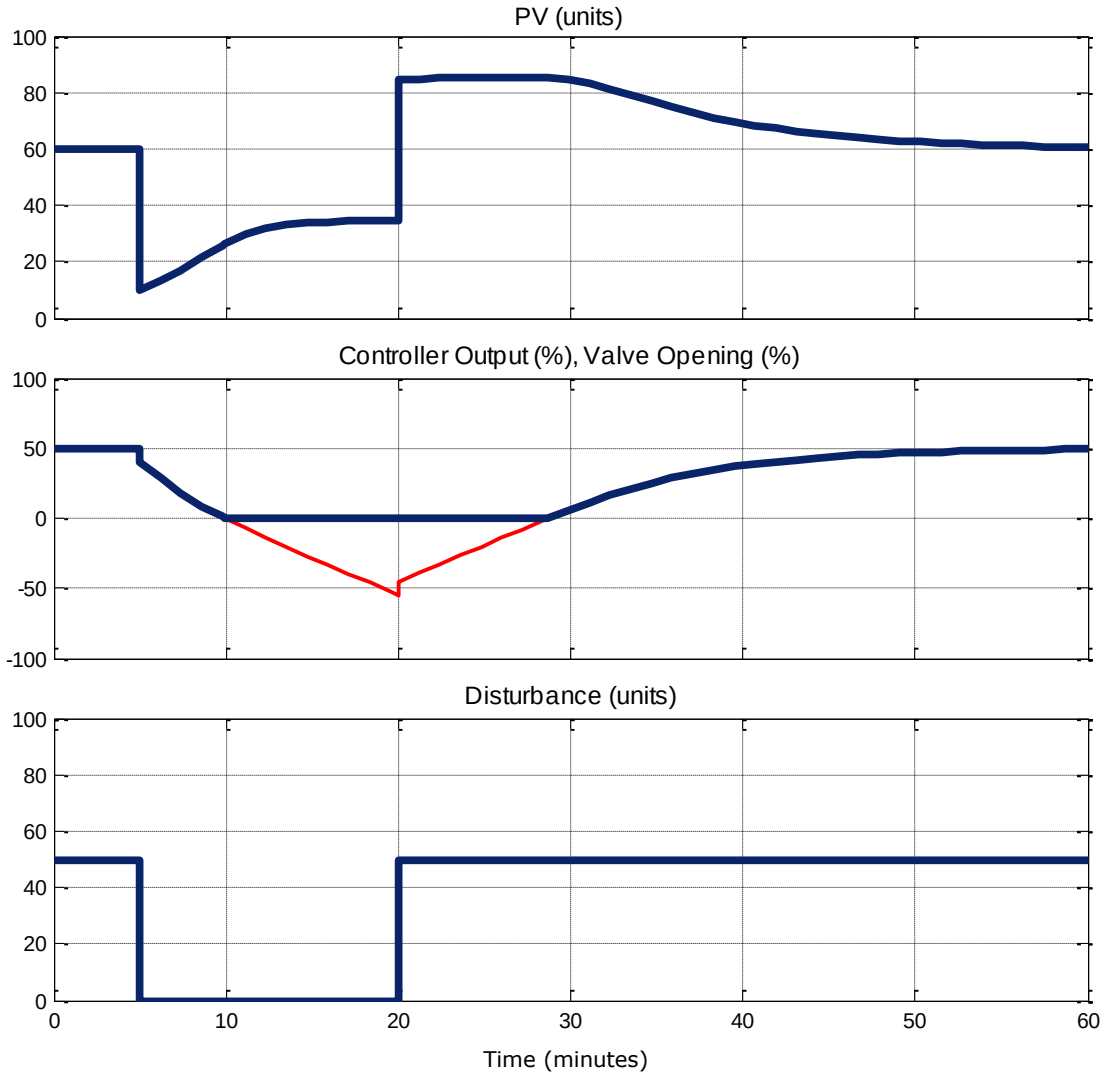

Figure 4.3: Process Simulation, Controller Integral Windup Beyond Valve Physical Limit

The objective of the system shown in Figure 4.3 is to maintain a set point PV = 60. At time = 5 minutes, a disturbance to the process occurs. The valve reaches its fully closed position at a controller output of 0%. The controller continues to wind up below 0%. When the disturbance is removed at time = 20 minutes, the controller output is well below the physical limit of the valve. The controller isn't able to affect the process until the controller output gets above 0% at time = 29 minutes.

Jacketing logic can be used to change the behavior of a controller under certain conditions. Jacketing logic can be applied to stop integral windup when the FCE reaches its limit. This type of jacketing logic is known as "anti-windup" logic. The simulation from Figure 4.3 is modified to include anti-windup logic to stop integral wind up when the controller output and valve reach 0%. The results are shown in Figure 4.4.

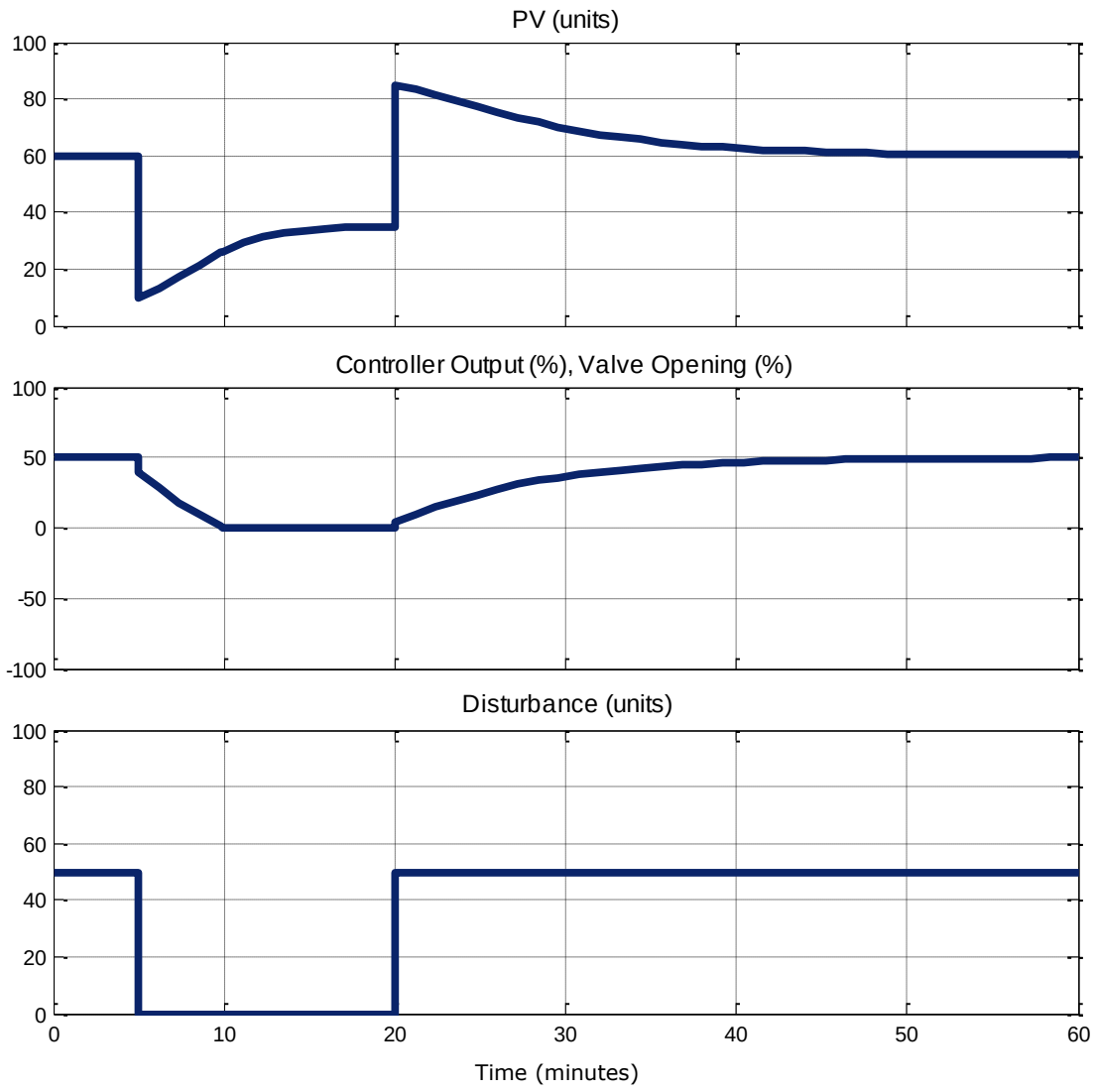

Figure 4.4: Process Simulation, Controller Anti-Windup Jacketing Logic

Again, a disturbance to the process occurs at time = 5 minutes. The valve reaches its fully closed position at a controller output of 0%. This time, the jacketing logic stops the controller output from winding up. When the disturbance is removed at time = 20 minutes, the controller output is able to resume control immediately.

4.3.2 Description of Dump Condenser Anti-Windup Issue

The process of Figure 4.4 is similar to the operation of the DCV→LP Steam Pressure process. Normally, the LP steam pressure is at 126 psi, below the LP steam pressure set point for the DCV→LP Steam Pressure process, 128 psi. This causes the DCV to fully close, and anti-windup jacketing logic is used to prevent the controller from integrating below zero.

The dump condenser is included in the piping and instrumentation diagram of the steam system provided in Figure 4.1. The dump condenser's role in the cogen steam pressure control system is included in Figure 4.2. When HP steam pressure is too high, the STG cascade stops controlling the LP side in order to control HP steam pressure. The LP steam pressure subsequently rises on the LP side until it becomes greater than 128 psi. When this happens, the DCV opens and begins to operate within its useful range, controlling the LP steam pressure at 128 psi.

The dump condenser anti-windup logic can also cause a control issue. When the STG cascade is controlling the LP steam pressure at 126 psi (below the dump condenser LP steam pressure set point), rapid movements may occur in the LP pressure. The dump condenser's PI controller with anti-windup can cause the DCV to "pop open," wasting

steam and degrading STG cascade pressure control. A plot of this phenomenon is provided in Figure 4.5.

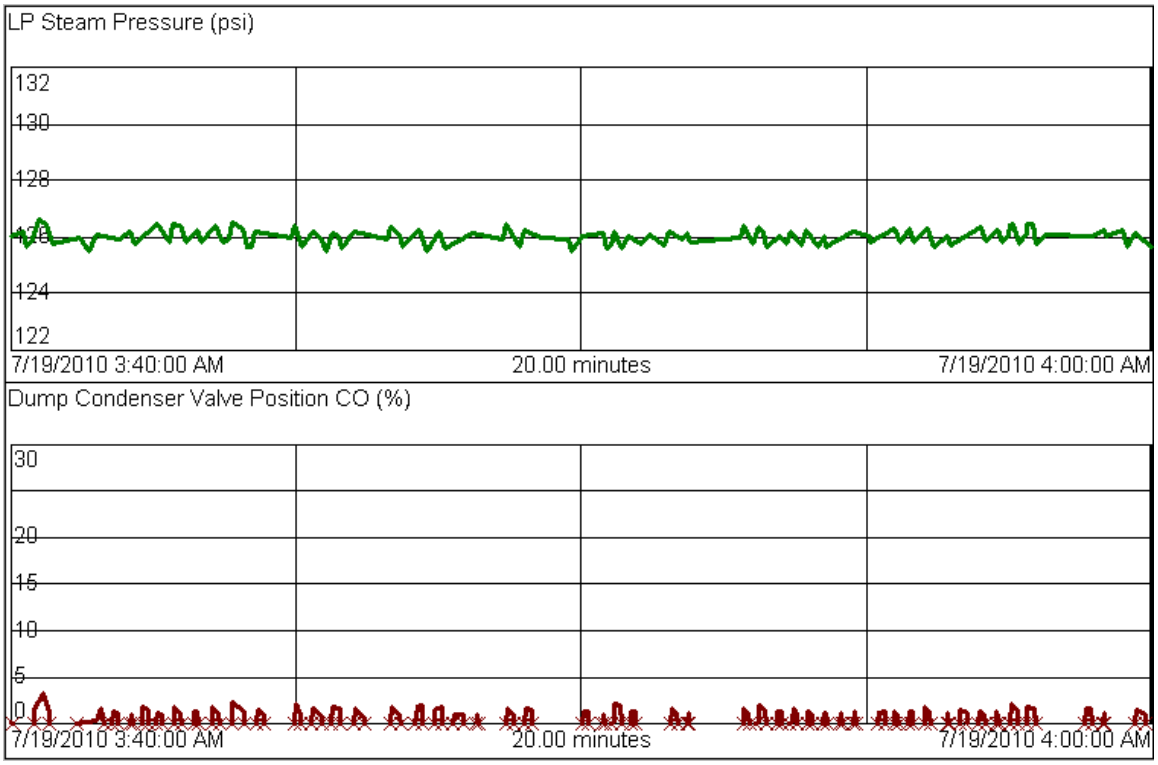

Figure 4.5: LP Steam Pressure, and DCV "Popping Open"

The phenomenon of Figure 4.5 can be explained by examining the math and logic used to generate a PI with anti-windup control signal. When a final control element is at its limit of operation, the controller output is clamped by the controller. If it has reached its lower limit, the controller output will not be allowed to decrease. The logic will only allow the controller output to change if the algorithm calls for an increase in controller output. The discretized velocity form of the PI controller, the algorithm used by the Allen-Bradley controllers at the UConn Cogen Plant, is given in Equation 4.1.

$$CO_n = CO_{n-1} + K_C(E_n - E_{n-1}) + K_I E_n \Delta t \qquad \text{Equation 4.1}$$

CO_n is the current controller output to the valve and CO_{n-1} is the controller output at the previous time step. E_n is the current error, calculated as SP-PV, and E_{n-1} is the error calculated at the previous time step. Δt is the elapsed time between time steps. K_C and K_I are the proportional and integral tuning values, respectively.

The discretized velocity form of the PI control algorithm stores the previous value of the controller output and makes changes based on previous and current values of error. When anti-windup jacketing logic is used, and the controller output is at its lower limit, the algorithm adjusts the controller output as follows:

$$CO_n{}' = CO_{n-1} + K_C(E_n - E_{n-1}) + K_I E_n \Delta t$$

$$IF(CO_n{}' > CO_{n-1}) \qquad THEN(CO_n = CO_n{}') \qquad ELSE(CO_n = CO_{n-1})$$

This introduces the potential for a problem. If the change in error times the proportional gain, $K_C(E_n - E_{n-1})$, is greater than the error times the integral gain times the time step, $K_I E_n \Delta t$, and in the opposite direction, then the controller could direct the final control element to change in a direction that would increase error. This problem is shown in the DCV→LP Pressure control loop in Figure 4.5.

4.3.3 FOPDT Modeling and PI Tuning Using the IMC Method

It's possible to add customized logic to help reduce the undesirable effect shown in Figure 4.5. However, any logic must consider that the dump condenser is a vital safety component in the steam system, and should not be disabled. Additionally, the dump condenser must act as the primary LP steam pressure controller when there is excess

steam in the system that needs to be dumped. It is good policy to search for a simpler solution before adding more logic complexity.

An inspection of the velocity form PI control algorithm, Equation 4.1, reveals, if $K_C(E_n - E_{n-1}) < K_I E_n \Delta t$, then the controller output will not be increased. Increasing the ratio of K_I/K_C would reduce the undesirable control action. To assess the feasibility of this strategy, the DCV→LP Steam Pressure process is bumped and modeled according to the strategy of Section 1.5. The results are shown in Figure 4.6.

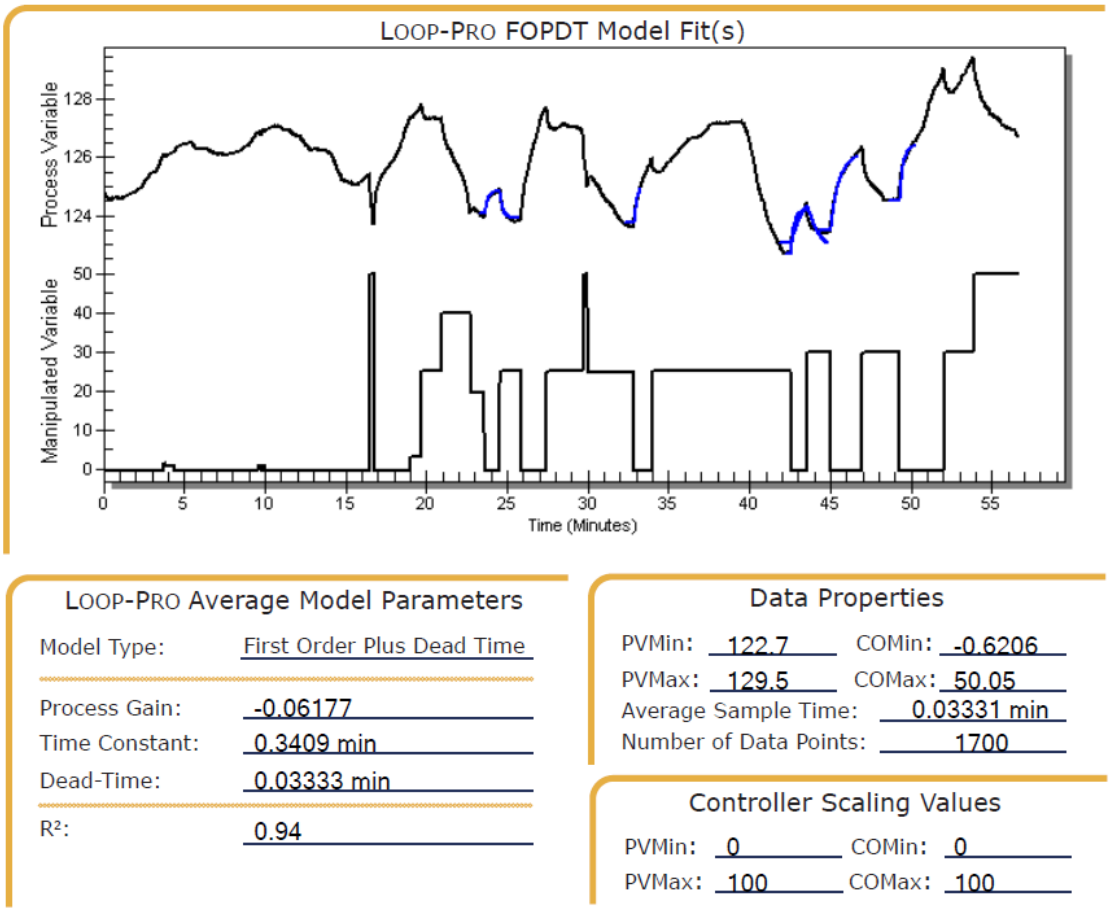

Figure 4.6: LP Steam Pressure Dynamic Response to Change in DCV Position and FOPDT Approximation

There are numerous disturbances to LP steam pressure during the tests, such as campus steam demand, which cannot be held constant. Large steps in DCV position are conducted so the effect of the DCV dominates the response in the LP steam pressure. An average of the individual step responses are taken to produce a process model. The model is used to derive PI tuning values according to the IMC strategy outlined in Section 1.5. The resultant dump condenser LP proportional gain, $K_{C,DCLP}$ and integral gain, $K_{I,DCLP}$, values are as follows:

$$K_{C,DCLP} = -17\ \%/psi \qquad K_{I,DCLP} = -49\ \%/psi \cdot min$$

The tuning values that were previously in place, which resulted in the dump condenser behavior of Figure 4.5, were as follows:

$$K_{C,DCLP} = -16\ \%/psi \qquad K_{I,DCLP} = -4\ \%/psi \cdot min$$

The new tuning values increase the K_I/K_C ratio from 0.25 to 2.9. This implies that the new values can help correct the anti-windup issue.

4.3.4 Results

The control action after the new tuning values are entered is shown in Figure 4.7.

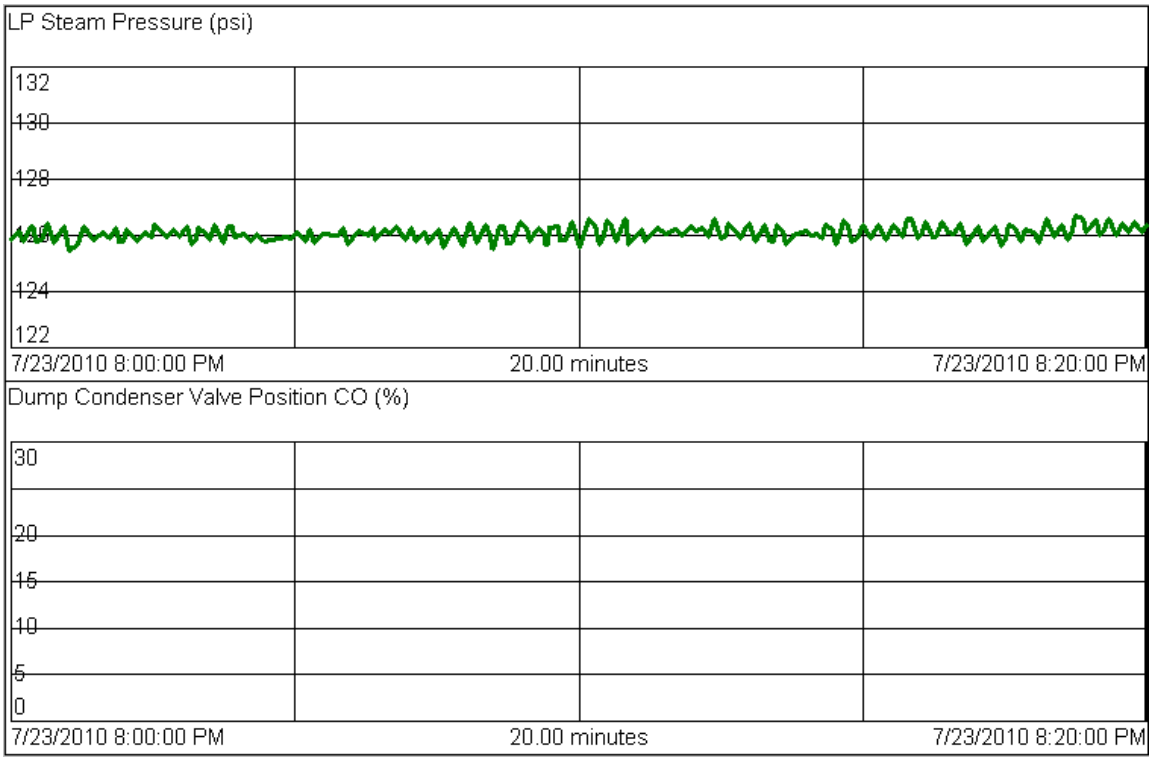

Figure 4.7: LP Steam Pressure, and Dump Condenser Valve Position with New Tuning

Figure 4.7 shows the dump condenser valve no longer "pops open" when the LP steam pressure is below the dump condenser pressure set point. It is also important that LP steam pressure is effectively controlled when the dump condenser is the primary controller. Figure 4.8 shows the LP steam pressure control when the dump condenser is in control, at set point = 128 psi. The control performance is shown before and after the new controller tuning values are entered.

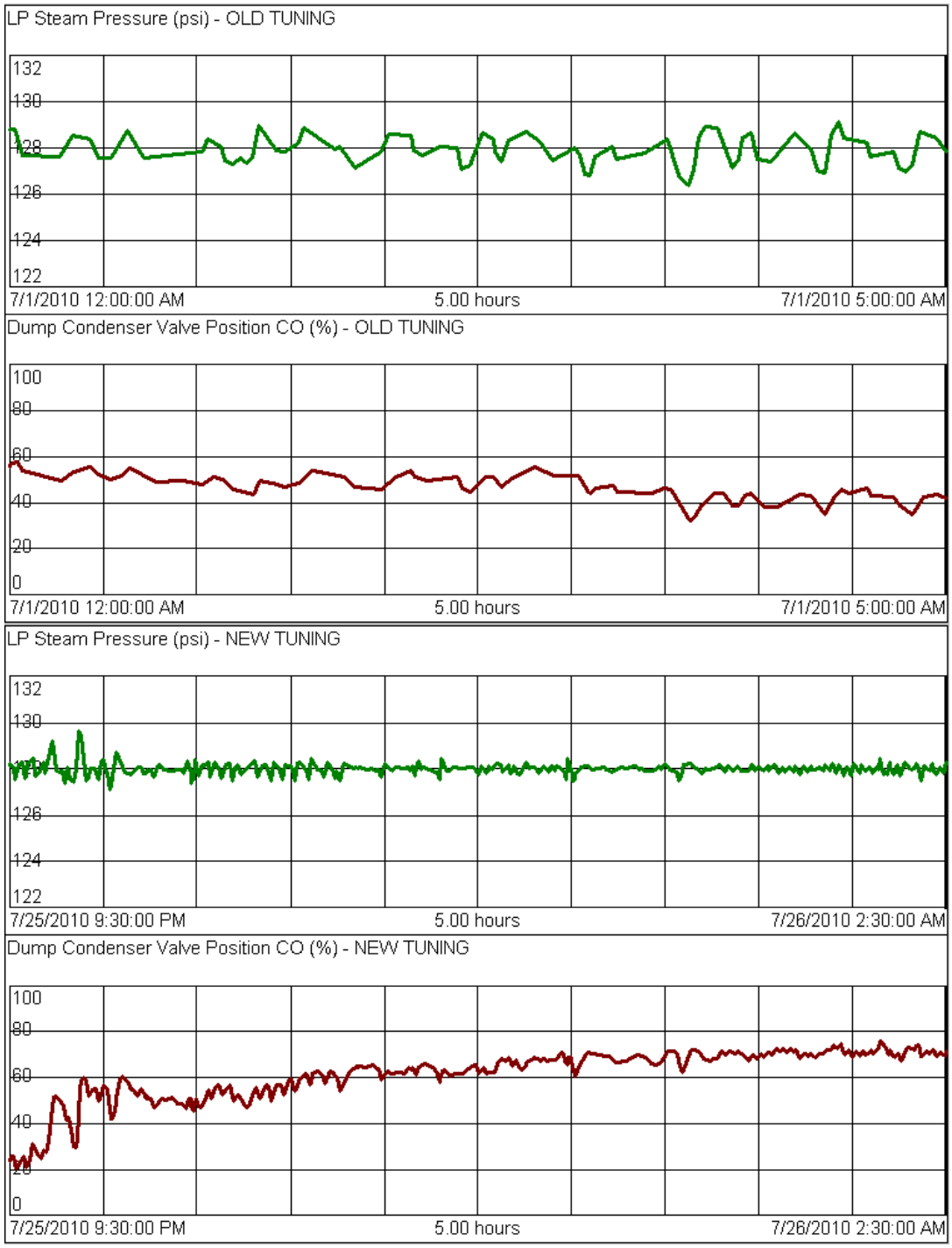

Figure 4.8: LP Steam Pressure, and Dump Condenser Valve Position Before and After Tuning

Figure 4.8 confirms that the new tuning values also improve LP steam pressure control when the dump condenser is the primary controller. The dump condenser also behaves as

a safety mechanism, preventing LP steam pressure from rising too high. It needs to be tuned aggressively to ensure the LP steam pressure doesn't become dangerously high. Both tuning values, $K_{C,DCLP}$ and $K_{I,DCLP}$, were increased. Therefore, the system is more aggressive than with the previous tunings, ensuring the safety functionality is preserved.

4.3.5 Conclusions

The new tuning values have improved the dump condenser functionality. The anti-windup issue has been corrected, main control functionality has been improved, and safety performance has been preserved. The classical SISO feedback structure, tuned using an FOPDT model from bump test data and IMC PI tuning correlations, is the most basic control strategy proposed in this paper. Its application to the dump condenser is further demonstration of its effectiveness in industrial process control.

4.4 Application of PID Control to LP Steam Temperature Process

4.4.1 Overview of the LP Steam Temperature Process and Oscillation Issue

The LP steam temperature is controlled by adjusting the amount of water sprayed into the LP steam using the desuperheater. The desuperheater is included in the piping and instrumentation diagram of the steam system provided in Figure 4.1. The temperature control system uses a traditional SISO feedback structure. In the past, a PI controller was used as shown in Figure 4.9.

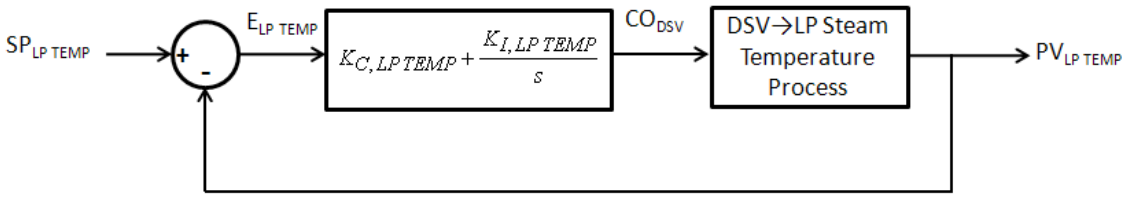

Figure 4.9: LP Steam Temperature Control Structure

The LP steam temperature, $PV_{LP\,TEMP}$, and the controller output to the DSV, CO_{DSV}, were exhibiting oscillations as shown in Figure 4.10.

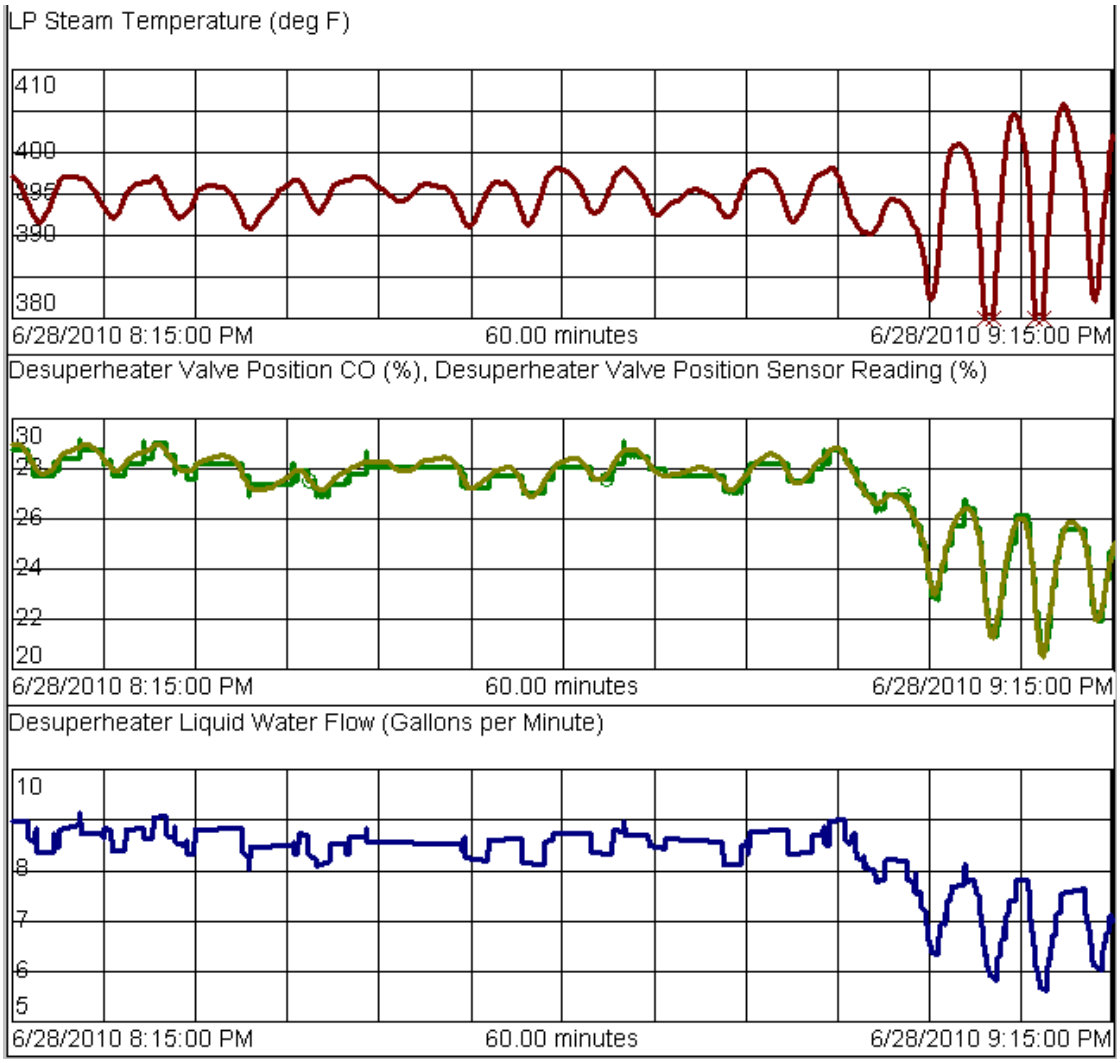

Figure 4.10: Oscillations in LP Steam Temperature, Controller Output to DSV, DSV Position Sensor Reading, Liquid Water Flow Rate to Desuperheater

The LP steam temperature appears to oscillate around the LP temperature set point, 390°F. When these oscillations cause steam temperature to drop below a certain point, the oscillations become worse. It is believed that when the steam temperature drops too low, liquid water sprayed by the desuperheater reaches the temperature sensor before a thermodynamic equilibrium is reached between the liquid and vapor phases. This causes the temperature sensor reading to drop dramatically, and control performance is ruined. This process nonlinearity is clearly shown in Figure 4.11. Once LP steam temperature

drops below a certain threshold, it tends to quickly fall to the LP steam saturation temperature, approximately 360°F.

Another control issue is evident in Figure 4.10. The DSV is equipped with a position sensor. Data from this sensor is superimposed on the CO_{DSV} data in Figure 4.8. The position should be tracking CO_{DSV}, however, the valve appears to be sticking, causing choppy movements and imprecise control. The valve issue is confirmed by the liquid water flow rate, which exhibits the same pattern, also shown in Figure 4.10.

4.4.2 FOPDT Modeling and PID Tuning using the IMC Method

PI controllers are typically favored over PID controllers in most processes. Theoretically, PID controllers can provide improved performance by speeding response time and damping oscillations [7]. This improved performance comes at a cost. The derivative term of the PID controller demands greater "effort" by the valve it controls. Small movements in the process variable and sensor noise are amplified by the derivative term causing strong and fast valve motion. This extra effort can cause increased wear and tear on valves. In practice, the derivative term is frequently cascaded through a low pass filter to reduce this high frequency amplification [1]. Because PI controllers generally provide adequate performance, the PID controller is sometimes avoided.

In the case of the LP temperature control system, a PID controller is appropriate. The system exhibits oscillations that require damping. The stronger control action produced by the PID controller is a benefit in this case. It can be used to help break through the valve stickiness. To tune the PID controller, the DSV→LP Steam Temperature process

is bumped and modeled according to the strategy of Section 1.5. The results are shown in Figure 4.11.

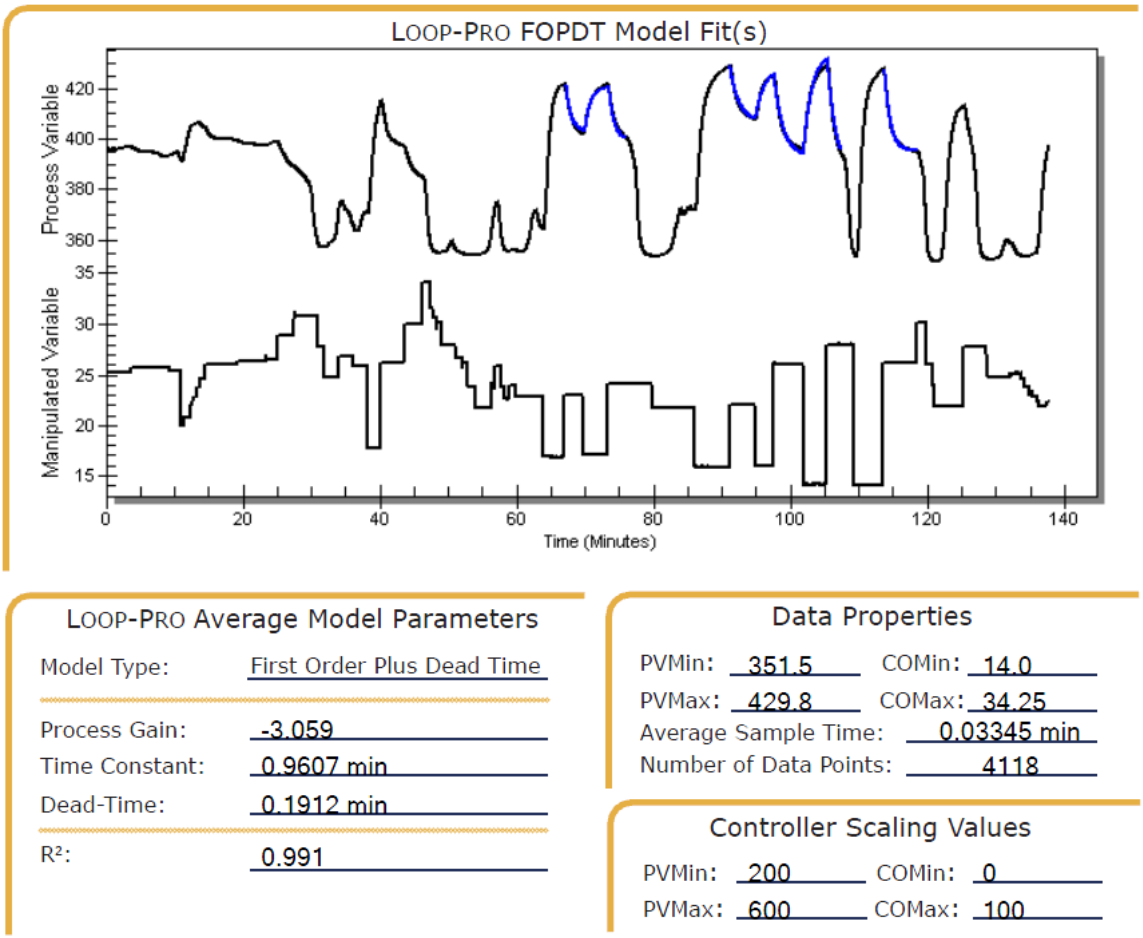

Figure 4.11: LP Steam Temperature Dynamic Response to Change in CO_{DSV} and FOPDT Approximation

The FOPDT model is used to generate tuning values using the IMC correlations for PID controllers. The correlations are as follows [5]:

$$K_C = \frac{\tau_P + 0.5\theta_P}{K_P(\tau_C + 0.5\theta_P)} \qquad K_I = \frac{K_C}{\tau_P + 0.5\theta_P} \qquad K_D = \frac{\tau_P \theta_P}{2K_P(\tau_C + 0.5\theta_P)}$$

The heuristic introduced in Section 1.5.2.1 is used to select a closed loop time constant, τ_C, for IMC tuning. The heuristic targets a 10-15% overshoot in the closed loop set point tracking response. The resultant PID tuning values for the LP temperature controller are:

$K_{C,LP\,TEMP} = -2.5\ \%/°\text{F}$ $K_{I,LP\,TEMP} = -2.4\ \%/°\text{F} \cdot min$

$K_{D,LP\,TEMP} = -0.22\ \% \cdot min/°\text{F}$

4.4.3 Results

The LP steam temperature process is shown in Figure 4.12. The new tuning values are entered approximately midway through the plot.

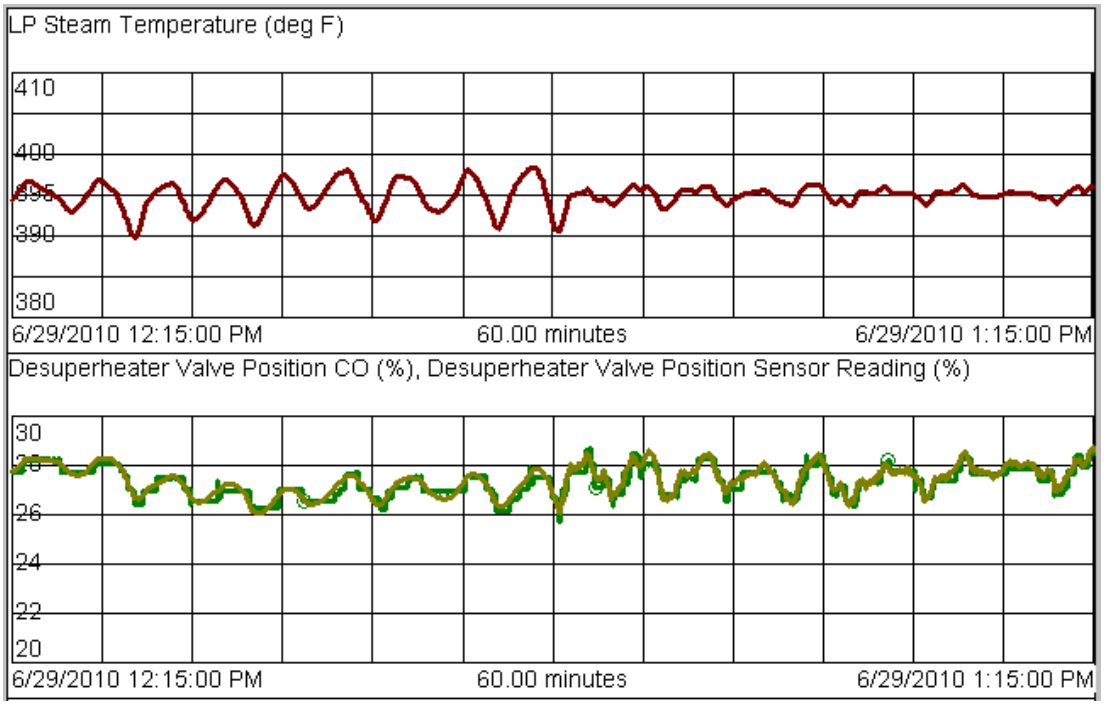

Figure 4.12: LP Steam Pressure Process Data, Showing the Switch from PI to PID control

Figure 4.12 shows that the PID controller reduced the amplitude of the oscillations in LP steam temperature from approximately 4°F to approximately 1°F. The increased control action of the DCV reduces the effects of valve sticking. The improved control stops the

LP steam temperature from dropping too low into its nonlinear range, protecting the effectiveness of the process.

4.4.4 Conclusions

The basic control strategy proposed in this paper has been adjusted to include a PID controller tuned using the IMC method. The PID controller and new tuning values reduce oscillations in LP steam temperature by 75% and enhance control performance. The SISO structure, FOPDT dynamic model and IMC PID tunings are applied successfully. The application of the strategy to the desuperheater is further proof of its dependability in industrial process control.

4.5 Boiler Feed Water Pressure Controller Tuning

4.5.1 Overview of Boiler Feed Water System

The UConn Cogen Plant operates boilers when the HRSGs cannot produce enough steam to meet campus steam load. High Pressure (HP) feed water at 800 psi is used for HRSG steam generation. This HP feed water is reduced to Low Pressure (LP) feed water at 225 psi and subsequently used by the boilers to generate LP steam. A simplified piping and instrumentation diagram of the process is presented in Figure 4.13. The LP steam from the boilers is shown entering the steam system's LP header in Figure 4.1.

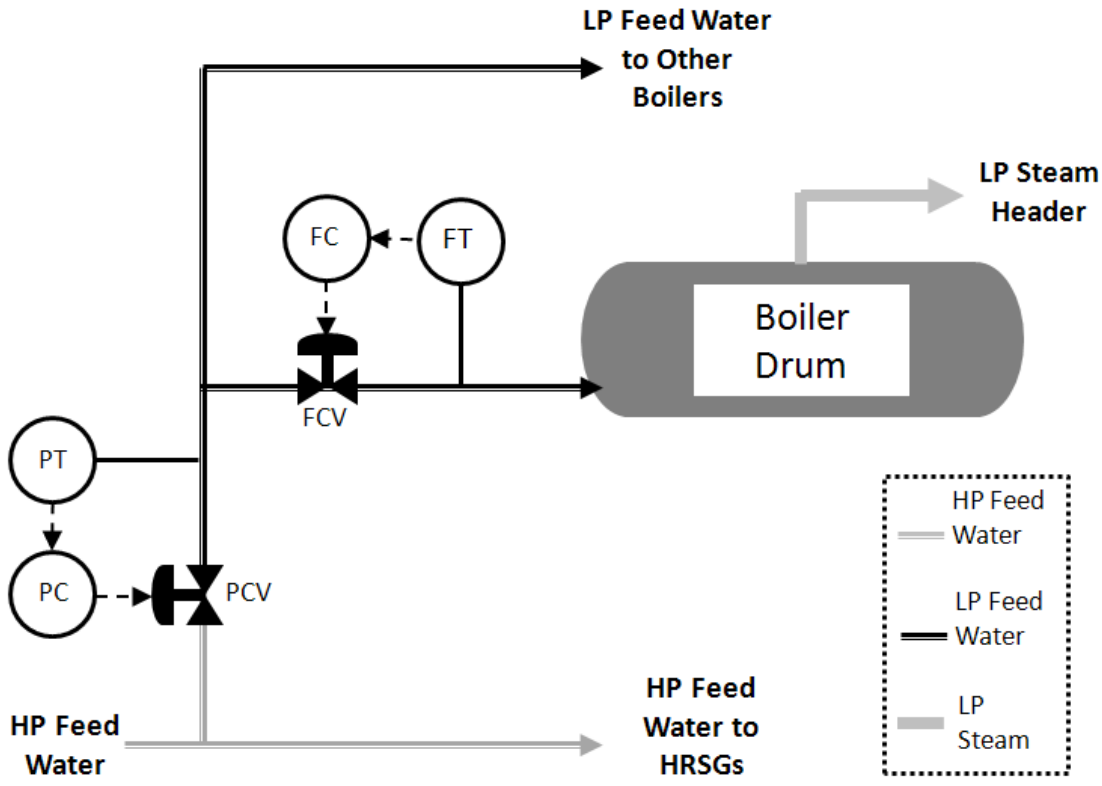

Figure 4.13: Simplified Piping & Instrumentation Diagram of Boiler Feed Water System

The LP feed water pressure is controlled by the pressure controller, PC, and actuated by the Pressure Control Valve, PCV. The pressure transmitter, PT, sends a pressure reading to the PC used for feedback control. The system reduces and controls feed water pressure, eliminating disturbances to the feed water flow control processes to each boiler.

4.5.2 FOPDT Modeling and PI Tuning using the IMC Method

The cogen plant commissioned a new PCV, which required tuning. The Flow Control Valve, FCV, to each boiler is held constant to perform bump tests of the PCV→LP Feed Water Pressure Process. An FOPDT model of the process is fit according to the tuning strategy of Section 1.5, and the results are presented in Figure 4.14.

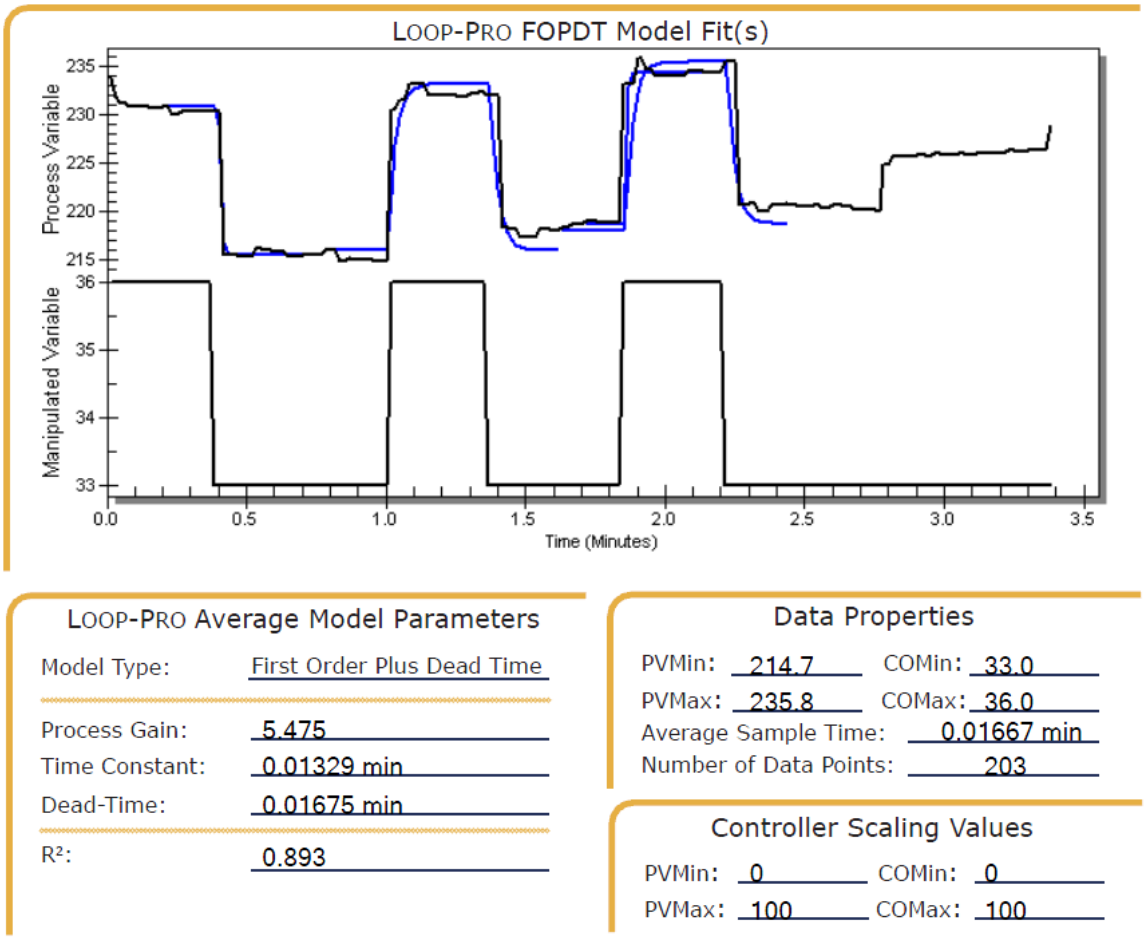

Figure 4.14: Boiler Feed Water Pressure Dynamic Response to Change in PCV CO and FOPDT Approximation

Multiple FOPDT models are fit to different pieces of the data of Figure 4.14. An average of the models is used for tuning purposes. The model is used to derive PI tuning values according to the IMC strategy outlined in Section 1.5. The resulting boiler feed water pressure tuning values, $K_{C,BFP}$ and $K_{I,BFP}$, are as follows:

$$K_{C,BFP} = 0.042\ \%/psi \qquad K_{I,BFP} = 3.2\ \%/psi \cdot min$$

4.5.3 Results

Although the system is used to reject disturbances to the LP feed water pressure, a closed loop, set point step response can be used to assess the effectiveness and stability of the tuning. Closed loop, LP feed water pressure, set point step response data is provided in Figure 4.15. Figure 4.15 shows that the tuning values provide set point tracking with a small overshoot.

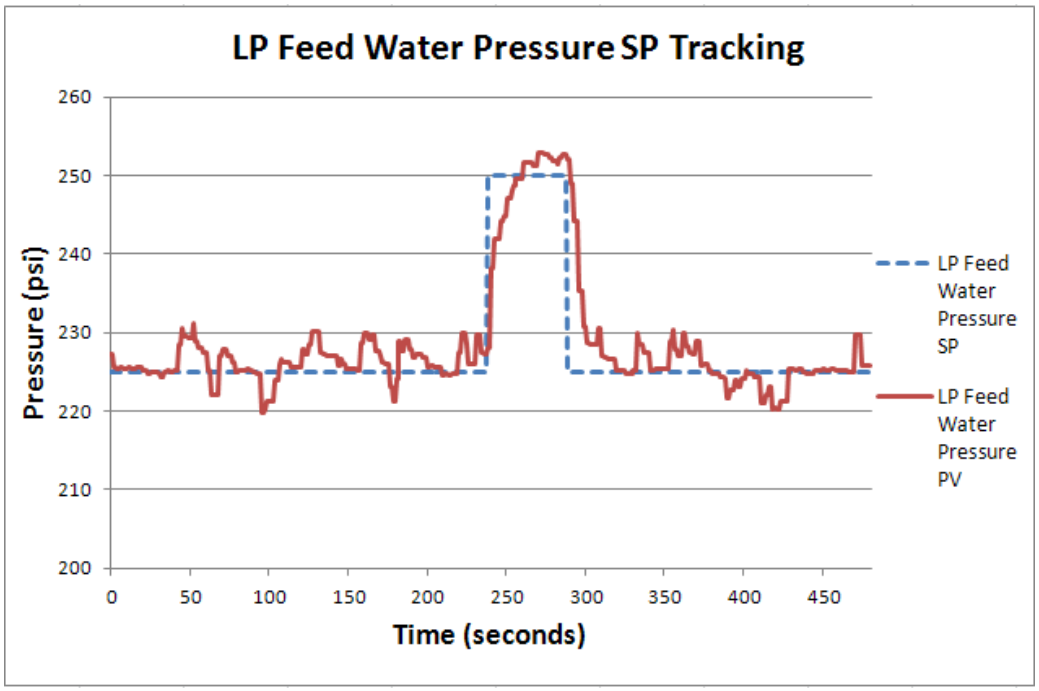

Figure 4.15: LP Feed Water Pressure Set Point Tracking Response

4.5.4 Conclusions

The boiler feed water pressure control response shows minimal overshoot, as preferred by the UConn Cogen Plant. A single bump test and simple calculation provided satisfactory control performance. The IMC tuning method allows the control engineer to tune processes with ease and confidence. These results are further evidence that the tuning strategy described in this thesis is effective and practical for industrial application.

GENERAL CONCLUSIONS

This thesis has demonstrated the effectiveness of several classical control strategies. The classical SISO feedback control structure, the FOPDT process model, the IMC PI tuning strategy, feed forward and cascade control are shown to provide satisfactory control in the studies presented. The strategies provide dependable dynamic process control. The simplicity and ease of implementation of the strategies presented are considered to be self-evident. Simplicity is essential to the UConn Cogen Plant, and other small scale, yet complex plants. The strategies produce effective control with simple logic, helping to simplify the maintenance of a plant's control systems along with the plant evolution.

REFERENCES

[1] Ang, Kiam Heong; Chong, Gregory; Li, Yun. "PID Control System Analysis, Design and Technology." IEEE Transactions of Control Systems Technology, Vol. 13, No. 4, 2005, p. 559-576.

[2] Bender, William R. "Lean Pre-Mixed Combustion." The Gas Turbine Handbook – National Energy Technology Labrotory. Accessed March 28, 2011. <www.netl.doe.gov/technologies/coalpower/turbines/refshelf/handbook/3.2.1.2.pdf>

[3] "Conservative Design Assures Top Operational Flexibility, Reliability." Combined Cycle Journal, Fourth Quarter 2007, p. 71-74.

[4] Cooper, Douglas J. "Practical Process Control: Proven Methods and Best Practices for Automatic Process Control." Accessed April 15, 2011 <www.controlguru.com>

[5] Cooper, Douglas J. “Practical Process Control using Loop-Pro Software.” Tolland: Control Station Inc., 2005.

[6] Doty, Steve; Turner, Wayne C. “Energy Management Handbook” 7th Edition. Lilburn: The Fairmont Press, Inc., 2009, p. 287-288.

[7] Franklin, Gene F.; Powell, J. D.; Emami-Naeini, Abbas. “Feedback Control of Dynamic Systems.” 6th Edition. Upper Saddle River: Pearson Higher Education Inc., 2010.

[8] Forzatti, Pio. “Present Status and Perspectives in De-NO_X SCR Catalysis,” Applied Catalysis A: General 222, 2001, p. 221.

[9] Krishnaswamy, R. Peruvemba; Rangaiah, Gade P.; Jha, Radha K.; Deshpande, Pradeep B. “When to Use Cascade Control.” Ind. Eng. Chem. 1990, 29, 2163–2166.

[10] Langston, Lee. “A Greener, Less Expensive Cogeneration Plant.” Mechanical Engineering Magazine, December 2006.

[11] Lietti, Luca; Nova, Isabella; Camurri, Stefano; Tronconi, Enrico; Forzatti, Pio. “Dynamics of the SCR-DeNO_X Recaction by the Transient-Response Method.” AIChE Journal, Vol. 43, No. 10, 1997, p. 2559-2570.

[12] Ljung, Lennart. “System Identification Theory for the User.” Englewood Cliffs: Prentice-Hall, Inc., 1987.

[13] Moran, Michael J.; Shapiro, Howard N.; Boettner, Daisie D.; Bailey, Margaret B. “Fundamentals of Engineering Thermodynamics.” 7th Edition. Hoboken: John Wiley and Sons, Inc., 2010, p. 741-762.

[14] Marlin, Thomas E. “Process Control: Designing Processes and Control Systems for Dynamic Performance.” 2nd Edition. Boston: McGraw Hill Inc., 2000, p. 462-492.

[15] Ogunnaike, B. A.; Ray, W. H. “Process Dynamics, Modeling, and Control.” New York: Oxford University Press, 1994, p. 533.

[16] Pavri, Roointon; Moore, Gerald D. “Gas Turbine Emissions and Control,” General Electric, 2001, p. 2.

[17] “Plant Overview.” UConn PI WebServer. Accessed May 1, 2011 <http://energyservices.uconn.edu/Cogen%20Plant/Plant%20Overview.aspx>

[18] Rivera, D. E.; Morari, M.; Skogestad, S. “Internal Model Control: PID Controller Design.” Ind. Eng. Chem. 1986, 25, 252–265.

[19] Smith, Carlos A.; Corripio, Armando B. “Principles and Practice of Automatic Process Control.” 2nd Edition. Hoboken: John Wiley and Sons, Inc., 1997, p. 494-518

[20] Stanford, Herbert W. “HVAC Water Chillers and Cooling Towers: Fundamentals, Application, and Operation” New York: Marcel Dekker, Inc., 2003.

[21] “Storrs Campus.” University of Connecticut Website. Accessed May 1, 2011 < http://www.uconn.edu/storrs-campus.php>.

APPENDIX A: Permission for Use of Copyrighted Material

Permission to Use Copyrighted Material

Dear Mr. Burns:

Control Station, Inc. hereby grants you permission to use parts of the following material:

Book Title: Practical Process Control
Author: Douglas J. Cooper
Copyright: 2005 by Control Station, Inc.

The material will be used as follows:

Incorporated into a thesis to be submitted in fulfillment of the requirements for the degree of Master of Science at the University of Connecticut, 2011.

Sincerely,

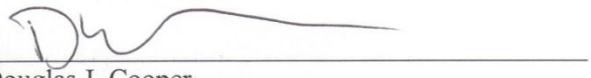

Douglas J. Cooper

Company: Control Station, Inc.

Date: 5/4/2011

APPENDIX B: Fan Speed→Temperature Process Bump Tests with FOPDT Approximations

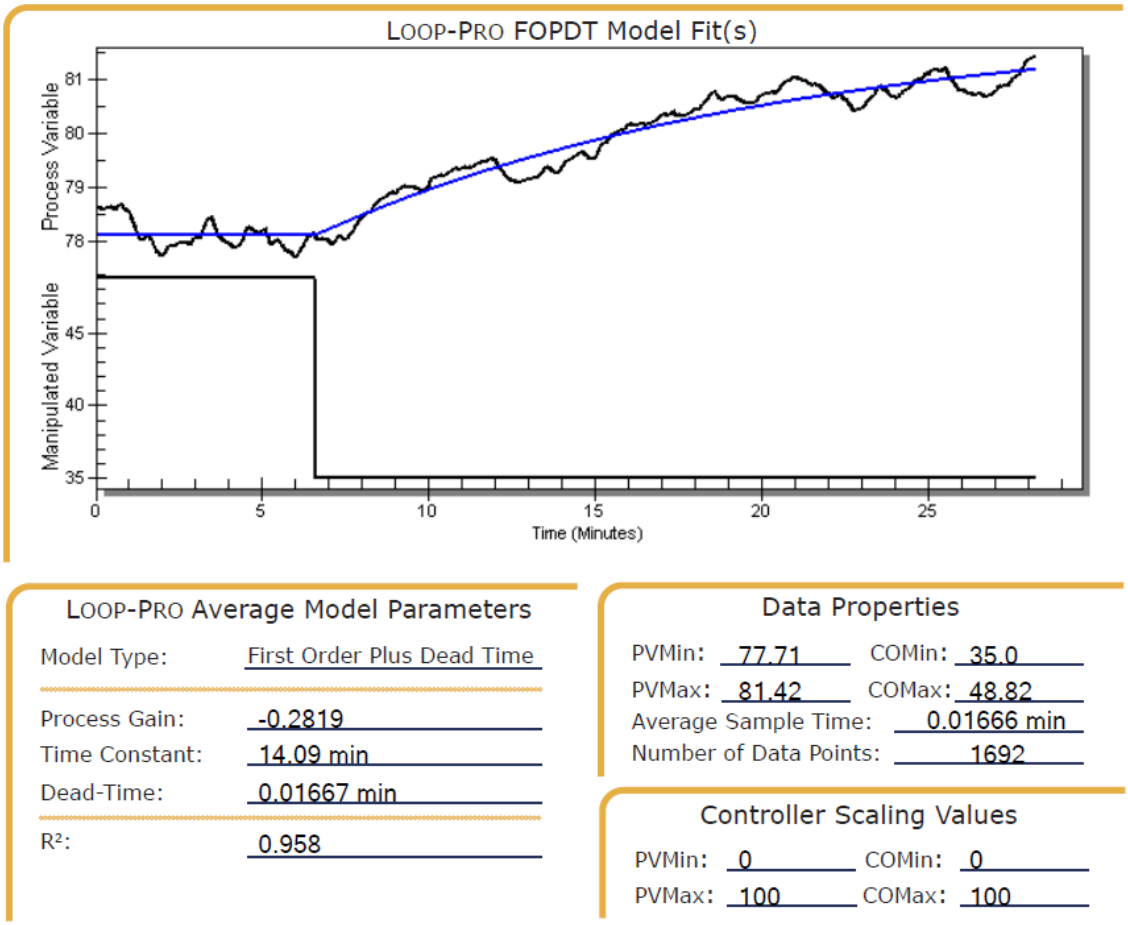

Figure B.1: Temperature Dynamic Response to Change in Fan Speed with 1 Fan Running and FOPDT Approximation

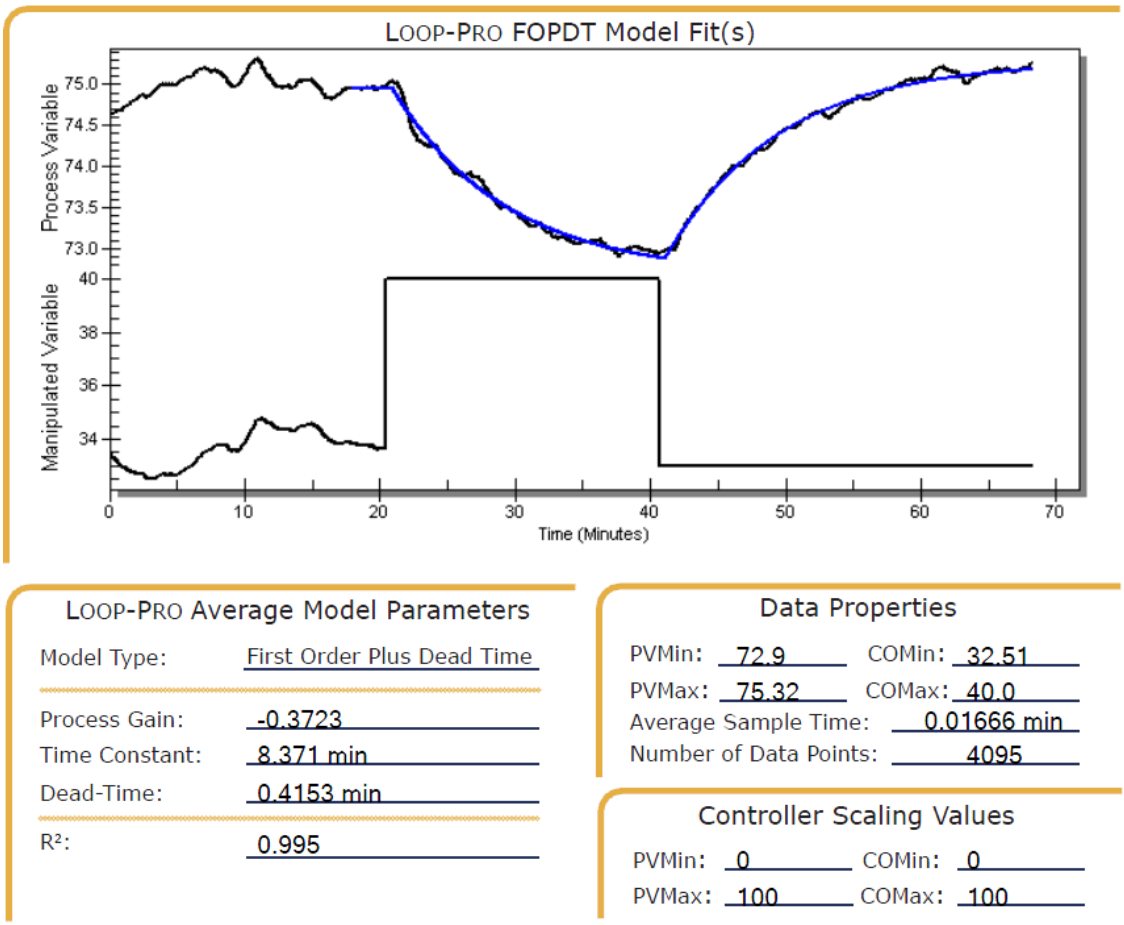

Figure B.2: Temperature Dynamic Response to Change in Fan Speed with 4 Fans Running and FOPDT Approximation

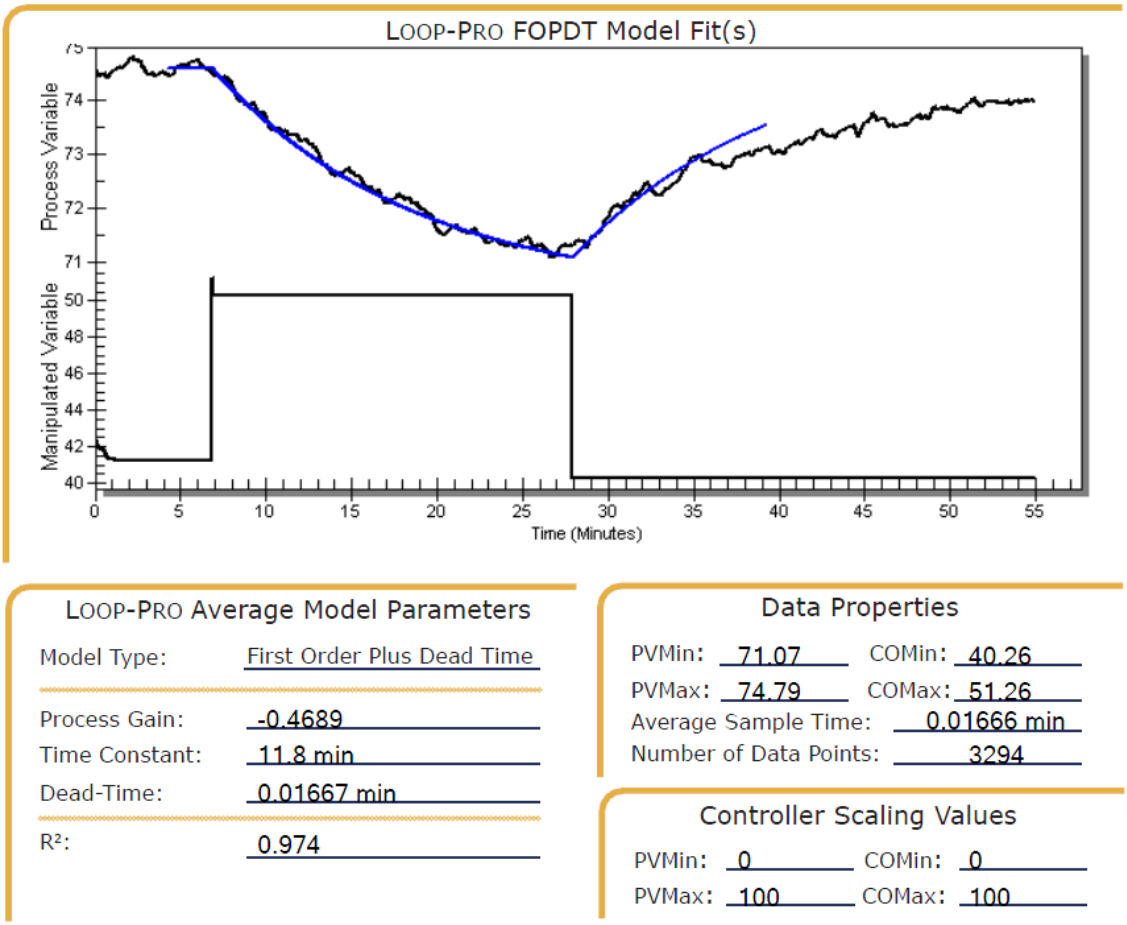

Figure B.3: Temperature Dynamic Response to Change in Fan Speed with 5 Fans Running and FOPDT Approximation

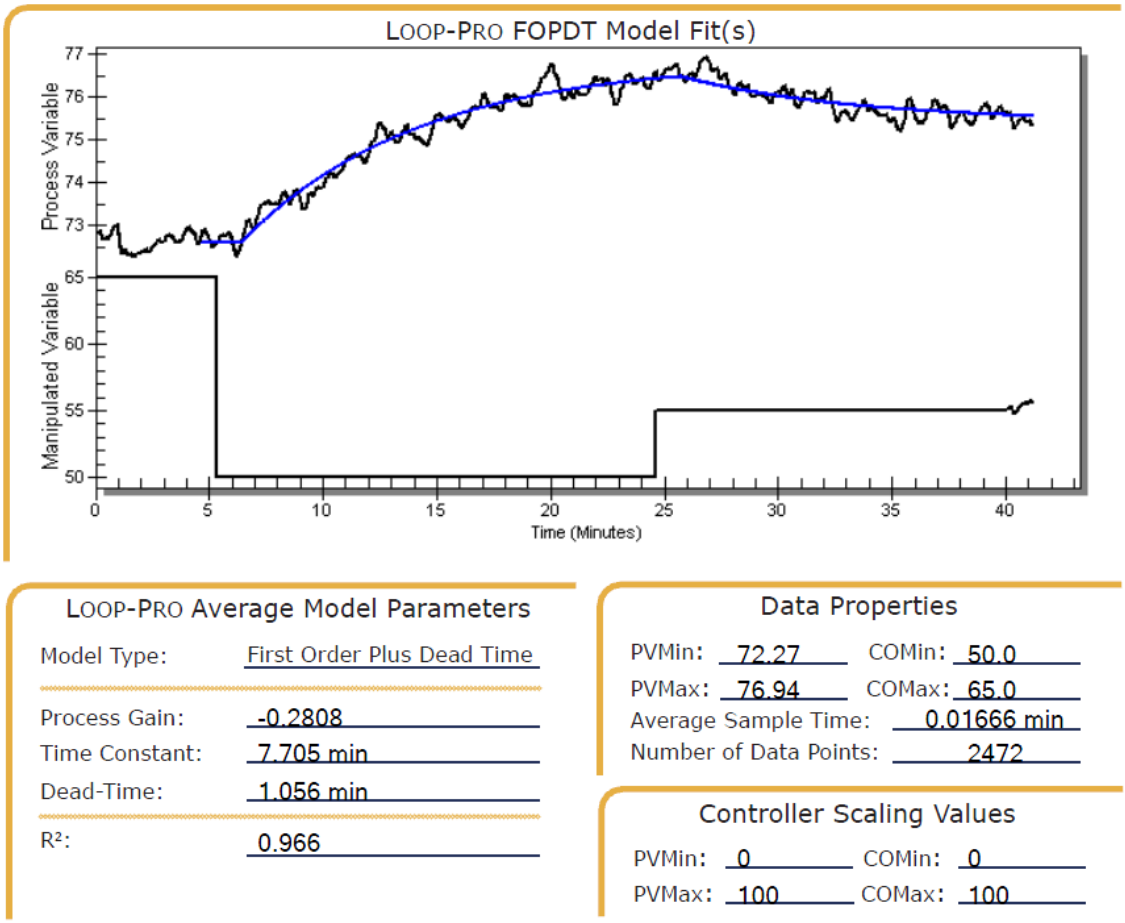

Figure B.4: Temperature Dynamic Response to Change in Fan Speed with 7 Fans Running and FOPDT Approximation

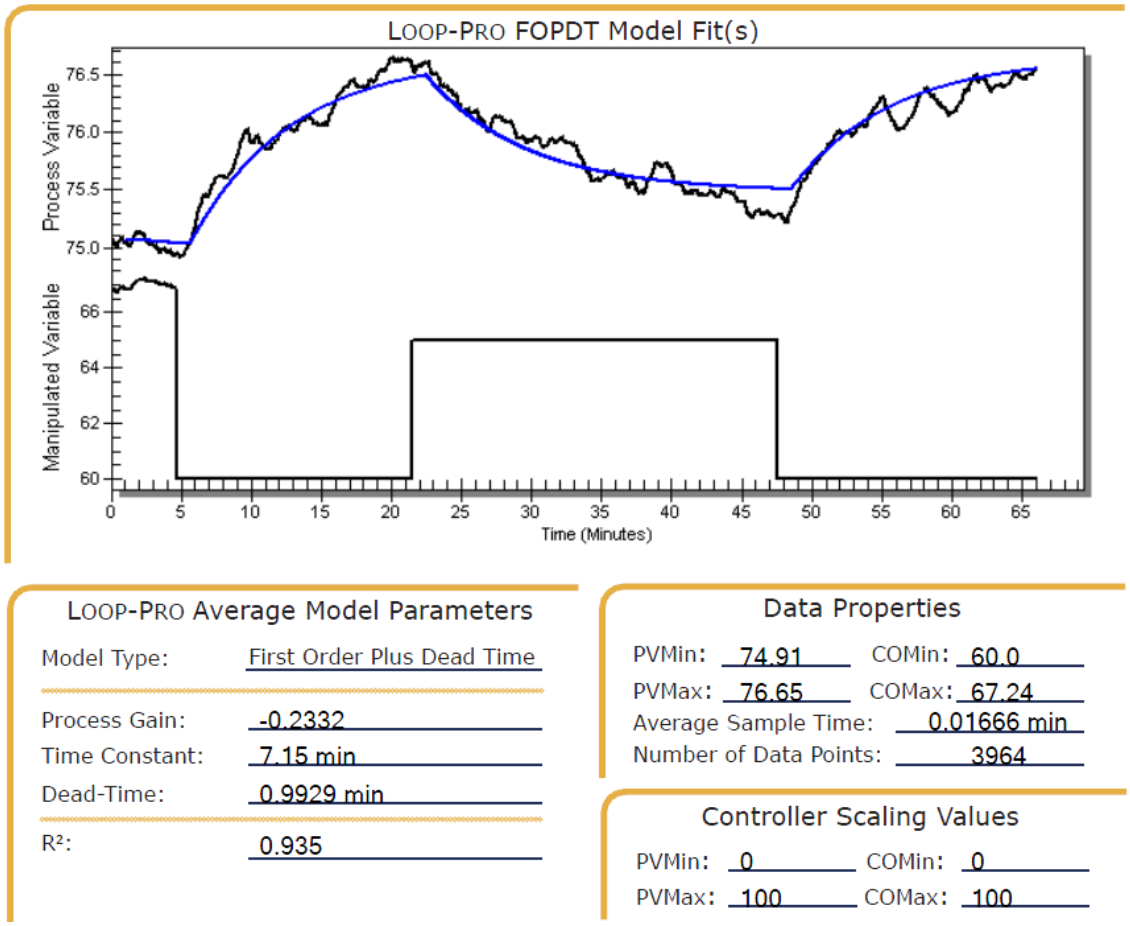

Figure B.5: Temperature Dynamic Response to Change in Fan Speed with 9 Fans Running and FOPDT Approximation

APPENDIX C: Cooling Water Temperature Regulation Performance Comparison Plots

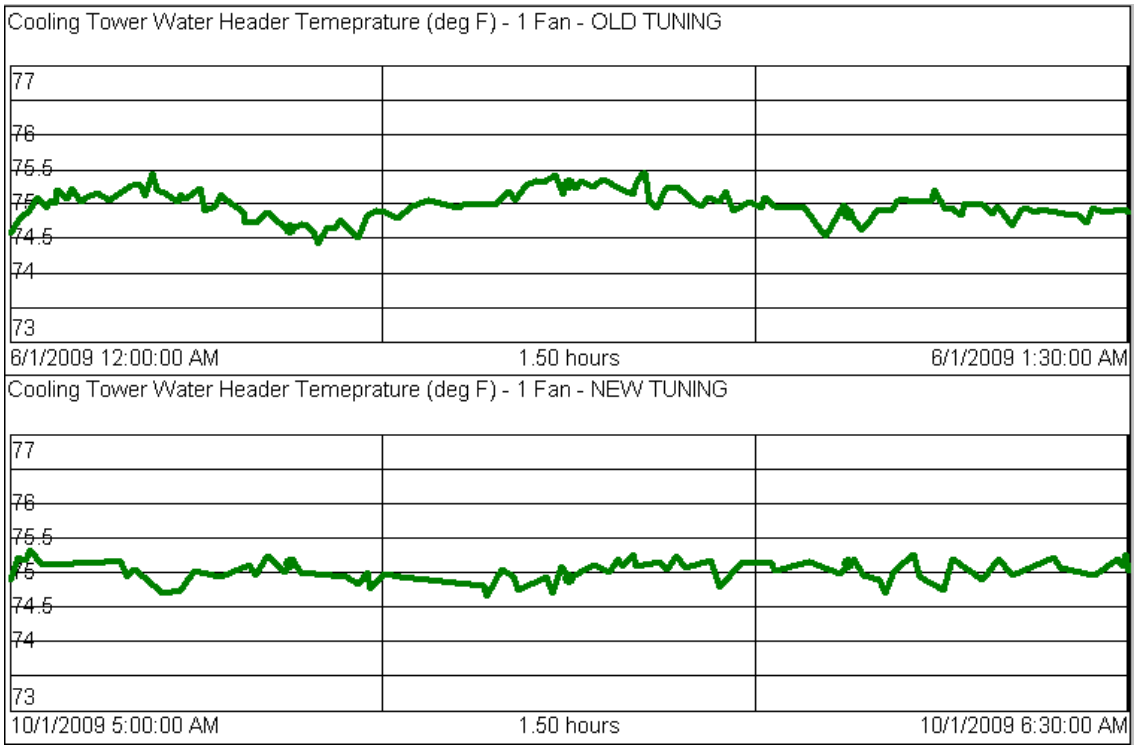

Figure C.1: Comparison of Temperature Regulation Performance with 1 Fan Operating Before and After Tuning

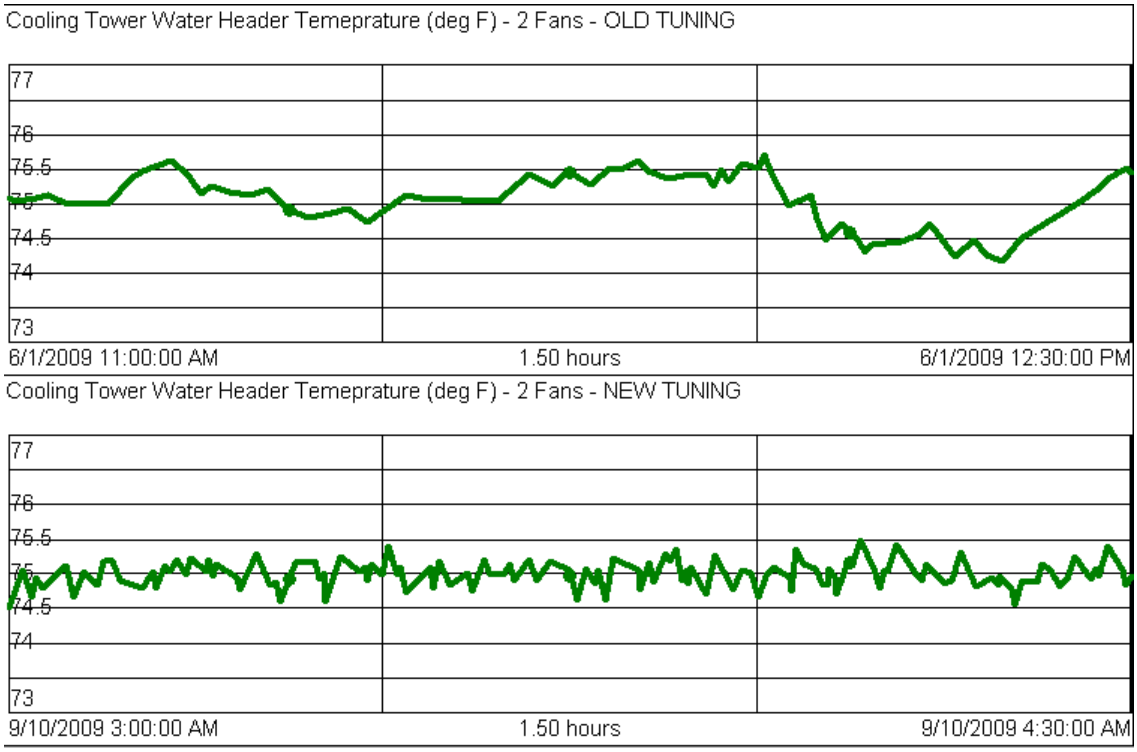

Figure C.2: Comparison of Temperature Regulation Performance with 2 Fans Operating Before and After Tuning

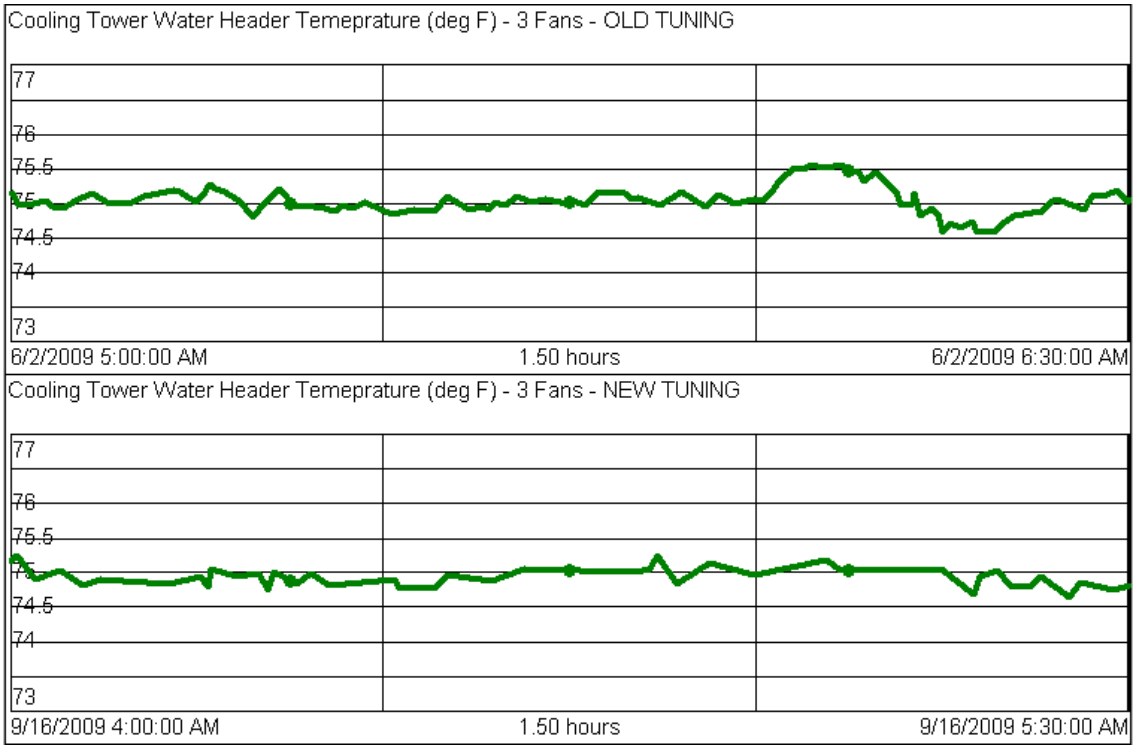

Figure C.3: Comparison of Temperature Regulation Performance with 3 Fans Operating Before and After Tuning

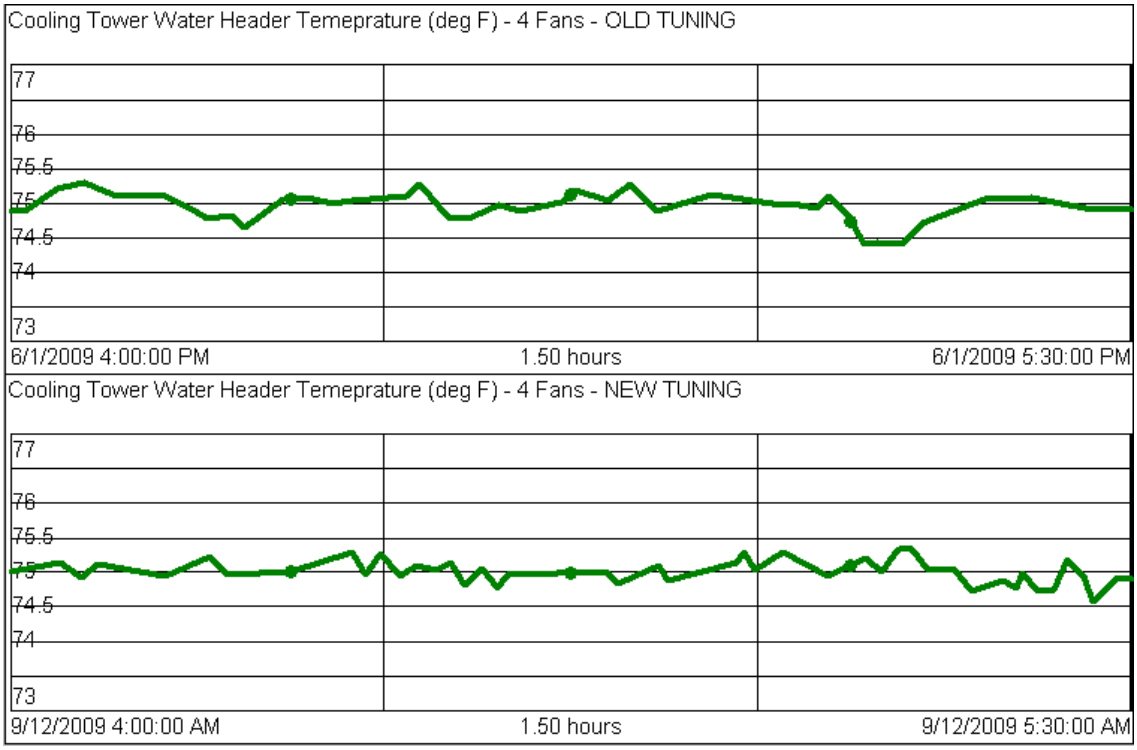

Figure C.4: Comparison of Temperature Regulation Performance with 4 Fans Operating Before and After Tuning

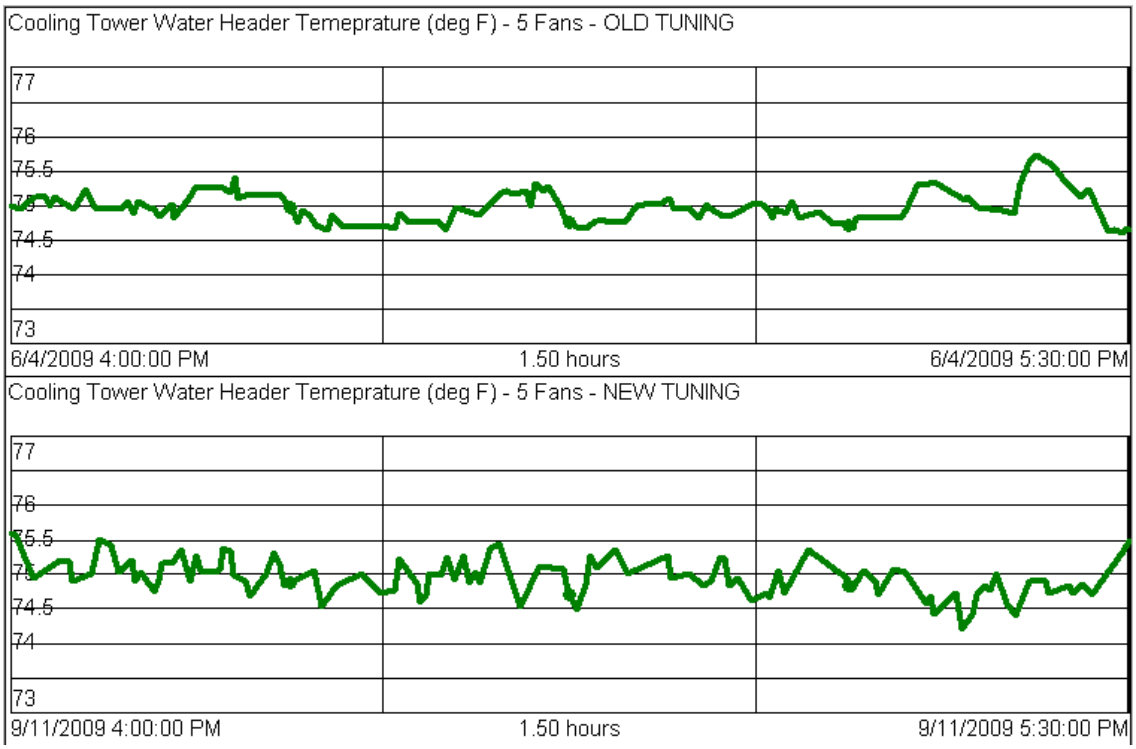

Figure C.5: Comparison of Temperature Regulation Performance with 5 Fans Operating Before and After Tuning

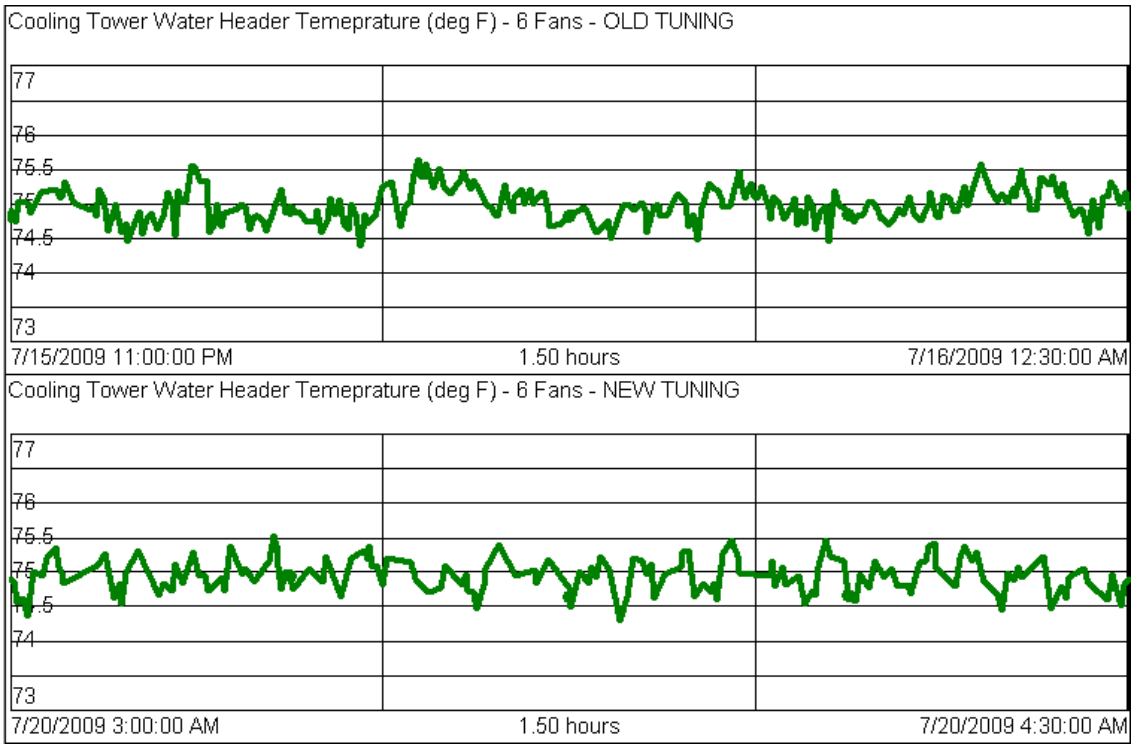

Figure C.6: Comparison of Temperature Regulation Performance with 6 Fans Operating Before and After Tuning

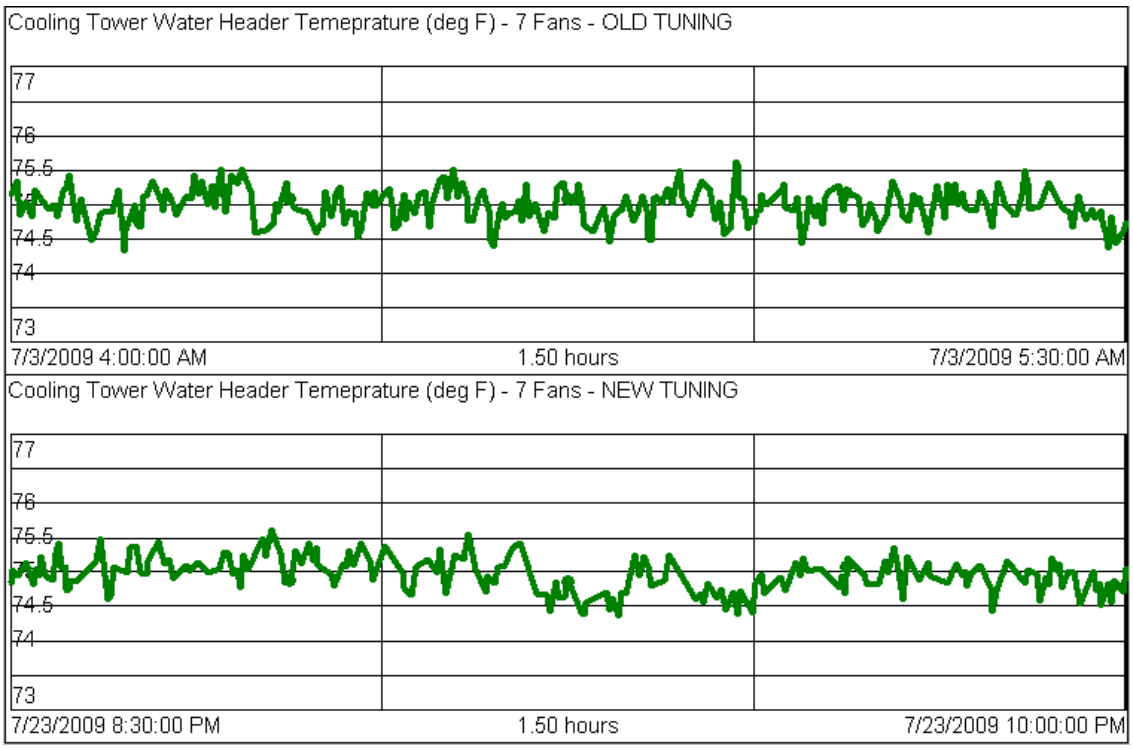

Figure C.7: Comparison of Temperature Regulation Performance with 7 Fans Operating Before and After Tuning

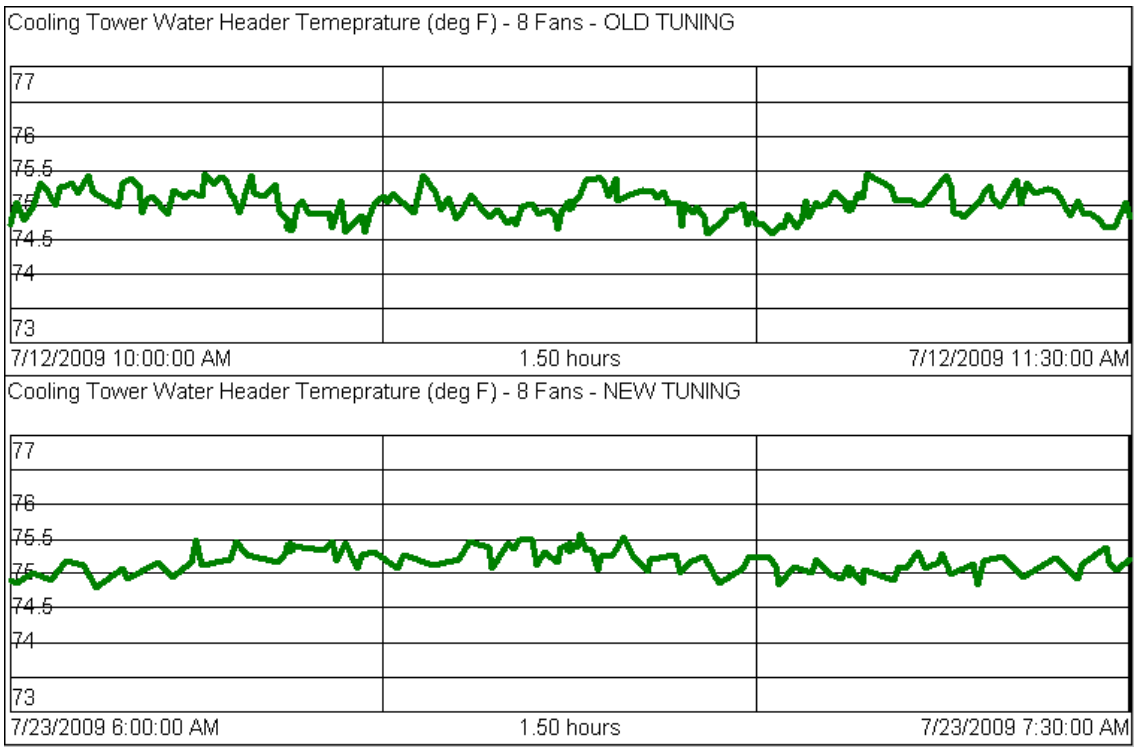

Figure C.8: Comparison of Temperature Regulation Performance with 8 Fans Operating Before and After Tuning

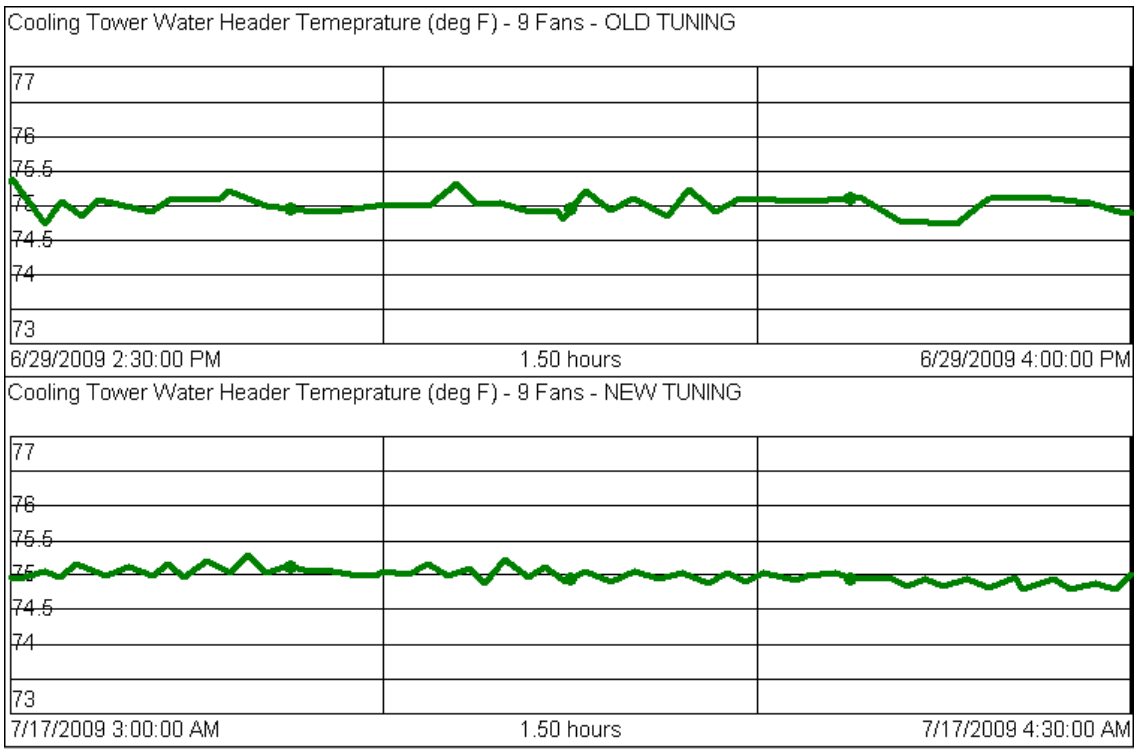

Figure C.9: Comparison of Temperature Regulation Performance with 9 Fans Operating Before and After Tuning

APPENDIX D: Fan Stop Disturbance Rejection Performance Comparison Plots

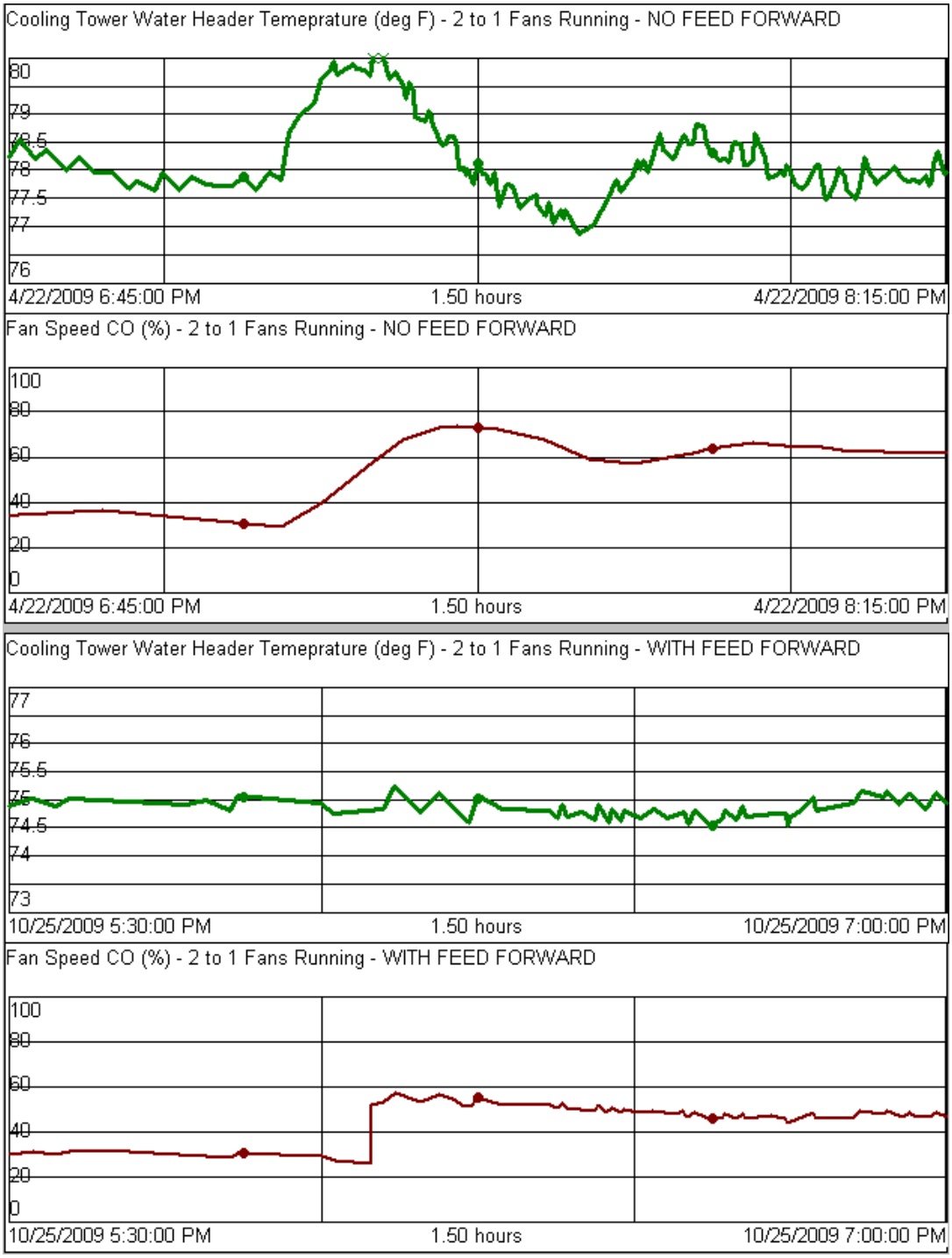

Figure D.1: Comparison of Disturbance Rejection Performance, No Feed Forward vs. Feed Forward, 2 Fans Initially Operating, 1 Fan Stopped

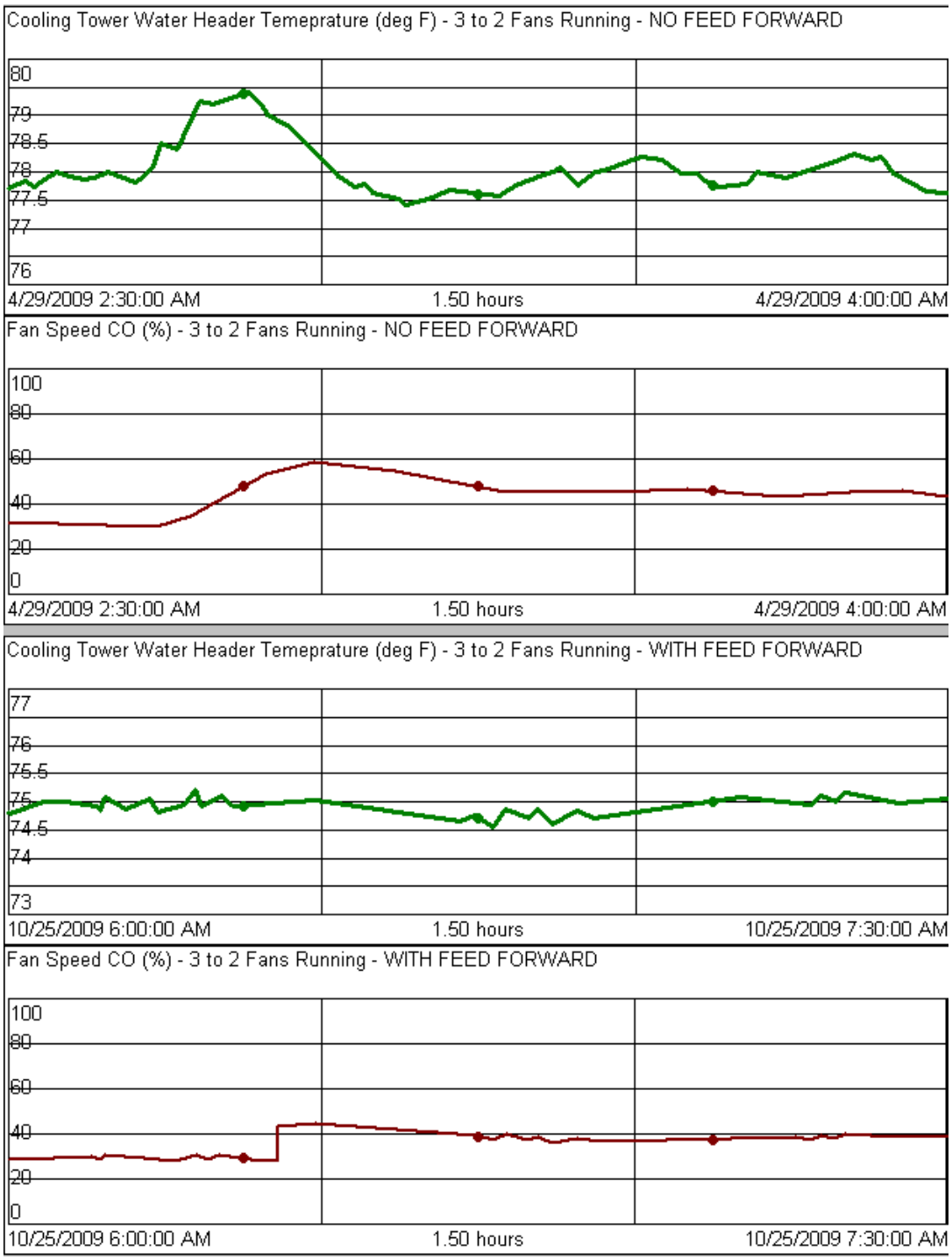

Figure D.2: Comparison of Disturbance Rejection Performance, No Feed Forward vs. Feed Forward, 3 Fans Initially Operating, 1 Fan Stopped

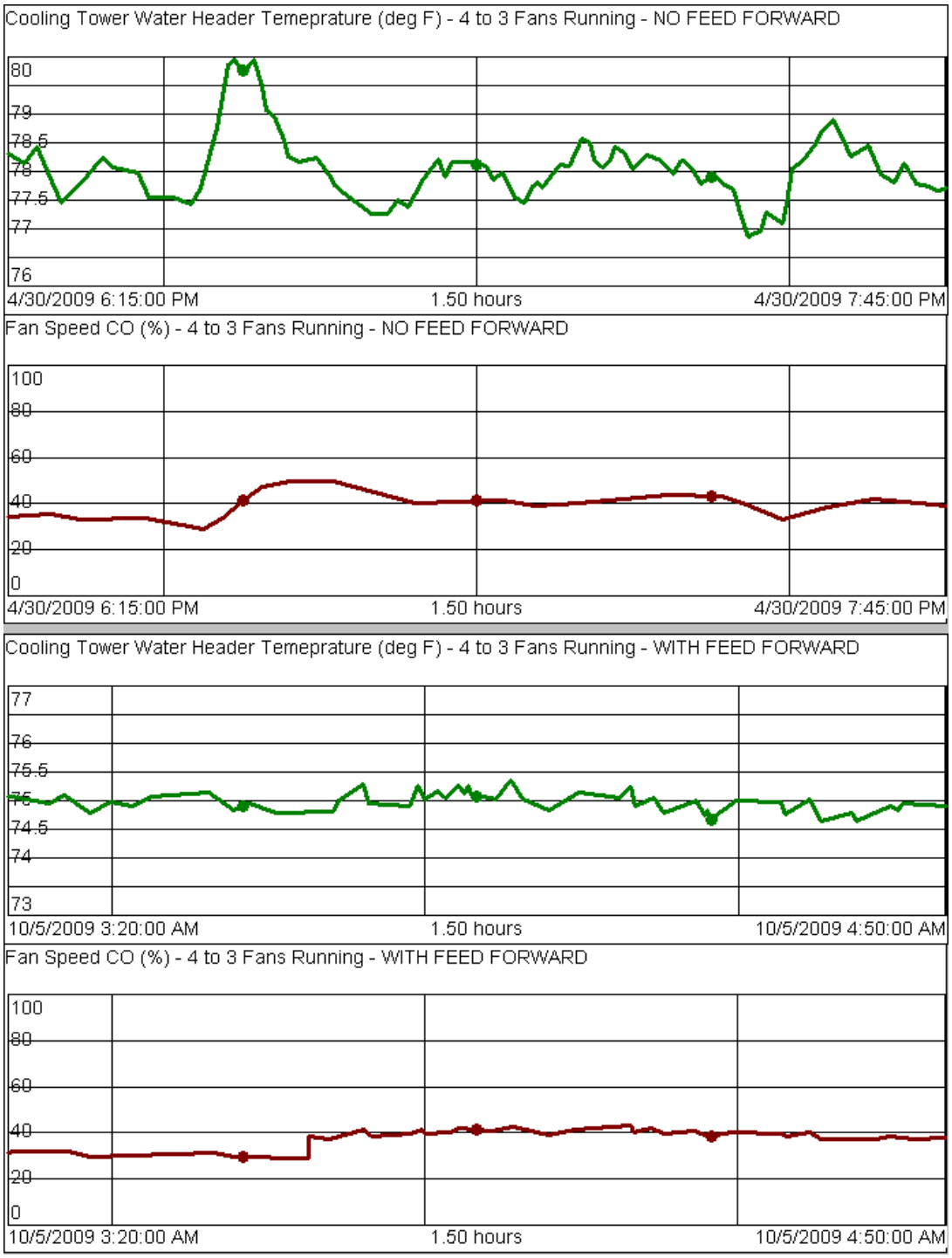

Figure D.3: Comparison of Disturbance Rejection Performance, No Feed Forward vs. Feed Forward, 4 Fans Initially Operating, 1 Fan Stopped

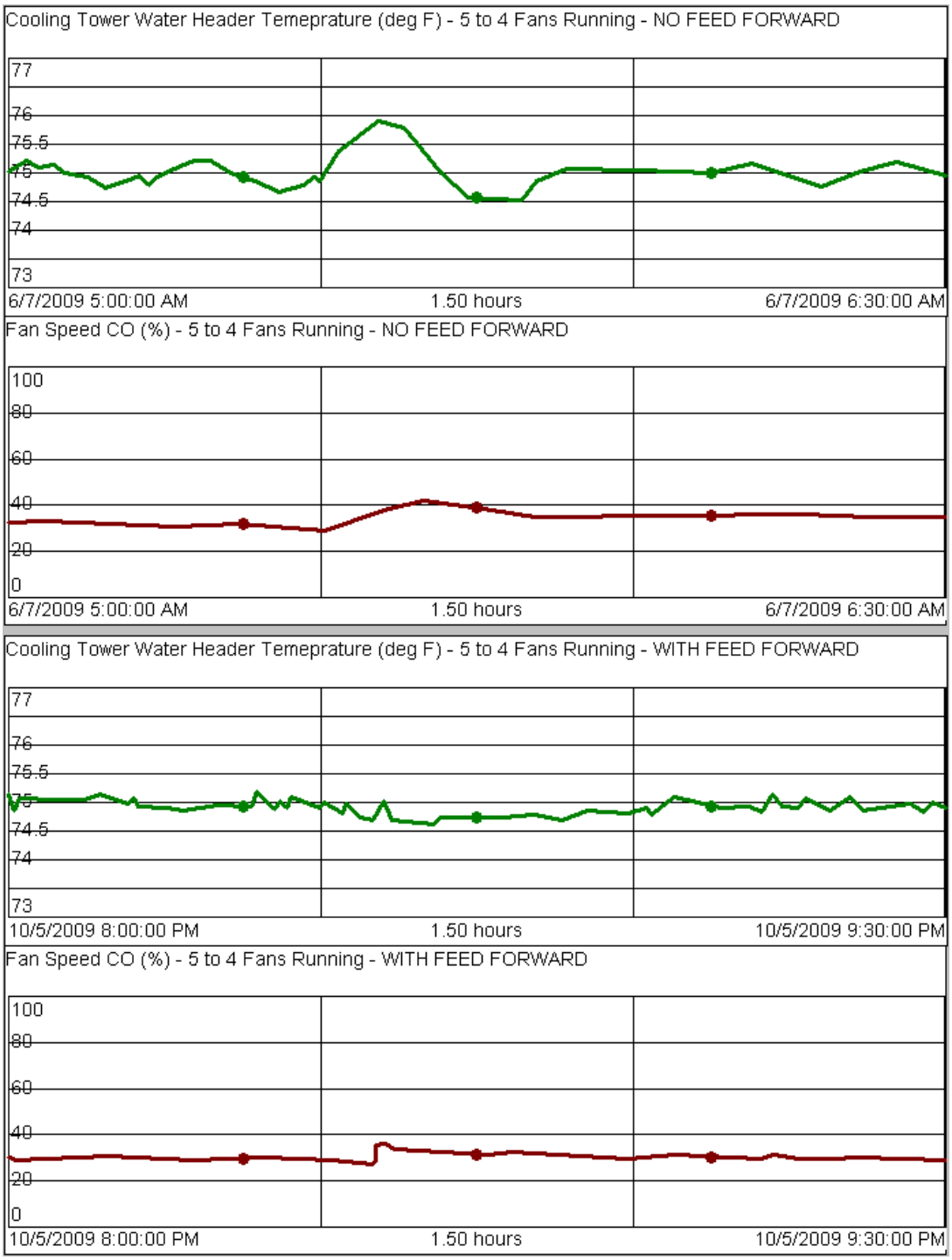

Figure D.4: Comparison of Disturbance Rejection Performance, No Feed Forward vs. Feed Forward, 5 Fans Initially Operating, 1 Fan Stopped

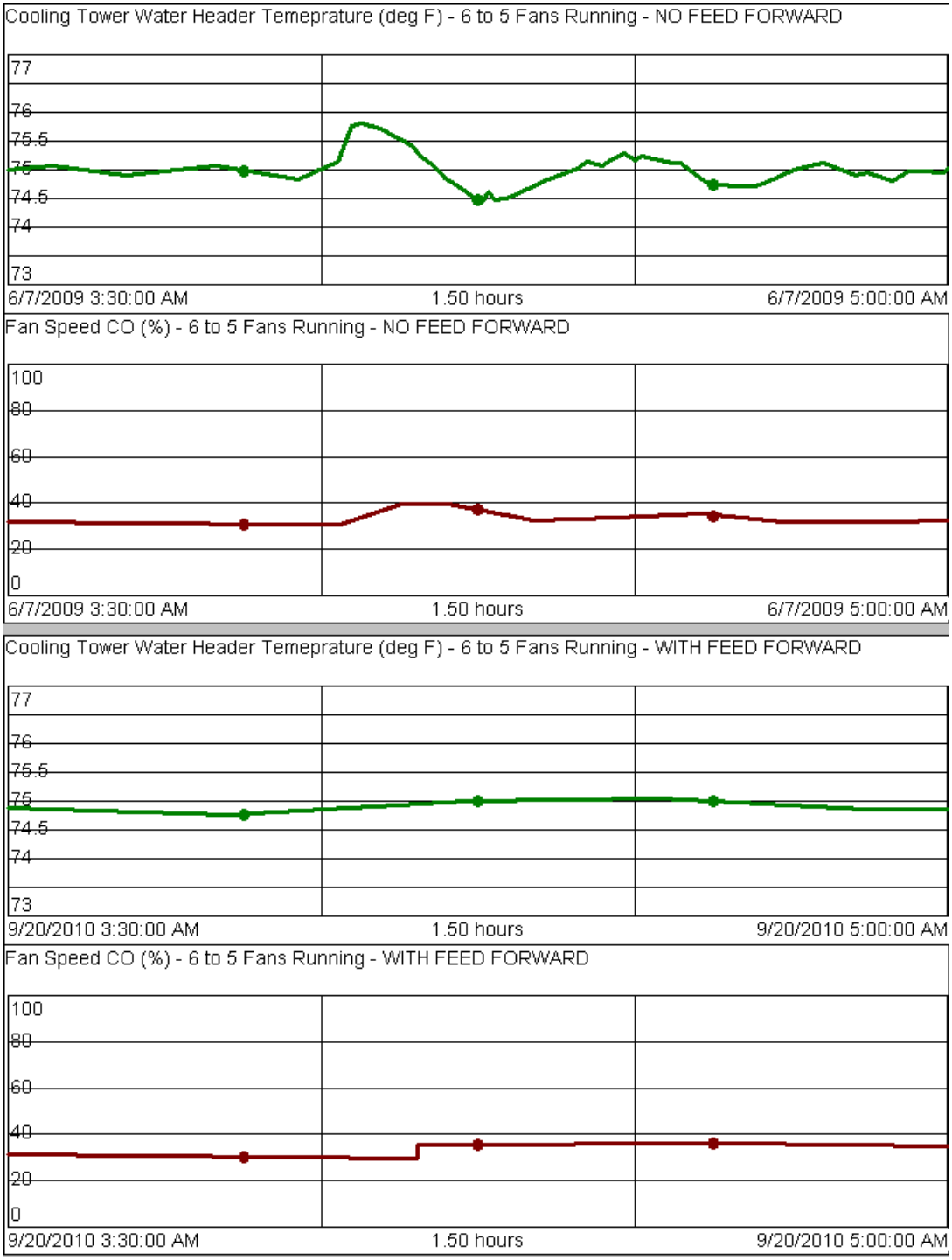

Figure D.5: Comparison of Disturbance Rejection Performance, No Feed Forward vs. Feed Forward, 6 Fans Initially Operating, 1 Fan Stopped

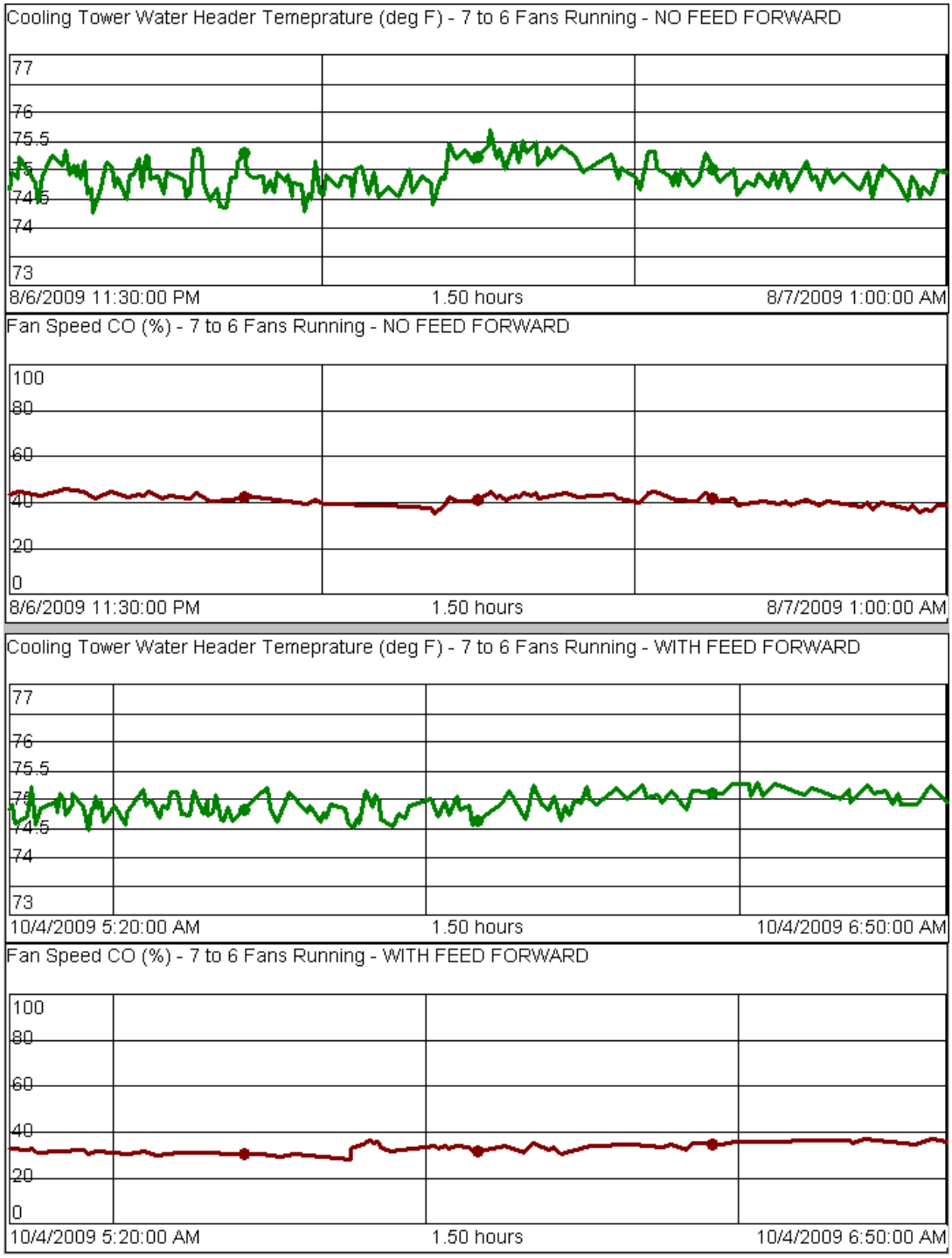

Figure D.6: Comparison of Disturbance Rejection Performance, No Feed Forward vs. Feed Forward, 7 Fans Initially Operating, 1 Fan Stopped

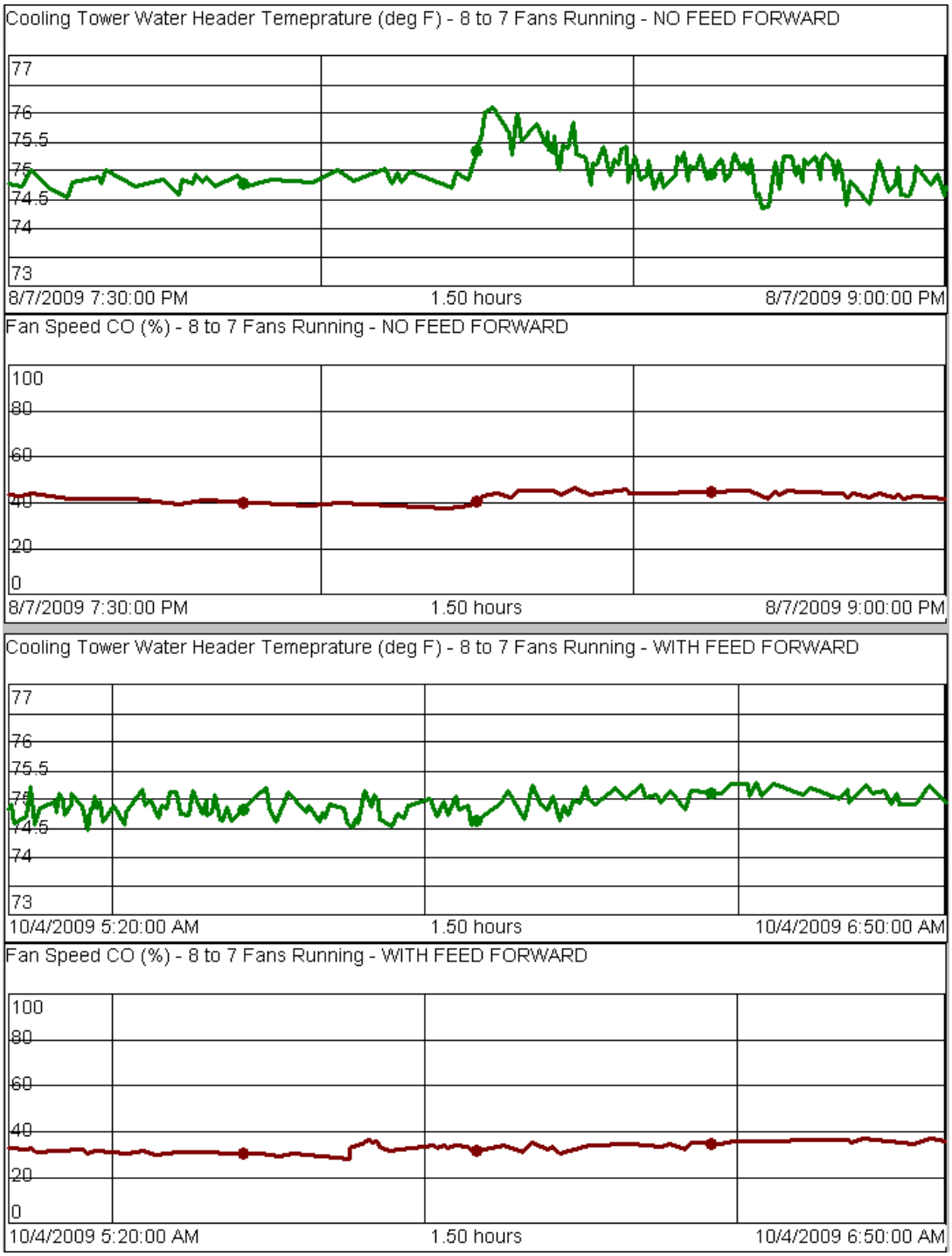

Figure D.7: Comparison of Disturbance Rejection Performance, No Feed Forward vs. Feed Forward, 8 Fans Initially Operating, 1 Fan Stopped

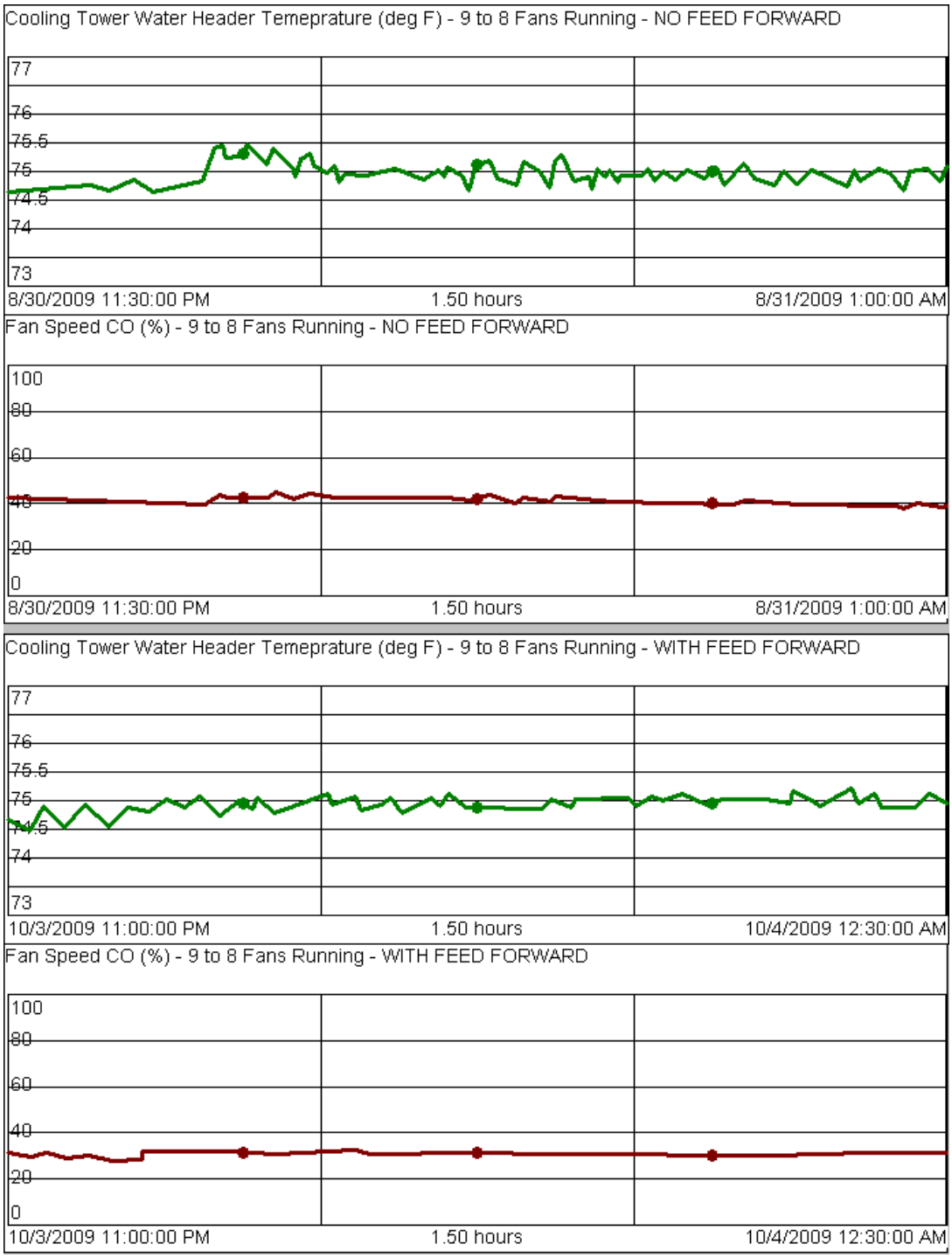

Figure D.8: Comparison of Disturbance Rejection Performance, No Feed Forward vs. Feed Forward, 9 Fans Initially Operating, 1 Fan Stopped